Fundamentals of Rotation-Vibration Spectra

S. Albert, K. Keppler Albert, H. Hollenstein, C. Manca Tanner, M. Quack

ETH Zürich, Laboratory of Physical Chemistry, Wolfgang-Pauli-Str. 10, CH-8093 Zürich, Switzerland, Email: Martin@Quack.ch

reprinted from

"Handbook of High-Resolution Spectroscopy",

Vol. 1, chapter 3, pages 117–173,
M. Quack, and F. Merkt, Eds. Wiley Chichester, 2011,
ISBN-13: 978-0-470-06653-9.
Online ISBN: 9780470749593,
DOI: 10.1002/9780470749593

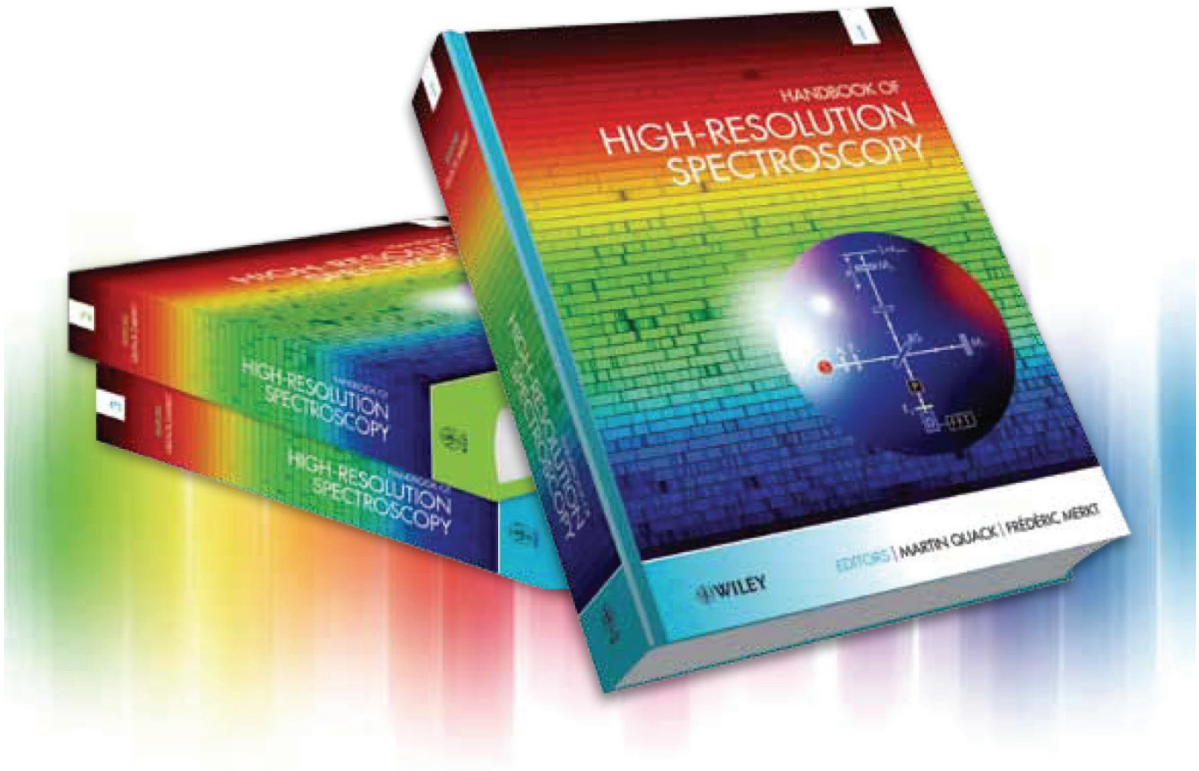

with compliments from Professor Martin Quack, ETH Zürich

Abstract

We provide a survey of fundamental aspects of rotation–vibration spectra. A basic understanding of the concepts is obtained from a detailed discussion of rotation–vibration spectra of diatomic molecules with only one vibrational degree of freedom. This includes approximate and exact separation of rotation and vibration, effective spectroscopic constants, the effects of nuclear spin and statistics, and transition probabilities derived from the form of the electric dipole moment function. The underlying assumptions and accuracy of the determination of molecular structure from spectra are discussed. Polyatomic molecules show many interacting vibrational degrees of freedom. Energy levels and spectra are discussed on the basis of normal coordinates and effective Hamiltonians of interacting levels in Fermi resonance, and in more complex resonance polyads arising from anharmonic potential functions. The resulting time-dependent dynamics of intramolecular energy flow is introduced as well. Effective Hamiltonians for interacting rotation–vibration levels are derived and applied to the practical treatment of complex spectra. Currently available computer programs aiding assignment and analysis are outlined.

Keywords: vibration-rotation spectra; intramolecular vibrational energy flow; fermi resonance; time-dependent vibrational dynamics; effective Hamiltonians; diatomic molecules; nuclear spin and statistics; electric dipole moment function; line intensities; band strengths

Fundamentals of Rotation–Vibration Spectra

Sieghard Albert, Karen Keppler Albert, Hans Hollenstein, Carine Manca Tanner and Martin Quack

Laboratorium für Physikalische Chemie, ETH Zürich, Zürich, Switzerland

1 INTRODUCTION

High-resolution infrared (IR) spectroscopy is the key to the quantum-state-resolved analysis of molecular rotation–vibration spectra and the consequent understanding of the quantum dynamics of molecules. Such quantum state resolution has been common in pure rotational spectra from the very beginning of this field after about 1945, on the basis of microwave (MW) technology (*see* Bauder 2011: **Fundamentals of Rotational Spectroscopy**, this handbook). In the IR range of the spectrum, however, which is important for the study of combined rotational–vibrational excitation, experimental resolution was sufficient in the past only for the simpler diatomic and polyatomic molecules, largely limited by the technology of grating or more generally dispersive spectrometers (Herzberg 1945, 1950, Nielsen 1962, Stoicheff 1962). There has been substantial development of IR and Raman spectroscopy at much higher resolution in recent decades, based on laser technology, on one hand, and interferometric Fourier transform infrared (FTIR) spectroscopy, on the other hand. This has made the rotation–vibration spectra of much more complex molecules accessible to the full analysis of the rotational–vibrational fine structure and the frontier in this area of research is moving toward even larger polyatomic molecules. Several articles in this handbook discuss these experimental developments (*see*, for instance, Albert *et al*. 2011: **High-resolution Fourier Transform Infrared Spectroscopy**, Snels *et al*. 2011: **High-resolution FTIR and Diode Laser Spectroscopy of Supersonic Jets**, Sigrist 2011: **High-resolution Infrared Laser Spectroscopy and Gas Sensing Applications**, Weber 2011: **High-resolution Raman Spectroscopy of Gases**, Havenith and Birer 2011: **High-resolution IR-laser Jet Spectroscopy of Formic Acid Dimer**, Hippler *et al*. 2011: **Mass and Isotope-selective Infrared Spectroscopy**, Amano 2011: **High-resolution Microwave and Infrared Spectroscopy of Molecular Cations**, Frey *et al*. 2011: **High-resolution Rotational Raman Coherence Spectroscopy with Femtosecond Pulses**, Demtröder 2011: **Doppler-free Laser Spectroscopy**, Stanca-Kaposta and Simons 2011: **High-resolution Infrared–Ultraviolet (IR–UV) Double-resonance Spectroscopy of Biological Molecules**, Flaud and Orphal 2011: **Spectroscopy of the Earth's Atmosphere** and Herman 2011: **High-resolution Infrared Spectroscopy of Acetylene: Theoretical Background and Research Trends**, among others, in this handbook).

In parallel to the experimental developments, there has been great progress in the theoretical understanding of the quantum mechanics of molecules on the basis of quantum chemical *ab initio* theory as well as quantum dynamics in general (*see* Yamaguchi and Schaefer 2011: **Analytic Derivative Methods in Molecular Electronic Structure Theory: A New Dimension to Quantum Chemistry and its Applications to Spectroscopy**, Tew *et al*. 2011: **Ab Initio Theory for Accurate Spectroscopic Constants and Molecular Properties**, Breidung and Thiel 2011: **Prediction of Vibrational Spectra from Ab Initio Theory**, Mastalerz and Reiher 2011: **Relativistic Electronic Structure Theory for Molecular Spectroscopy**, Marquardt and Quack 2011: **Global Analytical Potential Energy Surfaces for High-resolution Molecular Spectroscopy and Reaction Dynamics**, Watson 2011: **Indeterminacies of Fitting Parameters in Molecular**

Handbook of High-resolution Spectroscopy. Edited by Martin Quack and Frédéric Merkt. © 2011 John Wiley & Sons, Ltd.
ISBN: 978-0-470-74959-3.

Spectroscopy, Carrington 2011: **Using Iterative Methods to Compute Vibrational Spectra**, Tennyson 2011: **High Accuracy Rotation–Vibration Calculations on Small Molecules**, Boudon *et al*. 2011: **Spherical Top Theory and Molecular Spectra**, Köppel *et al*. 2011: **Theory of the Jahn–Teller Effect** and Field *et al*. 2011: **Effective Hamiltonians for Electronic Fine Structure and Polyatomic Vibrations**, this handbook). Thus, many aspects of rotation–vibration spectroscopy are covered in great detail in the individual articles of this handbook.

The goal of this article is to provide a brief, largely didactic discussion of some of the basic concepts, where one considers vibrational motion in addition to the rotational motion treated in the preceding article by Bauder 2011: **Fundamentals of Rotational Spectroscopy**, this handbook. This also helps in defining some of the basic concepts in this field (*see also* Stohner and Quack 2011: **Conventions, Symbols, Quantities, Units and Constants for High-resolution Molecular Spectroscopy**, this handbook). Further basic concepts related to the present article can be found in Merkt and Quack 2011: **Molecular Quantum Mechanics and Molecular Spectra, Molecular Symmetry, and Interaction of Matter with Radiation**, this handbook. We also discuss some aspects arising in the practical analysis of complex rotation–vibration spectra of polyatomic molecules, because this topic is not well covered in the traditional textbooks and has developed in more recent years through the development of new experimental possibilities. The structure arising from electronic excitation is covered in Wörner and Merkt 2011: **Fundamentals of Electronic Spectroscopy**, this handbook.

This article is organized as follows. We start with a detailed discussion of diatomic molecules in Section 2. Section 3 extends the treatment to polyatomic molecules with several interacting vibrations including anharmonic resonance. The time-dependent picture of intramolecuar motion and energy flow is presented in Section 4. Section 5 discusses the analysis of interaction of rotation and vibration, and Section 6 deals with pattern recognition and assignment aids for complex molecular spectra.

2 ENERGY LEVELS AND IR SPECTRA OF DIATOMIC MOLECULES: INTERACTION OF ROTATION AND VIBRATION AND EFFECTS OF NUCLEAR SPIN

This section considers some basic concepts of spectra of vibrating and rotating molecules, using diatomic molecules for illustration. These concepts also find their correspondence in polyatomic molecules, where, however, the situation is much more complex. We start from the Born–Oppenheimer approximation (*see* Bauder 2011: **Fundamentals of Rotational Spectroscopy**, Wörner and Merkt 2011: **Fundamentals of Electronic Spectroscopy** and Marquardt and Quack 2011: **Global Analytical Potential Energy Surfaces for High-resolution Molecular Spectroscopy and Reaction Dynamics**, this handbook), where the atoms or nuclei move in an effective potential $V(R)$ defined by the solution of the electronic Schrödinger equation. R is the distance between the nuclei. We consider molecules in their electronic ground state (*see* Wörner and Merkt 2011: **Fundamentals of Electronic Spectroscopy**, this handbook, for a discussion pertaining to molecules in excited electronic states). Indeed, one can consider "best" effective potentials $V(R)$ going beyond the Born–Oppenheimer approximation, still retaining the concept that the explicit motion of the electrons can be neglected and, thus, one has to consider only the dynamics of nuclear motion in this effective potential (Section 2.1). Because this effective potential, in general, has no simple form, there are consequently no simple analytical expressions available for the energy levels or rovibrational term values except for model potentials. Thus, in practical spectroscopy, one uses approximations leading to simple formulae for the term values, which can be expressed by tables of constants summarizing these term value expressions (Huber and Herzberg 1979). The approaches, starting either from "exact" solutions of the Schrödinger equation for nuclear motion in an effective potential or using simple term formulae for energy levels, are conceptually different, and similar conceptual differences also exist in the case of polyatomic molecules. Symmetry and nuclear spin introduce further effects in homonuclear diatomic molecules (Section 2.3). To describe spectroscopic transitions between energy levels, one has to furthermore consider the radiative transition probabilities, for example, in the electric dipole approximation for absorption spectra or related approximations for Raman spectra (Section 2.4). We also discuss concepts related to the determination of molecular structure from high-resolution IR spectra.

2.1 Quasi-exact Treatment of Rotation–Vibration States of Diatomic Molecules in the Framework of the Born–Oppenheimer Approximation or More General Effective Potentials

Figure 1 schematically shows a diatomic molecule with variable bond length R. For example, the reader may consider $^{12}C^{16}O$ (with no nuclear spin) or $^{1,2}H^{19}F$ (neglecting nuclear spin effects for now), both in their $^1\Sigma$ closed shell, nondegenerate electronic ground state in the

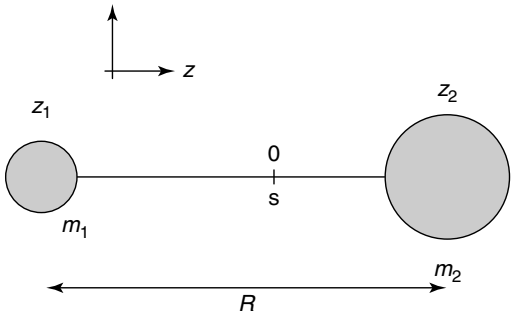

Figure 1 Diatomic molecule scheme. The origin of the molecule-fixed coordinate system is located at the center of mass (S) of the molecule.

Born–Oppenheimer approximation (*see* Bauder 2011: **Fundamentals of Rotational Spectroscopy** and Wörner and Merkt 2011: **Fundamentals of Electronic Spectroscopy**, this handbook). Restricting the motion to one dimension (along the z axis), one has a pure vibrational and translational problem; separating the center of mass (S) translational motion in a standard way (Cohen-Tannoudji *et al.* 1977, Demtröder 2003) and using momentum conservation for the molecule as a whole, one obtains the Hamiltonian operator for the internal (vibrational) motion:

$$\hat{H}_\mathrm{v} = \hat{T}_\mathrm{v} + \hat{V}_\mathrm{v} = \frac{\hat{p}^2}{2\mu} + V(R) \tag{1}$$

with the momentum operator $\hat{p}$ and the reduced mass μ,

$$\mu = \frac{m_1 m_2}{m_1 + m_2} \tag{2}$$

where m_1 and m_2 are the masses of the two nuclei (or atoms, see below).

Figure 2 shows two typical model potentials, as an illustration, for which the time-independent vibrational Schrödinger equation

$$\hat{H}_\mathrm{v}\Psi_\mathrm{v}(R) = E_\mathrm{v}\Psi_\mathrm{v}(R) \tag{3}$$

has simple solutions. With the harmonic potential $V_\mathrm{h}(R)$,

$$V_\mathrm{h}(R) = \frac{1}{2} f (R - R_\mathrm{e})^2 \tag{4}$$

one has

$$E_\mathrm{v} = h\nu \left(\mathrm{v} + \frac{1}{2}\right), \quad \mathrm{v} = 0, 1, 2 \ldots \tag{5}$$

or equivalently with vibrational wavenumbers ω_e

$$\frac{E_\mathrm{v}}{hc} = \omega_\mathrm{e} \left(\mathrm{v} + \frac{1}{2}\right) \tag{6}$$

$$\Psi_\mathrm{v}(Q) = N_\mathrm{v} H_\mathrm{v}(Q) \exp(-Q^2/2) \tag{7}$$

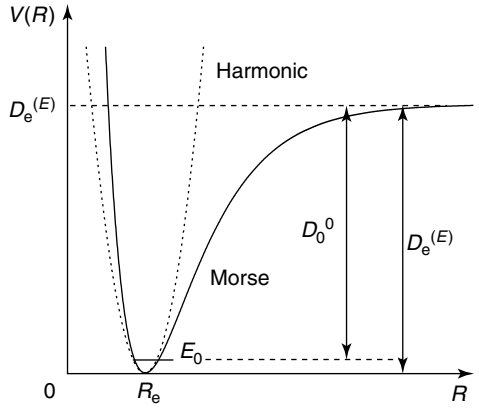

Figure 2 Morse potential $V(R)$, full line, and harmonic potential, dotted line. The relevant parameters are the zero-point energy E_0, the electronic dissociation energy $D_\mathrm{e}^{(E)}$, and the thermodynamic bond dissociation energy at 0 K $D_0^0 = \Delta_\mathrm{diss} H_0^0 / N_\mathrm{A} = D_\mathrm{e}^{(E)} - E_0$.

with the reduced coordinate

$$Q = (R - R_\mathrm{e})\sqrt{f/h\nu} \tag{8}$$

Because of close analogies with the classical mechanics of oscillation, one uses the concept of the force constant

$$f = \left(\frac{\partial^2 V(R)}{\partial R^2}\right)_{R=R_\mathrm{e}} \tag{9}$$

and the classical oscillation frequency $\nu = c\omega_\mathrm{e}$

$$\nu = \frac{1}{2\pi}\sqrt{\frac{f}{\mu}} \tag{10}$$

The normalization factors N_v in equation (7) are obtained from

$$\int_{-\infty}^{+\infty} \Psi_\mathrm{v}^* (Q)\Psi_\mathrm{v}(Q)\,\mathrm{d}Q = 1 \tag{11}$$

$$N_\mathrm{v} = \left\{\sqrt{\pi}\,\mathrm{v}!2^\mathrm{v}\right\}^{-1/2} \tag{12}$$

and the Hermite polynomials $H_\mathrm{v}(Q)$

$$H_\mathrm{v}(Q) = (-1)^\mathrm{v} \exp(Q^2) \frac{\mathrm{d}^\mathrm{v}}{\mathrm{d}Q^\mathrm{v}} \exp(-Q^2) \tag{13}$$

Similarly, with the "anharmonic" Morse potential

$$V_\mathrm{M}(R) = D_\mathrm{e}^{(E)} \{1 - \exp[-a(R - R_\mathrm{e})]\}^2 \tag{14}$$

one obtains

$$\frac{E_\mathrm{v}}{hc} = \omega_\mathrm{e} \left(\mathrm{v} + \frac{1}{2}\right) - \omega_\mathrm{e} x_\mathrm{e} \left(\mathrm{v} + \frac{1}{2}\right)^2 \tag{15}$$

with the usual spectroscopic constants ω_e and $\omega_e x_e$ in units of wavenumbers (m^{-1} or cm^{-1}, *see* Stohner and Quack 2011: **Conventions, Symbols, Quantities, Units and Constants for High-resolution Molecular Spectroscopy**, this handbook)

$$\omega_e x_e = \frac{\omega_e^2}{4D_{eM}} \tag{16}$$

$$D_{eM} = \frac{D_e^{(E)}}{hc} \tag{17}$$

Equation (15) is valid for discrete energies $E_{v \le v_{max}}$, where v_{max} is given by the highest bound level with $E_{v_{max}} < D_e^{(E)}$. Figure 3 shows in an exemplary manner the lowest six energy levels, wavefunctions Ψ_v, and probability densities $|\Psi_v|^2$ for the harmonic oscillator and the anharmonic Morse oscillator. The conventional spectroscopic constants of the anharmonic Morse oscillator are related to the properties of the potential

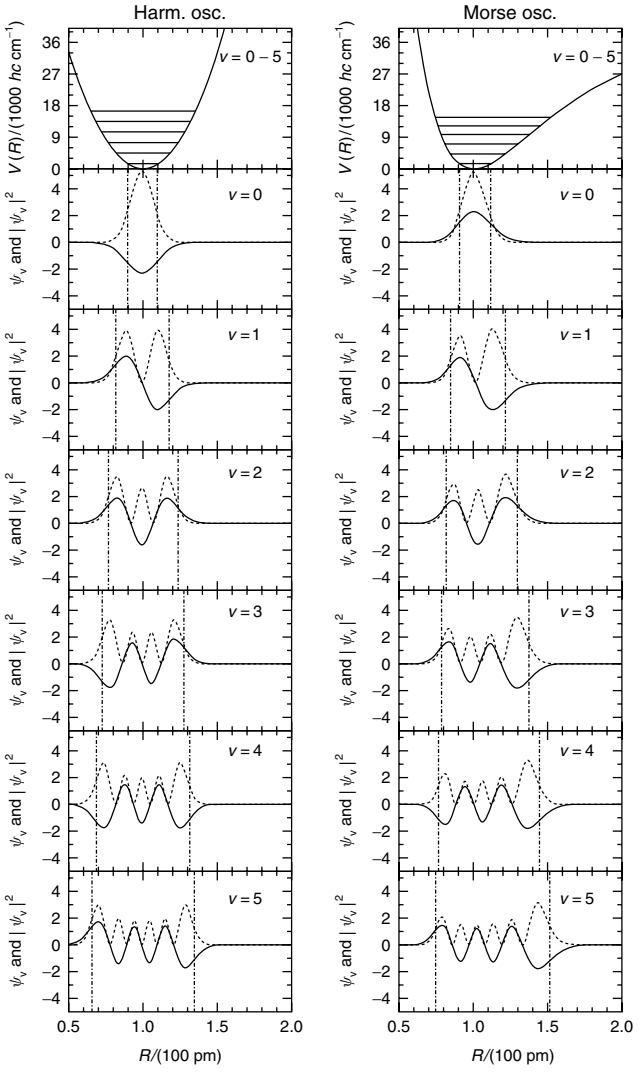

Figure 3 Eigenfunctions (full line) and probability densities (dotted line) of the harmonic oscillator (left) and the anharmonic Morse oscillator (right).

$$\omega_e = \frac{1}{2\pi c}\sqrt{\frac{f}{\mu}} = a\left[\frac{D_{eM}h}{2\pi^2 c\mu}\right]^{1/2} \tag{18}$$

with the force constant f being defined by equation (9). One can also write

$$\omega_e x_e = \frac{ha^2}{8\pi^2 c\mu} \tag{19}$$

$$a = \omega_e\sqrt{2\pi^2 c\mu/(D_{eM}h)} \tag{20}$$

$$a \simeq 1.2177 \times 10^7 \omega_e \sqrt{\frac{\mu/\mathrm{Da}}{D_{eM}/\mathrm{cm}^{-1}}} \tag{21}$$

where the last approximate equation is useful for practical calculations with constants given in spectroscopic units.

Rewriting the energy levels as a difference measured from the zero point level, one finds

$$\frac{(E_v - E_0)}{hc} = (\omega_e - \omega_e x_e)v - \omega_e x_e v^2 \tag{22}$$

$$\frac{(E_v - E_0)}{hc} = \omega_0 v - \omega_0 x_0 v^2 \tag{23}$$

with the new constants $\omega_0 = \omega_e - \omega_e x_e$ and $\omega_0 x_0 = \omega_e x_e$ for the Morse oscillator.

The energy difference of adjacent energy levels is a linear function of v:

$$\frac{\Delta E(v)}{hc} = \frac{(E_{v+1} - E_v)}{hc} = (\omega_0 - \omega_0 x_0) - 2\omega_0 x_0 v \tag{24}$$

This relation can be used for practical determination of the spectroscopic constants from a linear graph (Figure 4). One readily also sees that there is a finite number of discrete levels with

$$v_{max} \simeq \frac{2D_{eM}}{\omega_e} \tag{25}$$

Thus one has about twice as many levels as the number of harmonic levels up to dissociation. The first interval $\Delta E(0)/hc = \tilde{\nu}_{fM}$ is also called the *anharmonic fundamental wavenumber* of the Morse oscillator (y-intercept, Figure 4).

The one-dimensional motion can be extended to three dimensions by using angular momentum conservation in isotropic space (Cohen-Tannoudji *et al.* 1977, Zare 1988, Demtröder 2003). This allows for an exact separation of the wavefunction in polar coordinates (R, ϑ, φ) according to equation (26):

$$\Psi(R, \vartheta, \varphi) = \Phi_{v,J}(R) Y_{J,M_J}(\vartheta, \varphi) \tag{26}$$

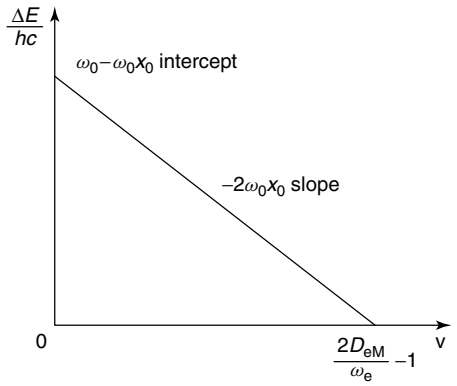

Figure 4 Term values as differences $f(\mathrm{v}) = \Delta E(\mathrm{v})/(hc)$; see equation (24).

$Y_{J,M_J}(\vartheta, \varphi)$ are the spherical harmonics; here we use the conventional symbols for the angular momentum quantum number J and the quantum number M_J for the z component of the angular momentum. The angular dependence of the "rotational" wavefunctions is, thus, the same as for the hydrogen atom, with the conventional notation $Y_{l,m_l}(\vartheta, \varphi)$. The "vibrational" wavefunctions $\Phi_{\mathrm{v},J}(R)$ depend upon the double index v, J because they are solutions of a one-dimensional Schrödinger equation with an effective J-dependent potential

$$V_{\mathrm{eff}}(R, J) = V(R) + \frac{h^2}{8\pi^2\mu R^2} J(J+1) \qquad (27)$$

$$V_{\mathrm{eff}}(R, J) = V(R) + V_{\mathrm{cent}}(J) \qquad (28)$$

where $V_{\mathrm{cent}}(J)$ is interpreted as a centrifugal potential. The effectively one-dimensional differential equation to be solved is thus

$$\hat{H}\Phi_{\mathrm{v},J}(R) = E_{\mathrm{v},J}\Phi_{\mathrm{v},J}(R) \qquad (29)$$

with

$$\hat{H} = -\frac{h^2}{8\pi^2\mu R^2}\left[\frac{\partial}{\partial R}R^2\frac{\partial}{\partial R}\right] + V_{\mathrm{eff}}(R, J) \qquad (30)$$

or rewriting the differential equation in the practical form (Demtröder 2003)

$$\frac{1}{R^2}\frac{\mathrm{d}}{\mathrm{d}R}\left(R^2\frac{\mathrm{d}\Phi_{\mathrm{v},J}(R)}{\mathrm{d}R}\right) + \frac{8\pi^2\mu}{h^2}\left[E_{\mathrm{v},J} - V_{\mathrm{eff}}(R, J)\right]\Phi_{\mathrm{v},J}(R) = 0 \qquad (31)$$

The one-dimensional differential equation is readily solved by numerical methods, for instance, using the Numerov–Cooley algorithm, and programs are available that are specifically designed for diatomic molecule problems (Le Roy 2007). In general, there are no simple energy level formulae available. However, we mention the close analogy to the hydrogen atom, where $V(R)$ is the Coulomb potential ($V(R) \propto -e^2/R$). Indeed, the problem at hand is the general problem of two point masses separated by R and moving in free space under the influence of an interaction potential $V(R)$.

Figure 5 shows the lowest "rotation–vibration energies" for the Coulomb potential in the corresponding effective potentials $V_{\mathrm{eff}}(R, l)$, where the "rotational" quantum number is labeled "l" by convention for the orbital angular momentum. Because of the special nature of the Coulomb potential, the "vibrational ground state" for each effective potential $V_{\mathrm{eff}}(R, l)$ is degenerate with excited states arising from lower values of l ($l-1, l-2, \ldots 0$), leading to the well-known "Coulomb degeneracy" (slightly lifted in reality). For diatomic molecules, no such degeneracy arises because $V(R)$ is qualitatively very different from the Coulomb potential. Indeed, in general, no simple exact term formulae arise.

In this respect an exception results for the Morse potential. As shown by Pekeris (1934), and Nielsen (1951, 1959), one finds

$$\frac{E_{\mathrm{v},J}}{hc} = \omega_{\mathrm{e}}\left(\mathrm{v}+\frac{1}{2}\right) - \omega_{\mathrm{e}}x_{\mathrm{e}}\left(\mathrm{v}+\frac{1}{2}\right)^2 + B_{\mathrm{v}}J(J+1) - D_{\mathrm{v}}J^2(J+1)^2 \qquad (32)$$

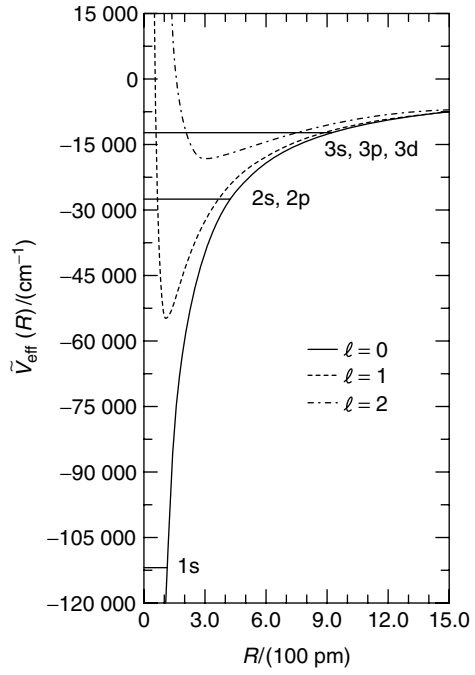

Figure 5 Potential functions with vibrational eigenvalues for the hydrogen atom (for $l = 0, 1, 2$).

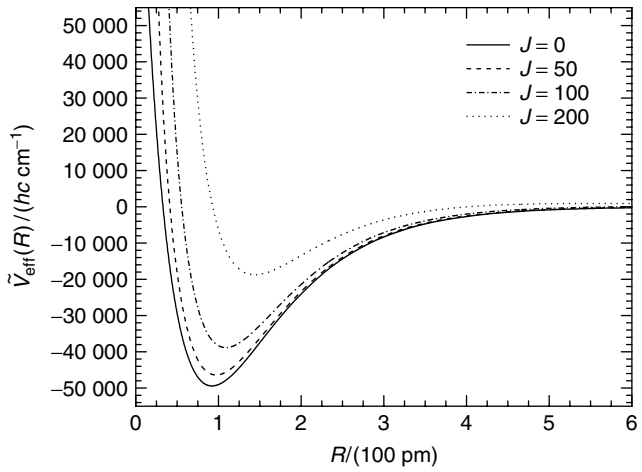

Figure 6 Morse potential $\tilde{V}_{\text{eff}}(R)$ of the HF molecule from the SO-3 potential (Klopper *et al*. 1998) and effective potential for various values of J.

$$B_{\text{v}} = B_{\text{e}} - \alpha_{\text{e}}\left(\text{v} + \frac{1}{2}\right) \tag{33}$$

$$B_{\text{e}} = \frac{h}{8\pi^2 c\mu R_{\text{e}}^2} \tag{34}$$

$$\alpha_{\text{e}} = \frac{3h^2\omega_{\text{e}}}{16\pi^2\mu R_{\text{e}}^2 D_{\text{e}}}\left(\frac{1}{aR_{\text{e}}} - \frac{1}{a^2R_{\text{e}}^2}\right) \tag{35}$$

$$D_{\text{v}} = D_{\text{e}} + \beta_{\text{e}}\left(\text{v} + \frac{1}{2}\right) \tag{36}$$

$$\beta_{\text{e}} = D_{\text{e}}\left(\frac{8\omega_{\text{e}}x_{\text{e}}}{\omega_{\text{e}}} - \frac{5\alpha_{\text{e}}}{\omega_{\text{e}}} - \frac{\alpha_{\text{e}}^2\omega_{\text{e}}}{24B_{\text{e}}^3}\right) \tag{37}$$

$$D_{\text{e}} = \frac{4B_{\text{e}}^3}{\omega_{\text{e}}^2} \tag{38}$$

The comparatively simple formula (equation (32)) for the rotation–vibration energy levels of a Morse oscillator suggests a generalization in terms of simple power series expansions as a function of v and J. Before addressing such equations, we show the effect of the centrifugal potential for a typical example (Figure 6). For low J, there is little change in the effective potential, very different from the hydrogen atom. For $J = 1$ and 2, the effects would not be visible in the figure. Large effects arise only for $J > 100$, which is a further reason to look for another simple treatment of the rotation–vibration problem.

Here, it is necessary to make a remark on the calculation of the effective reduced masses μ in these equations. In the practical analysis of spectra, the most commonly used assumption is to introduce the *atomic* masses m_i in equation (2), i.e., including the masses of the electrons in the atoms with the masses m_i. It is, however, by no means obvious that this is the best choice. In calculating effective rotational energies following equation (27), one would assume that the moment of inertia indeed includes the masses of the electrons which are, however, not incorporated at the position of the two nuclei separated by R.

A better assumption would be to compute the moments of inertia by means of the actual probability distributions of the electrons arising from the ground-state electronic wavefunction. Nevertheless, in the first approximation, the use of atomic masses might be plausible for the calculation of the effective rotational reduced mass μ_{r} to be used in equation (27). On the other hand, for the purely vibrational problem, the most logical interpretation in the framework of the straight Born–Oppenheimer (BO) approximation would be a motion of the bare nuclei in the effective potential field generated by the electronic motion (*see* Bauder 2011: **Fundamentals of Rotational Spectroscopy**, this handbook). In principle, for very simple molecules such as H_2^+ or H_2 one could treat the quantum mechanical problem directly as a three or four particle system, without need for the BO approximation.

However, particularly for the heavier atoms, it seems physically obvious that the inner shell electrons are so tightly bound to the nuclei that they effectively move with the nuclei and thus contribute to the effective vibrational reduced masses μ_{v}. One might, thus, include some useful fraction of the total number of electrons of the "atoms" with masses "m_i" in the calculation of the reduced masses μ_{v} in equation (2). The situation is by no means trivial and is related to replacing the true many-body Hamiltonian by an effective few-body Hamiltonian (two-body Hamiltonian for diatomic molecules). The uncertainties in these masses are thus directly linked to the Born-Oppenheimer or other related effective Hamiltonian approximations. There has been some debate on which is the "best" choice for effective reduced masses μ_{v} and μ_{r}; for further discussion, we refer to the review by Tennyson 2011: **High Accuracy Rotation–Vibration Calculations on Small Molecules**, this handbook and the papers by Kutzelnigg (2007), Bunker and Moss (1977), Schwartz and Leroy (1987) and Coxon and Hajigeorgiou (1999). At ultrahigh precision, the mass distribution within the extended nuclei must also be taken into account.

2.2 Effective Treatment in Terms of Spectroscopic Constants

Equation (32) for the Morse oscillator lends itself to a simple interpretation. The purely v-dependent terms are the results of the anharmonic vibrational motion alone. Neglecting the small centrifugal distortion term $D_{\text{v}}J^2(J+1)^2$, the rotational term $B_{\text{v}}J(J+1)$ corresponds

to the rigid rotor energy levels, with an effective rotational constant B_v.

Separating the fast vibrational motion from the rotational motion in a Born–Oppenheimer-like adiabatic manner, B_v is interpreted as the expectation value of the rotational constant over the vibrational wavefunction:

$$B_v \simeq \left\langle \Psi_v \left| \frac{h}{8\pi^2 c\mu R^2} \right| \Psi_v \right\rangle \tag{39}$$

It is furthermore common to allow for a representation of energy levels by simply extending the power series of equation (32) to higher powers by adding further empirically adjustable constants (Huber and Herzberg 1979). Thus, one can write the vibrational term values as

$$\frac{E_v}{hc} = G(v) = \omega_e \left(v + \frac{1}{2}\right) - \omega_e x_e \left(v + \frac{1}{2}\right)^2 + \omega_e y_e \left(v + \frac{1}{2}\right)^3 + \omega_e z_e \left(v + \frac{1}{2}\right)^4 + \cdots \tag{40}$$

and add to this the rotational term values defined by

$$\frac{E_{J(v)}}{hc} = F_v(J) = B_v J(J+1) - D_v J^2(J+1)^2 + H_v J^3(J+1)^3 + \cdots \tag{41}$$

to give the total rotational–vibrational energy

$$\frac{E_{v,J}}{hc} = G(v) + F_v(J) \tag{42}$$

Furthermore, one uses the expansions

$$B_v = B_e - \alpha_e \left(v + \frac{1}{2}\right) + \gamma_e \left(v + \frac{1}{2}\right)^2 + \cdots \tag{43}$$

$$D_v = D_e + \beta_e \left(v + \frac{1}{2}\right) + \delta_e \left(v + \frac{1}{2}\right)^2 + \cdots \tag{44}$$

One notes the slight inconsistencies in the sign convention: to have commonly positive $\omega_e x_e$, α_e, and D_e, the corresponding terms in the power series are defined with a negative sign, whereas all further terms have a positive sign.

These equations are used in the least squares adjustment of the corresponding "effective spectroscopic constants" (ω_e, $\omega_e x_e$, B_e, α_e, D_e, β_e, etc.) to the measured transition frequencies (Albritton *et al.* 1976). One should not overinterpret the physical significance of such parameters, but they can be considered as resulting from the diagonalization of an effective Hamiltonian matrix to appropriate order to obtain its diagonal (eigenvalue) form.

A slightly different development was proposed by Dunham (1932):

$$\frac{E_{v,J}}{hc} = \sum_j \sum_k y_{jk} \left(v + \frac{1}{2}\right)^j [J(J+1)]^k \tag{45}$$

One can use the following relations (Herzberg 1950, Demtröder 2003)

$$y_{10} \simeq \omega_e \tag{46}$$

$$y_{20} \simeq -\omega_e x_e \tag{47}$$

$$y_{30} \simeq \omega_e y_e \tag{48}$$

$$y_{01} \simeq B_e \tag{49}$$

$$y_{02} \simeq -D_e \tag{50}$$

$$y_{11} \simeq -\alpha_e \tag{51}$$

$$y_{12} \simeq -\beta_e \tag{52}$$

$$y_{21} \simeq \gamma_e \tag{53}$$

$$y_{00} \simeq \frac{B_e - \omega_e x_e}{4} + \frac{\alpha_e \omega_e}{12 B_e} + \frac{\alpha_e^2 \omega_e^2}{144 B_e^2} \tag{54}$$

For the Morse potential, only y_{10}, y_{20}, y_{01}, y_{02}, y_{11}, and y_{12} are different from zero and one can establish exact relationships to the more conventional spectroscopic parameters. However, in general, equations (46)–(54) are approximate.

Also, in a real molecule, one might absorb some effects from higher terms in the lower terms by setting all terms after some point in the expansion to zero. These facts have to be observed when comparing results arising from different fits to experimental data in the literature.

2.3 Symmetry, Nuclear Spin, and Statistics in Homonuclear Diatomic Molecules

Other important effects in the energy level structures arise for homonuclear diatomic molecules from symmetry, nuclear spin, and statistics. The generalized Pauli principle is one of the fundamental laws of atomic and molecular science, going beyond the mere laws of quantum mechanics (*see* Quack 2011: **Fundamental Symmetries and Symmetry Violations from High-resolution Spectroscopy**, this handbook). The consequences of the Pauli principle on the electronic structure due to the indistinguishability of electrons are discussed in an article by Wörner and Merkt 2011: **Fundamentals of Electronic Spectroscopy**, this handbook. There are, however, further important consequences on rotation–vibration spectra arising from the identity of nuclei. Indeed, we know that the solution of the Schrödinger equation in the Born–Oppenheimer approximation may generally be written as

$$\Psi_{\text{tot}}(r_e, R_n \ldots) = \Psi_e(r_e, R_n \ldots)\Psi_v^{(e)}(R_n) \cdot \Psi_r^{(ev)}(\vartheta, \varphi, \chi)\Psi_{ns}^{(evr)}(\sigma) \quad (55)$$

$$E_{\text{tot}} = E_e + E_v^{(e)} + E_r^{(ev)} + E_{ns}^{(evr)} \quad (56)$$

Here, the upper indices indicate the implicit dependence upon electronic (e), vibrational (v), and rotational (r) states by computing the appropriate expectation values in the given state. For the diatomic molecule, we obviously have $R_n = R$.

The wavefunction of equation (55) is a solution of the Schrödinger equation within appropriate approximations, but it is still incomplete because it does not satisfy the symmetry requirements imposed by the generalized Pauli principle. A proper Ψ_{tot} must be antisymmetric with respect to the permutation of two fermions (particles with half odd integer spin) and symmetric with respect to the permutation of two bosons (particles with integer spin). We shall assume that electrons have been dealt with by an appropriate electronic structure treatment for the electronic ground state (*see* Wörner and Merkt 2011: **Fundamentals of Electronic Spectroscopy**, this handbook), resulting in allowed electronic ground-state terms. We now consider the effect on rotational–vibrational structure arising from identical nuclei.

We start with the simple and historically important case of H_2 (*see also* Quack 2011: **Fundamental Symmetries and Symmetry Violations from High-resolution Spectroscopy**, this handbook). The ground-state electronic term is $^1\Sigma_g^+$, the electronic wavefunction, thereby satisfying the Pauli principle for electrons. This totally symmetric term in the point group $D_{\infty h}$ is also symmetrical upon the permutation of the two protons in H_2. The vibrational wavefunction $\Psi_v^{(e)}(R)$ or $\Phi_{v,J}(R)$ depends on the magnitude of separation R of the two nuclei and, thus, is also symmetric with respect to a permutation of the coordinates of the two protons. For a diatomic molecule, the rotational wavefunction $\Psi_r^{(ev)}(\vartheta, \varphi, \chi)$ reduces to the spherical harmonics Y_{J,M_J} (equation (26)). These are symmetric under permutation of the coordinates of the two nuclei for even J and antisymmetric for odd J as can be seen by the inspection of the spherical harmonics. We discuss next the symmetry of the nuclear spin functions $\Psi_{ns}^{(evr)}(\sigma)$. Each proton may exist in two spin states, depending on the magnetic quantum number m_p for the projection of the proton spin on the z-axis, which we define as

$$\psi_{\text{spin, p}_{1,2}}(m_p = +1/2) \equiv \alpha(j = 1, 2) \quad (57)$$

$$\psi_{\text{spin, p}_{1,2}}(m_p = -1/2) \equiv \beta(j = 1, 2) \quad (58)$$

Depending on whether we consider the first or the second proton ($j = 1, 2$), we write $\alpha(1)$, $\alpha(2)$, or $\beta(1)$, $\beta(2)$. The total spin wavefunction can be written as a product of the individual wavefunctions, at least as far as its symmetry properties are concerned, which results in a total of four possibilities with appropriate symmetry with respect to permutation of the indices 1 and 2 and satisfying the triangle condition for the total nuclear spin I

$$|I_1 - I_2| \leq I \leq I_1 + I_2 \quad (59)$$

1. The three normalized symmetrical functions have total nuclear spin $I = 1$:

$$\varphi_{s_1} = \frac{1}{\sqrt{2}}[\alpha(1)\beta(2) + \alpha(2)\beta(1)] \quad \text{with} \quad M_I = 0 \quad (60)$$

$$\varphi_{s_2} = \alpha(1)\alpha(2) \quad \text{with} \quad M_I = 1 \quad (61)$$

$$\varphi_{s_3} = \beta(1)\beta(2) \quad \text{with} \quad M_I = -1 \quad (62)$$

2. The one antisymmetrical wavefunction has $I = 0$ (and $M_I = 0$):

$$\varphi_a = \frac{1}{\sqrt{2}}[\alpha(1)\beta(2) - \alpha(2)\beta(1)] \quad (63)$$

Because of the generalized Pauli principle, the total wavefunction Ψ_{tot} must be antisymmetric with respect to the permutation (12) of the indices of the two protons; thus,

$$(12)\Psi_{\text{tot}} = -\Psi_{\text{tot}} \quad (64)$$

Considering the properties of the product wavefunction (equation (55)), one can thus either combine symmetric rotational functions with even J with the antisymmetric nuclear spin function (equation (63)) or else combine the antisymmetric rotational wavefunctions with odd J with the three symmetric nuclear spin functions with an extra degeneracy due to $M_I = 0, \pm 1$, giving an extra nuclear spin statistical weight 3 for all odd J (in addition to the $(2J + 1)$ degeneracy resulting from M_J). These two sets of states of hydrogen do not interconvert easily because of the dynamical principle of approximate nuclear spin symmetry conservation (*see* Quack 2011: **Fundamental Symmetries and Symmetry Violations from High-resolution Spectroscopy**, this handbook). They behave like different isomers of hydrogen H_2 (called *nuclear spin isomers*), which can be separated and can be stable for months at room temperature in the absence of catalysts for interconversion.

The more abundant nuclear spin isomer with the higher nuclear spin statistical weight 3 (and odd J for H_2) is called *ortho*-hydrogen, while the less abundant nuclear spin isomer with nuclear spin statistical weight 1 (and even J for H_2) is called *para*-hydrogen. In ordinary hydrogen gas, the two forms coexist as a mixture. Because of the extra nuclear

spin statistical weights (3 and 1), in samples at thermal equilibrium with many J populated, there will be an intensity alternation (3 : 1) in spectral lines associated with odd or even J in the ground state of the relevant transition (for instance, in the rotation–vibration Raman spectrum of H_2; *see* Weber 2011: **High-resolution Raman Spectroscopy of Gases**, this handbook). Similar effects arise for all homonuclear diatomic molecules with nuclei of spin 1/2 (for instance, $^{15}N_2$). For nuclear spins $I_i > 1/2$, one can readily show, by inspection of the functions generated following the triangle condition (equation (59)), that the total number of symmetrical nuclear spin functions is

$$N_s = \frac{(2I_i + 1)^2 + 2I_i + 1}{2} \tag{65}$$

and the total number of antisymmetrical functions is

$$N_a = \frac{(2I_i + 1)^2 - 2I_i - 1}{2} \tag{66}$$

Obviously, with $I_i > 1/2$, one has more than two possible values of I in equation (59). The deuterium nucleus, for instance, has $I_D = 1$ and thus $I = 0, 1, 2$ with $N_s = 6$ and $N_a = 3$, in the case of D_2.

Because the deuteron is a boson, the total wavefunction Ψ_{tot} must be symmetrical; thus, even J (for the electronic ground state $^1\Sigma_g^+$) combine with the six symmetrical nuclear spin wavefunctions and are called *ortho*-deuterium (because of the higher abundance, see above) and odd J combine with the three antisymmetrical wavefunctions (*para*-deuterium).

Several further considerations are now in order. Equation (55) is an approximation, and, in particular, nuclear spin–rotation interactions can couple states of different nuclear spin as non-Born–Oppenheimer interactions can couple different electronic states. Nevertheless, it is possible to obtain the proper symmetry relations from the approximation (equation (55)), as can be seen from the exact wavefunction, which in general will be a sum of infinitely many terms of the form of equation (55):

$$\Psi_{tot,exact} = \sum_j c_j \Psi_{tot}^j(r_e, R_n, \ldots) \tag{67}$$

Our discussion following equation (55) concerned only the dominant leading term with the largest $|c_j|$ in equation (67). However, all further terms Ψ_{tot}^j must satisfy the generalized Pauli principle in the same way as the leading term, even though they may mix individual terms in the products (vibronic mixing, nuclear spin rotation mixing, etc.). It is thus sufficient to consider only the leading term, if one is only interested in the symmetry properties. Mixing may, however, decrease degeneracies (nuclear spin degeneracy will be lifted slightly for instance) and more generally lead to further deviations from the expression for E_{tot} in equation (56).

A second consideration concerns the symmetry properties of electronic terms under permutation of identical nuclei. We illustrate this with the example of the $O_2(^3\Sigma_g^-)$ ground state, which has led to some confusion not only in the textbook literature (for instance, Demtröder 2003, but also in a number of other cases). This is because of the understanding of the symmetry property of the electronic term $^3\Sigma_g^-$ (in $D_{\infty h}$) as related to the symmetry under the permutation (12) of the two nuclei. It is, thus, necessary to consider the permutation of the two nuclei arising from a sequence of point group operations as follows:

1. Rotate the molecule by 180°.
2. Invert the electrons back through the center of symmetry.
3. Reflect the electrons at the plane containing the molecular symmetry axis 1–2 perpendicular to the axis of rotation involved in operation 1.

Operation 1 changes the sign of the rotational wavefunction for odd rotational angular momentum quantum numbers J as discussed above, or N, in conventional notation, if J contains an electronic spin contribution (as in the triplet ground state of $O_2(^3\Sigma_g^-)$, $|N - S| \leq J \leq N + S$ with total electronic spin $S = 1$ for a triplet). Operation 2 changes the sign of the electronic wavefunction for *ungerade* terms (Σ_u, Π_u, Δ_u, . . .). For *gerade* terms such as Σ_g, the sign remains unchanged. Operation 3 changes the sign of the electronic wavefunction for X^- terms (here Σ^-). For degenerate electronic terms Π, Δ, . . . the twofold degeneracy with $\Lambda = \pm|\Lambda|$ is slightly lifted by molecular rotation (Λ-doubling, see below and *see also* Wörner and Merkt 2011: **Fundamentals of Electronic Spectroscopy**, this handbook) containing a symmetric and an antisymmetric function under this reflection. The total wavefunction must, thus, be symmetric including the sequence of the three operations above for bosons, and antisymmetric for fermions.

Applying this to $^{16}O_2(^3\Sigma_g^-)$, one thus finds that the electronic term is antisymmetric with respect to the permutation of the nuclei. The total wavefunction must be symmetric, because the ^{16}O nucleus with nuclear spin $I = 0$ is a boson. Thus, only odd rotational angular momenta $N = 1, 3, 5$ result in allowed states for $O_2(^3\Sigma_g^-)$ (with nuclear spin statistical weight 1). The same is true for $^{18}O_2$ with the boson ^{18}O having $I = 0$. Thus, these molecules have a "zero point rotation", which affects the dissociation energy $\Delta_{diss}H_0^0$ of $^{16}O_2$ and $^{18}O_2$, but not of $^{16}O^{18}O$, which has all rotational angular momenta allowed ($N = 0, 1, 2, \ldots$), because there are no symmetry restrictions.

For ^{17}O, one has $I = 5/2$ and thus this nucleus is a fermion. The total wavefunction Ψ_{tot} must be antisymmetric. Therefore, the antisymmetric $^3\Sigma_g^-$ electronic ground state can combine with antisymmetric (odd N) rotational wavefunctions and antisymmetric nuclear spin wavefunctions ($N_a = 15$ from equation (66), *para*-$^{17}O_2$) or with symmetric (even N) rotational wavefunctions and symmetric nuclear spin wavefunctions ($N_s = 21$ according to equation (65), *ortho*-$^{17}O_2$). Figure 19 in the article by Wörner and Merkt 2011: **Fundamentals of Electronic Spectroscopy**, this handbook, gives a summary of the symmetry properties of a number of electronic terms of diatomic molecules. We have introduced these basis concepts of symmetry, nuclear spin, and statistics for the simplest case of diatomic molecules. The general concept is of relevance for more complex symmetric molecules with identical nuclei, in which the use of group theory becomes necessary (*see* Oka 2011: **Orders of Magnitude and Symmetry in Molecular Spectroscopy** and Quack 2011: **Fundamental Symmetries and Symmetry Violations from High-resolution Spectroscopy**, this handbook). The intensity alternations resulting from nuclear spin statistical weights in spectral line patterns are among the more powerful "practical" instruments in the symmetry assignment of molecular states. Good examples of diatomic molecule spectra with intensity alternations are given in Weber 2011: **High-resolution Raman Spectroscopy of Gases**, this handbook. For spectra of polyatomic molecules, *see* Albert *et al.* 2011: **High-resolution Fourier Transform Infrared Spectroscopy**, this handbook.

Apart from the practical importance in the assignment of high-resolution spectra, the role of nuclear spin, symmetry, and statistics has been of fundamental importance for the understanding of nuclear structure in a historical context. Before the discovery of the neutron, one hypothesis of nuclear structure assumed that the heavier nuclei contained electrons, bound to protons within the nucleus by a special force, in order to neutralize part of the proton charges. In this case, the deuteron would consist of two protons and an electron tightly bound together. Such a "deuteron" would have half odd integer spin and be a fermion, leading to a quite different nuclear spin statistics than observed in reality. The historical example was actually $^{14}N_2$, where the real ^{14}N nucleus is a boson of spin 1 (similar to the deuteron), whereas the hypothetical "electron binding" $^{14}_{7}N$ would consist of seven electrons and 14 protons, resulting again in a "fermion ^{14}N" with half-odd integer spin. The intensity alternation actually observed in the Raman spectra of $^{14}N_2$ demonstrated the boson (spin 1) nature of ^{14}N (resulting from seven protons and seven neutrons), thus excluding the "electron binding" model of the nucleus. Early high-resolution spectroscopy thus helped to shape nuclear theory and anticipated the neutron as a component of the nucleus. Intensity alternation in spectra was discovered by Mecke (1925) and discussed by Hund (1927) (*see also* Rasetti 1930, Heitler and Herzberg 1929). Some of the interesting history is covered by Herzberg (1939, 1950) (*see also* Quack 2011: **Fundamental Symmetries and Symmetry Violations from High-resolution Spectroscopy**, this handbook).

The fact that the neutron (free or bound in the nucleus) cannot be an electron bound to a proton is also clear from the spin and statistical properties: the neutron has spin 1/2 and is a fermion, whereas the electron binding proton would be a boson with spin 0 or 1. Thus, the radioactive β^- decay also

$$n \rightarrow p^+ + e^- \quad \text{(incomplete)} \tag{68}$$

cannot be complete, because of the statistics and spin, and now we know that the symmetry properties are saved by the electron antineutrino, a fermion of spin 1/2

$$n \rightarrow p^+ + e^- + \overline{\nu}_e \quad \text{(correct)} \tag{69}$$

Thus, while the neutrino was postulated historically by Pauli in order to preserve the symmetry law of energy conservation in β-decay, a second route to this hypothesis would be spin and statistics (*see also* Quack 2011: **Fundamental Symmetries and Symmetry Violations from High-resolution Spectroscopy**, this handbook).

A note is also relevant concerning the nature of nuclear "spin": this property would better be called nuclear angular momentum, because in general it contains contributions from orbital angular momentum in current nuclear models. This fact is actually also important for nuclear parity and quadrupole moments. Table 1 lists a small selection of properties of particularly important nuclei in molecular spectroscopy; a more detailed table is given by Hippler *et al.* 2011: **Mass and Isotope-selective Infrared Spectroscopy**, this handbook and Cohen *et al.* (2007). This table is instructive because it shows the apparent complexity of the patterns of nuclear angular momenta and parities given by I^{Π} as understood on the basis of the relatively simple nuclear shell model of Goeppert–Mayer and Jensen including orbital angular momenta. Some simple (and obvious) rules include the absence of nuclear spin for gg nuclei (*gerade–gerade* for even numbers of protons and even numbers of neutrons). Nuclei with $I \geq 1$ have quadrupole moments, leading, in general, to more easily visible hyperfine structure in rotation–vibration spectra. Magnetic moments m_N are of obvious relevance for magnetic resonance spectroscopy (Ernst *et al.* 1987). We note that the masses m given in Table 1 are atomic masses (including the electron masses). Table 2 gives for further illustration some ground state properties of

Table 1 Ground-state properties of some selected light nuclei: charge number Z, element symbol, mass number A, atomic mass m, natural abundance as mole fraction x in terms of percent, nuclear "spin" I and parity Π, magnetic moment m_N (in units of the Bohr magneton μ_N), and quadrupole moment Q.

Z	Symbol	A	m/Da	$100x$	I^Π	m_N/μ_N	Q/fm^2
1	H	1	1.007825032	99.9885	$(1/2)^+$	+2.7928473	0
	D	2	2.014101777	0.0115	1^+	+0.8574382	+0.286
5	B	10	10.012937	19.9	3^+	+1.800644	+8.47
		11	11.009305	80.1	$(3/2)^-$	+2.688648	+4.07
6	C	12	12.0 (defined)	98.93	0^+	0	0
		13	13.003354837	1.07	$(1/2)^-$	+0.702411	0
		14	14.003241989	–	0^+	0	0
7	N	14	14.003074004	99.636	1^+	+0.403761	+2.001
		15	15.000108898	0.364	$(1/2)^-$	−0.2831888	0
8	O	16	15.994914619	99.757	0^+	0	0
		17	16.99913170	0.038	$(5/2)^+$	−1.89379	−2.578
		18	17.999161	0.205	0^+	0	0
9	F	19	18.9984032	100	$(1/2)^+$	+2.628868	0

Table 2 Ground-state properties of some molecules: electronic ground-state term symbol $^{2S+1}\Gamma_x$, the ground-state N value, angular momentum quantum number J, total nuclear spin I, and total angular momentum F with total parity Π in the ground state.

Molecule	$^{2S+1}\Gamma_x$	N	J	I	F^Π
H_2	$^1\Sigma_g^+$	0	0	0	0^+
$^{12}C^{16}O$	$^1\Sigma^+$	0	0	0	0^+
$^{13}C^{16}O$	$^1\Sigma^+$	0	0	1/2	$(1/2)^-$
$^{14}C^{16}O$	$^1\Sigma^+$	0	0	0	0^+
$^{12}C^{17}O$	$^1\Sigma^+$	0	0	5/2	$(5/2)^+$
$^{15}N_2$	$^1\Sigma_g^+$	0	0	0	0^+
$^{14}N^{15}N$	$^1\Sigma^+$	0	0	1/2	$(1/2)^-$
		0	0	3/2	$(3/2)^-$
$^{16}O_2$	$^3\Sigma_g^-$	1	0	0	0^+
			1	0	1^+
			2	0	2^+
$^{19}F_2$	$^1\Sigma_g^+$	0	0	0	0^+

molecules, the complete ground state having well defined "particle properties" (including nuclear parity) and might be considered similar to a fundamental particle of some relevance for applications in fundamental physics (*see* Quack 2011: **Fundamental Symmetries and Symmetry Violations from High-resolution Spectroscopy**, this handbook).

The total angular momentum quantum number $|I - J| \leq F \leq I + J$ arises from the combination of the J (= N if $S = 0$) and nuclear spin (I) angular momentum.

2.4 Radiative Transitions and Spectra of Diatomic Molecules

The rotation–vibration spectra of heteronuclear diatomic molecules are readily observed by IR absorption and emission and the spectra of homonuclear diatomic molecules are observable by Raman spectroscopy (*see* Merkt and Quack 2011: **Molecular Quantum Mechanics and Molecular Spectra, Molecular Symmetry, and Interaction of Matter with Radiation**, this handbook). To discuss the structure of actually observed line spectra, we have to address the consequences of selection rules and relative and absolute intensities of the lines. For electric dipole transitions, the integrated line strength G_{fi} (or integrated absorption cross section) is proportional to the absolute square of the matrix element of the electric dipole operator:

$$G_{fi} = \frac{8\pi^3}{3hc_0(4\pi\epsilon_0)} |M_{fi}|^2 \tag{70}$$

with G_{fi} being given by the appropriate integration over the molecular absorption cross section:

$$G_{fi} = \int_{line} \sigma_{fi}(\tilde{\nu})\tilde{\nu}^{-1} d\tilde{\nu} \tag{71}$$

and

$$|M_{fi}|^2 = \sum_\rho \left|\langle f | \mu_\rho | i \rangle\right|^2 \tag{72}$$

where the sum is extended over the space-fixed Cartesian coordinates with the components μ_ρ of the electric dipole operator ($\rho = x, y, z$)

$$\boldsymbol{\mu} = \sum_\rho \mu_\rho \boldsymbol{e}_\rho = \sum_i \boldsymbol{r}_i q_i \tag{73}$$

q_i are the charges of the quasi-point particles in the molecule (electrons and nuclei), $\boldsymbol{r}_i$ the corresponding position vectors, and $\boldsymbol{e}_x$, $\boldsymbol{e}_y$, and $\boldsymbol{e}_z$ the unit vectors. Analysis of

the rotational wavefunctions (*see* Merkt and Quack 2011: **Molecular Quantum Mechanics and Molecular Spectra, Molecular Symmetry, and Interaction of Matter with Radiation**, this handbook) results in the angular momentum selection rule for an allowed rotational–vibrational transition in a diatomic molecule in a $^1\Sigma$ state such as CO

$$\Delta J = \pm 1 \tag{74}$$

The group of lines corresponding to $\Delta J = +1$ is called the R-branch with (initially) increasing wavenumber and the group of lines with $\Delta J = -1$ the P-branch, with (initially) decreasing wavenumber. Figure 7 shows a CO spectrum with assignment of the observed transitions given as P(J'') and R(J''), where J'' is the angular momentum quantum number of the lower level, as illustrated by the level scheme of Figure 8.

The figures also clearly illustrate how energy intervals in the vibrational ground state can be obtained by "ground-state combination differences" (GSCDs), i.e., differences of spectral line frequencies. For example, the difference $\tilde{\nu}$[R(0)] − $\tilde{\nu}$[P(2)] corresponds to $[E(J'' = 2) - E(J'' = 0)]/(hc)$ in the vibrational ground state. Thus, IR rotation–vibration spectroscopy at high resolution provides an alternative to pure rotational (MW of far IR) spectroscopy for determining rotational energies in the vibrational ground state. Similarly, excited state rotational energies can be isolated by appropriate combination differences, for example, $\tilde{\nu}$[R(1)] − $\tilde{\nu}$[P(1)] in Figure 8.

To obtain exact absolute transition intensities for rotation–vibration transitions, one has to evaluate the integral in equation (72) using the exact wavefunction from equation (26), where $\Phi_{\mathrm{v},J}(R)$ is in general not simple. However, because it depends upon R, we have to consider the R-dependent dipole moment function $\mu(R)$. The qualitative behavior and even the semiquantitative behavior of

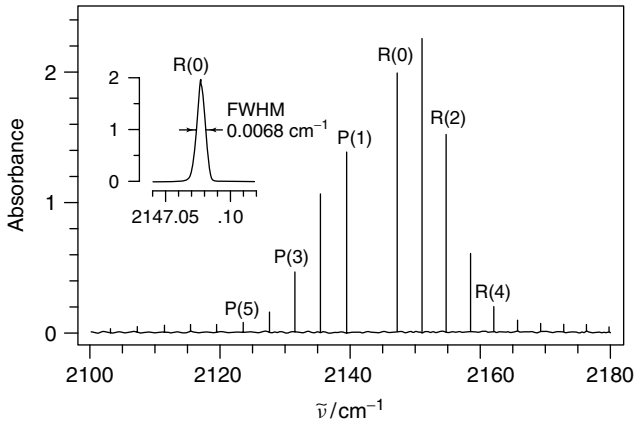

Figure 7 CO spectrum measured at low temperature ($T \approx 13$ K) in a supersonic jet. [Reproduced with permission from Amrein *et al*. (1988b).]

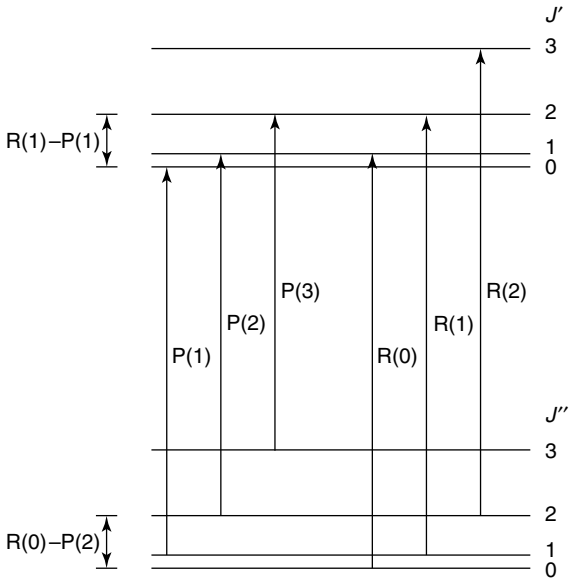

Figure 8 Rotational levels in the lower vibrational state (referred to as J'') and in the upper vibrational state (referred to as J'). Some transitions of the P- and R-branch as well as combination differences are also indicated.

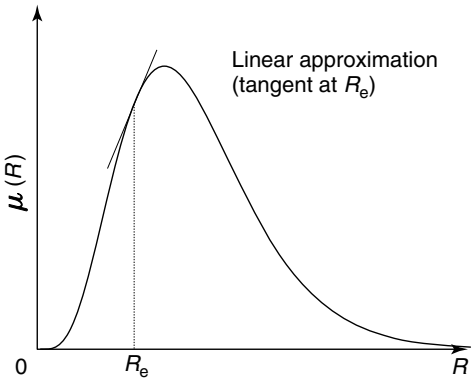

Figure 9 Dipole moment $\mu(R)$ of a diatomic molecule as a function of the distance between the nuclei R.

these electric dipole functions are often well described by a function proposed by Mecke (1950) and shown graphically in Figure 9:

$$\mu(R) = bR^n \exp(-\alpha R) \tag{75}$$

where b, n, and α are adjustable parameters to describe the behavior of $\mu(R)$. It is obvious that homonuclear diatomic molecules do not show electric dipole pure rotation–vibration spectra, because $\mu(R)$ vanishes for symmetry reasons at all values of R.

To derive some further simple approximate rules, one sometimes considers pure vibrational wavefunctions $\Psi_{\mathrm{v}} \equiv \Phi_{\mathrm{v},J=0}(R)$ as an approximation for the vibrational part of the wavefunction, also for higher J, and one describes the

dipole function with a Taylor series expansion:

$$\mu(R) = \mu(R_e) + \left(\frac{\partial \mu}{\partial R}\right)_{R_e} (R - R_e) + \frac{1}{2}\left(\frac{\partial^2 \mu}{\partial R^2}\right)_{R_e} (R - R_e)^2 + \cdots \qquad (76)$$

Thus, one can define a purely vibrational transition moment

$$M_{vv'} = \mu(R_e)\langle \Psi_v | \Psi_{v'} \rangle + \left(\frac{\partial \mu}{\partial R}\right)_{R_e} \langle \Psi_v | (R - R_e) | \Psi_{v'} \rangle + \frac{1}{2}\left(\frac{\partial^2 \mu}{\partial R^2}\right)_{R_e} \langle \Psi_v | (R - R_e)^2 | \Psi_{v'} \rangle + \cdots \qquad (77)$$

The first term in equation (77) vanishes for $v \neq v'$, because of the orthogonality of the vibrational eigenfunctions. For $v = v'$, it results in the "permanent electric dipole moment" of the molecule, leading to pure rotational transitions.

For harmonic oscillator functions, one has a selection rule $\Delta v = \pm 1$ for the second term and $\Delta v = 0, \pm 2$ for the third term. This nonlinear term thus provides intensity for overtone transitions $\Delta v = 2$ even in the harmonic oscillator (one refers figuratively to "electrical anharmonicity" due to this term). On the other hand, if one has anharmonic (Morse oscillator-like) wavefunctions Ψ_v, $\Psi_{v'}$, then even the linear term in the dipole moment $(\partial \mu/\partial R)_{R_e}(R - R_e)$ leads to a nonvanishing electric dipole matrix element for $|\Delta v| > 0$. Thus, one refers to the intensity of the overtone transition being due to "mechanical anharmonicity". In general, both effects are important and for diatomic molecules, it is in fact not very difficult to carry out the integration exactly, provided that $\mu(R)$ is known. For polyatomic molecules, the situation is more complex and, therefore, many calculations of vibrational intensities are carried out for separable normal vibrations in the so-called double harmonic approximation, which assumes harmonic oscillator wavefunctions and retains only the linear term in the Taylor series expansion of the dipole moment function. Obviously, this can at best give an approximation for "fundamental" vibrational transitions (i.e., $\Delta v = 1$ from $v = 0$) as overtone transitions vanish in this approximation.

Figure 10 illustrates electric dipole functions for the rather localized CH-stretching normal vibrations in CHF_3 and $CHCl_3$ ("quasi-diatomic vibration" but including some motion of the heavy atoms). Although a linear approximation might be acceptable for CHF_3, the dipole functions of $CHCl_3$ show a maximum in $\mu(R)$ near $R_e \approx 1$ Å; thus, $(\partial \mu/\partial R)_{R_e}$ is zero or very small, which is reflected by the overtone intensity ($\Delta v = 2$) for CH-stretching in $CHCl_3$, which is larger than that for the fundamental transition ($\Delta v = 1$), because the contribution to the transition intensity from the term with $(\partial^2 \mu/\partial R^2)_{R_e}$ is larger than the contribution from the term $(\partial \mu/\partial R)_{R_e}$. Such phenomena must be considered when using quantum chemical program packages computing approximate ("double harmonic") vibrational band intensities, but they are obviously not of fundamental importance, because more accurate calculations are possible. For intensities and selection rules in Raman spectra, we refer the reader to Merkt

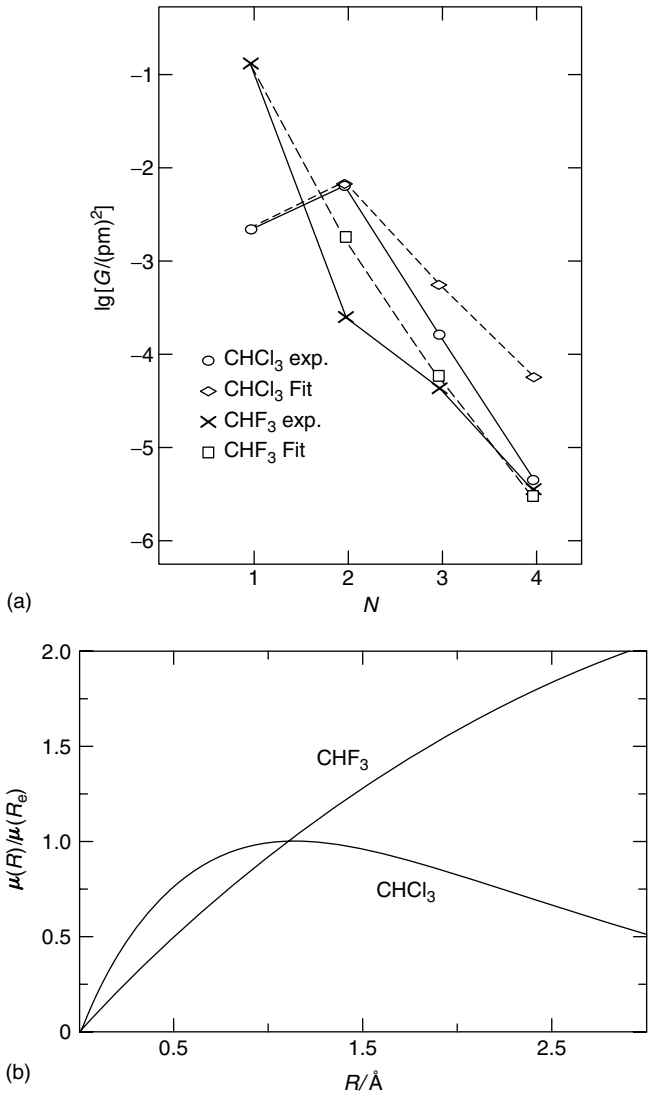

Figure 10 (a) Overtone intensities for the CH chromophore (quantum number N) $0 \rightarrow N$ transition (after Lewerenz and Quack 1986). Experimental and theoretical fit for CHF_3 ($R_m/R_e = 6.0$, i.e., $\gg 1$) and for $CHCl_3$ ($R_m/R_e = 1.05$). (b) Empirical dipole functions, approximately valid around $R_e \pm 0.3$ Å and extrapolated with the Mecke function outside this range. For CHF_3 and CDF_3 $\mu(R_e)$ would be 1.01 and 1.3 D, for $CHCl_3$ 3.8 D, and for $CDCl_3$ 1.5 D, when adjusted to the fundamental band strength with the Mecke function (note that permanent dipole moments μ_0 are for CHF_3 1.6 ± 0.1 D and for $CHCl_3$ 1.4 ± 0.5 D in qualitative agreement). See Lewerenz and Quack (1986) for precise definitions and parameters and further discussion.

and Quack 2011: **Molecular Quantum Mechanics and Molecular Spectra, Molecular Symmetry, and Interaction of Matter with Radiation** and Weber 2011: **High-resolution Raman Spectroscopy of Gases**, this handbook.

2.5 Diatomic Radicals in Degenerate Electronic Ground States

This topic is closely related to the electronic structure and spectra discussed in detail by Wörner and Merkt 2011: **Fundamentals of Electronic Spectroscopy**, this handbook. We give here just a short account of some of the most important consequences in rotation–vibration spectra observed in the IR and illustrate these with two prominent examples. For degenerate electronic ground states of diatomic radicals, one uses the following nomenclature for the electronic angular momentum quantum number Λ, which gives the absolute magnitude of the projection of the electronic angular momentum on the molecular axis $\left(\left|J_z^{\mathrm{el}}\right| = \hbar\Lambda\right)$

$$\Lambda = 0,\ 1,\ 2,\ 3,\ \ldots \tag{78}$$

$$\text{nomenclature} \quad \Sigma, \Pi, \Delta, \Phi$$

The analogy to the nomenclature S, P, D, and F for atomic terms with $L = 0, 1, 2, 3$ is readily seen, although the physical significances of L and Λ are quite different. Similarly, the spin quantum number S for the electronic term is given by the upper left exponent in the electronic term symbol:

$$^{(2S+1)}\Lambda_{\Sigma+\Lambda} \tag{79}$$

The quantum number Σ for the projection of the electron spin onto the molecular axis can take $2S + 1$ values:

$$\Sigma = -S, -S+1, -S+2, \ldots, S-1, S \tag{80}$$

For instance, in the case of the doublet ground states of the important NO and OH radicals, one has $\Lambda = 1$ and thus a $^2\Pi$ term with the two possibilities

$$^2\Pi_{1/2} \quad \text{and} \quad ^2\Pi_{3/2} \tag{81}$$

In addition to the rotational energy given by the term formulae in Section 2.2, one has the extra "electronic" term for the rotation vibration structure:

$$T_{\mathrm{e}} = T_0 + A\Lambda\Sigma \tag{82}$$

The spin–orbit coupling constant A can be positive or negative. For the NO ground state, one has $A = 123.1\ \mathrm{cm}^{-1}$; thus, $^2\Pi_{1/2}$ is lower than $^2\Pi_{3/2}$ in energy, whereas for the OH radical ground state, one has $A = -139\ \mathrm{cm}^{-1}$, and $^2\Pi_{3/2}$ is lower in energy than $^2\Pi_{1/2}$. There is a contribution to the rotational energy from the electronic angular momentum with the quantum number $\Omega = |\Sigma + \Lambda|$:

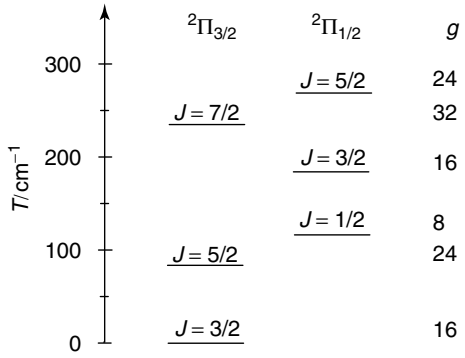

Figure 11 Level scheme for the lowest states of the OH radical.

$$T_{\mathrm{rot}}(J, \Omega) = B_{\mathrm{v}}[J(J+1) - \Omega^2] \quad \text{with} \quad J \geq \Omega \tag{83}$$

The resulting term values are thus approximately

$$T = T_{\mathrm{e}} + T_{\mathrm{rot}} = T_0 + A\Lambda\Sigma + B_{\mathrm{v}}[J(J+1) - \Omega^2] \tag{84}$$

Figure 11 shows the level scheme for OH relative to the lowest level with $J = 3/2$.

The degeneracies in these levels are partly lifted by Λ-doubling and hyperfine splittings. The two Λ components correspond to eigenfunctions of slightly different energy and angular dependence

$$\Psi_{\Lambda\pm} = \frac{1}{\sqrt{2}}\left[\exp(-\mathrm{i}\Lambda\varphi) \pm \exp(\mathrm{i}\Lambda\varphi)\right] \tag{85}$$

with φ being the angle of rotation with respect to the molecular axis. This "Λ-doubling" in OH is in the gigahertz range. Finally, hyperfine coupling of the molecular angular momentum J with nuclear spin I leads to levels with total angular momentum quantum numbers:

$$|J - I| \leq F \leq J + I \tag{86}$$

For the ground state of OH with $J = 3/2$ and $I = 1/2$ for the proton, thus one has two possibilities with $F = 1$ or 2. The corresponding level scheme is shown in Figure 12.

We have provided this discussion to give an idea of the orders of magnitude expected for high-resolution spectra. For much more detailed discussion of the corresponding spectral structures, we refer the reader to Zare (1988), Brown and Carrington (2003) and the article by Wörner and Merkt 2011: **Fundamentals of Electronic Spectroscopy**,

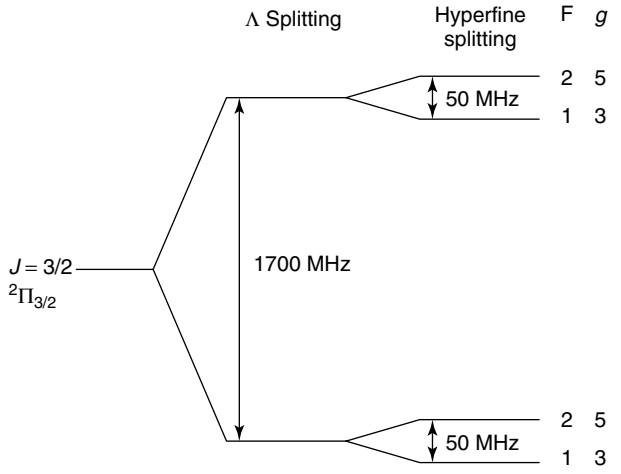

Figure 12 Level scheme for the OH radical including hyperfine splittings (schematic, not to scale).

this handbook (*see also* Western 2011: **Introduction to Modeling High-resolution Spectra**, this handbook).

In practice, one can use the following approximate term formulae:

$$T(^2\Pi_{3/2}) = \frac{\overline{A}}{2} + B_{\text{eff}+}\left[(J+1/2)^2 - \Lambda^2\right] \quad (87)$$

$$T(^2\Pi_{1/2}) = \frac{-\overline{A}}{2} + B_{\text{eff}-}\left[(J+1/2)^2 - \Lambda^2\right] \quad (88)$$

$$\overline{A} = A - 2B \quad (89)$$

$$B_{\text{eff}\pm} = B\left[\frac{1 \pm B}{\overline{A}\Lambda}\right] \quad (90)$$

If one has $\Lambda = 0$, one uses the term formulae for the sublevels of a $^2\Sigma$ state:

$$T_1(N) = BN(N+1) + \frac{\gamma N}{2} \quad \text{for} \quad J = N + \frac{1}{2} \quad (91)$$

$$T_2(N) = BN(N+1) - \frac{\gamma(N+1)}{2} \quad \text{for} \quad J = N - \frac{1}{2} \quad (92)$$

The spectroscopic constant γ is frequently very small.

For $^3\Sigma$ states, one has three sublevels for each rotational quantum number N:

$$T_1(N) = BN(N+1) - \lambda + B(2N+3) - B\left[a^2 - 2a + (2N+3)^2\right]^{1/2} + \gamma(N+1) + \frac{\gamma}{2} \quad \text{for} \quad J = N+1 \quad (93)$$

$$T_2(N) = BN(N+1) \quad \text{for} \quad J = N \quad (94)$$

$$T_3(N) = BN(N+1) - \lambda - B(2N-1) + B\left[a^2 - 2a + (2N-1)^2\right]^{1/2} - \gamma N - \frac{\gamma}{2} \quad \text{for} \quad J = N-1 \quad (95)$$

with $a = \lambda/B$. The coupling constant λ is frequently on the order of rotational constants.

If one has an electronic angular momentum $\Lambda > 0$, the selection rules for IR rotation vibration transitions are

$$\Delta J = 0, \pm 1 \quad (96)$$

where the $\Delta J = 0$ transitions correspond to a Q-branch. Figure 13 shows as an example the low-temperature vibrational spectrum of NO with one Q-branch because at the low temperature of about 17 K in a supersonic jet expansion, only the $^2\Pi_{1/2}$ ground state is populated. At higher temperatures, one finds a second Q-branch arising

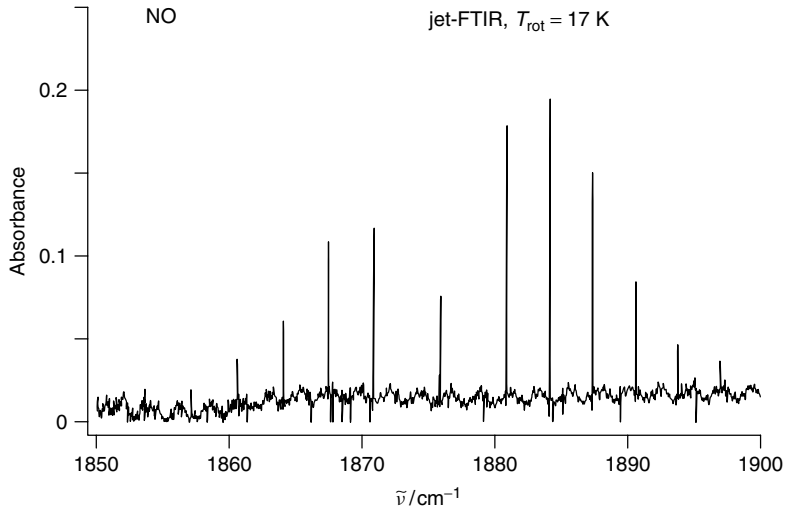

Figure 13 Spectrum of NO at low temperature (17 K) in a supersonic jet. Here, the Napierian absorbance $\ln(I_0/I)$ is shown, see also Amrein *et al*. (1988b).

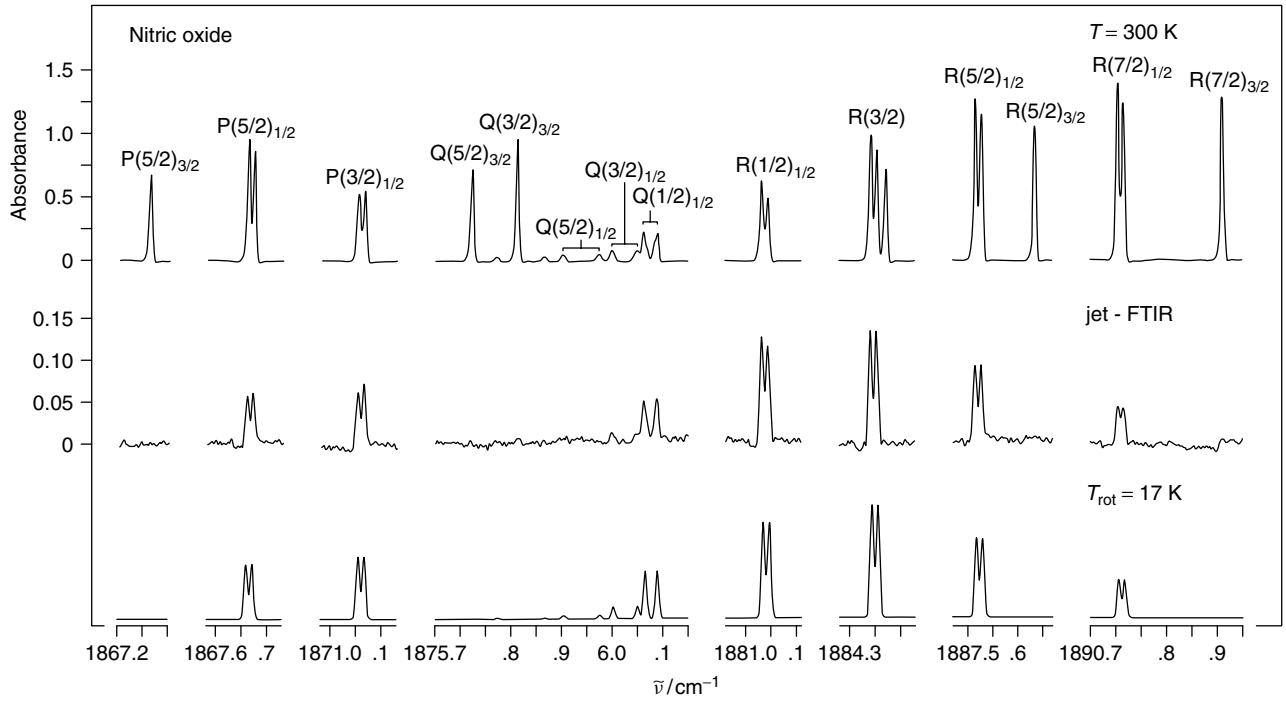

Figure 14 High-resolution (0.004 cm^{-1} FWHM) FTIR spectra of neat nitric oxide. Only small regions of the spectra containing spectral lines are displayed on an expanded scale (0.05 cm^{-1} per division). Top: spectrum recorded in a static cell at room temperature (T = 300 K). Center: jet-FTIR spectrum. (Nozzle diameter 100 μm, distance from the nozzle $z = 6$ mm, backing pressure 650 kPa, background pressure 0,6 Pa.) Note the absence of lines of the excited electronic state $^2\Pi_{3/2}$. Bottom: computed spectrum for a rotational temperature of 17 K. [Reproduced with permission from Amrein *et al.* (1988b).] The Napierian absorbance $\ln(I_0/I)$ is shown.

Table 3 Summary of the conventions for the various angular momentum quantum numbers.

Quantum number	Description
Λ	Projection of electronic angular momentum
Σ	Projection of electronic spin
$\Omega = \lvert\Lambda + \Sigma\rvert$	Projection as given by formula (sometimes $\Omega \doteq \Lambda + \Sigma$)
N	Angular momentum from rotation excluding spins
S	Electronic spin
$\lvert N - S\rvert \le J \le N + S$	Angular momentum including electronic spin
I_i	Nuclear spin of nucleus i
I	Total nuclear spin
$\lvert I - J\rvert \le F \le I + J$	Total angular momentum

from $^2\Pi_{3/2}$ and also the corresponding P- and R-branch transitions; Figure 14 shows expanded sections of the spectrum, in which the effects of Λ-doubling are visible.

Table 3 provides a brief didactic summary of the conventions for the various angular momentum quantum numbers (*see also* Stohner and Quack 2011: **Conventions, Symbols, Quantities, Units and Constants for High-resolution Molecular Spectroscopy** and Wörner and Merkt 2011: **Fundamentals of Electronic Spectroscopy**, this handbook).

2.6 The Determination of Molecular Structures from Infrared and Raman Rotation–Vibration Spectra

The article by Bauder 2011: **Fundamentals of Rotational Spectroscopy**, this handbook, has already provided an extensive discussion of the practice of determination of structure from pure rotation (MW) spectra. We complement this here with some additional aspects arising in the analysis of rotation–vibration spectra in terms of molecular structure. We use diatomic molecules for illustrating the basic concepts because of their relative simplicity. Most of the concepts can be readily transferred to the much more complex situation of polyatomic molecules.

In Section 2.4, we have already discussed the determination of the vibrational ground-state rotational level structures from GSCDs in rotation–vibration spectra. Thus, with such data, essentially all the methods discussed in Bauder 2011: **Fundamentals of Rotational Spectroscopy**, this handbook, for the analysis of pure rotational MW spectra can be applied to determine the molecular structure.

Usually, the MW data are much more precise, whereas the IR GSCDs frequently cover a much larger range of rotational levels up to very high J for the heavier polyatomic molecules. If both sets of data are available, a combined analysis using a weighted least squares adjustment is frequently in order.

The new aspect of rotation–vibration data consists in obtaining results for excited vibrational states in terms of B_v, D_v, etc. Adjustment of the appropriate constants in equations (43) and (44) to the observed spectroscopic data results, among other constants in values for the "equilibrium rotational constant B_e", is frequently possible with a precision of five to six significant digits. This can be translated into an equilibrium bond length R_e of similar accuracy by means of equation (34) provided that the uncertainty in the reduced masses μ is negligible or disregarded and that the physical significance of R_e as the position of the minimum of the potential function can be justified within the framework of an accurate effective Hamiltonian model. Both these aspects leave room for some doubt. We have already discussed uncertainties in the definitions of reduced masses in Section 2.3. The first uncertainty results from the point mass assumption for nuclei, which have extensions in the femtometer range. For typical bond lengths, in the 100 pm range (1 Å), the relative uncertainty due to this approximation is about 10^{-5}, similar to common experimental uncertainties. The relative uncertainties related to the treatment of electronic masses when calculating μ can be similarly estimated to be about 10^{-5} to about 10^{-4} (given the electron: proton mass ratio of 5×10^{-4}). An even more serious uncertainty might arise from the concept of an effective potential. Using slightly different effective ("BO-like") Hamiltonians, different definitions of these potentials lead to different minima. This effect is not easily estimated. However, different R_e obtained for different isotopomers can give an indication of the actual uncertainties. For example, for $^1H^{19}F$, one finds $R_e^H = 91.6808$ pm and for $D^{19}F$ one has $R_e^D = 91.694$ pm (Huber and Herzberg 1979). The relative difference is on the order of 10^{-4} and can be considered to arise from a combination of several of the uncertainties discussed. Thus, while it is possible to determine "apparent" R_e in a self-consistent way from spectroscopic data to within uncertainties of 10^{-5} or 10^{-6} (and even better), one should be cautious about claiming relative uncertainties of less than about 10^{-4}, when the underlying physical assumptions and significance are considered.

From another point of view, one could argue that the actual uncertainty in molecular structures (here, the bond lengths of diatomic molecules) is related to the root-mean-square deviation of distances measured in actual scattering experiments. This can be readily calculated from the ground-state probability distributions derived from the vibrational wavefunctions, and for a typical X–H bond length, one obtains relative uncertainties in the range 5–8%, for heavier molecules, thus, in the percent range. Moving beyond this, one could argue that certain parameters of these distributions can be derived more accurately (for instance, the expectation value of the distribution, or the maximum in the distribution). These will be isotope dependent, but still would be empirically well defined. One could argue that the physical sizes, say, of HF and DF are actually different, for instance, when interacting with other molecules. With very accurate data, one might expect then to get again relative uncertainties in the 10^{-4}–10^{-5} range.

However, one probably must be extremely cautious when interpreting structural data at a higher relative accuracy. While the frequencies in spectra can, of course, be measured to much higher accuracy, their interpretation in terms of structure should probably in general not claim accuracies corresponding to relative uncertainties better than 10^{-4}–10^{-5} at best, in terms of their real physical significance, regardless of which concept or definition of structure is used.

3 POLYATOMIC MOLECULES

3.1 General Aspects

The treatment of the rotation–vibration dynamics and spectra of polyatomic molecules is conceptually similar but more complex than that for diatomic molecules because of the larger number of internal degrees of freedom. Indeed, in the adiabatic or Born–Oppenheimer approximation and related approximations the potential function $V(R)$ in equation (1) now is to be replaced by a potential energy hypersurface $V(q_1, q_2, q_3, \ldots, q_{3N-6})$ depending on $3N - 6$ degrees of freedom, where N is the number of atoms or nuclei in the molecule. At present we take the q_i to be some kind of generalized coordinate (see below).

In principle, any consistent set of coordinates could be chosen to formulate the Hamiltonian for the quantum dynamics of the molecule given an appropriate effective potential energy hypersurface. A conceptually and dynamically simple choice consists of simply taking the Cartesian coordinates of the atoms (or nuclei) $x_1, y_1, z_1, \ldots, x_i, y_i, z_i \ldots, x_N, y_N, z_N$. In practice, it is, however, desirable to reduce the number of degrees of freedom by appropriate (exact) separation of the center of mass motion and approximate separation of rotational motion. Often, there are special physical aspects of the internal molecular motion that suggest the use of other special sets of coordinates, for

instance, for low-frequency internal degrees and other large amplitude motions (*see* Bauder 2011: **Fundamentals of Rotational Spectroscopy**, this handbook). There is, however, one set of coordinates that finds, by far, the widest range of applications for ordinary rigid molecules: normal coordinates make the vibrational problem separable in the limit of the harmonic (multidimensional) potential function. The vibrational Hamiltonian can be written as a sum of Hamiltonians of harmonic oscillators. We introduce here the basic concepts of the normal coordinate treatment, just in order to define the main features, nomenclature, and conventions. A fairly complete treatment from the point of view of molecular spectroscopy can be found in Wilson *et al.* (1955) and numerous other papers.

3.2 Normal Coordinates and Normal Vibrations

We start by writing the classical Hamiltonian for the motion of N atoms in Cartesian coordinates $x_1, x_2, \ldots, x_i, \ldots, x_{3N}$:

$$H = \sum_{i=1}^{3N} \frac{m_i}{2} \left(\frac{\mathrm{d}x_i}{\mathrm{d}t} \right)^2 + V(x_1, \ldots, x_{3N}) \tag{97}$$

We consider the potential function with a well-defined minimum at the equilibrium geometry of the molecule defined by x_i^{e}. It is then convenient to introduce mass-weighted displacement coordinates q_i defined by

$$q_i = \sqrt{m_i}\Delta x_i = \sqrt{m_i}(x_i - x_i^{\mathrm{e}}) \tag{98}$$

The kinetic energy remains exactly separable in these coordinates. One uses a Taylor expansion for the potential around the minimum ($x_i = x_i^{\mathrm{e}}$):

$$V = V_0 + \sum_{i=1}^{3N} \left(\frac{\partial V}{\partial q_i} \right)_0 q_i + \frac{1}{2} \sum_{i=1}^{3N} \sum_{j=1}^{3N} \left(\frac{\partial^2 V}{\partial q_i \partial q_j} \right)_0 q_i q_j + \cdots \tag{99}$$

where V_0 is a constant, which can be set to zero. The first derivatives are zero at the minimum of the potential. The second derivatives are the force constants F_{ij}. We now neglect higher terms of the expansion. The classical Hamiltonian takes the following form:

$$H = T + \frac{1}{2} \sum_{i=1}^{3N} \sum_{j=1}^{3N} F_{ij} q_i q_j \tag{100}$$

with

$$T = \frac{1}{2} \sum_{i=1}^{3N} \left(\frac{\mathrm{d}q_i}{\mathrm{d}t} \right)^2 \tag{101}$$

With this simplified classical Hamiltonian, the dynamics are separable. One can show that there is an orthogonal transformation to the set of normal coordinates Q_k (Wilson *et al.* 1955):

$$Q_k = \sum_{i=1}^{3N} L_{ik} q_i \tag{102}$$

After this orthogonal transformation with $\boldsymbol{L}^{-1} = \boldsymbol{L}^{\mathrm{T}}$, one can write the kinetic energy T as

$$T = \frac{1}{2} \sum_{i=1}^{3N} \left(\frac{\mathrm{d}Q_i}{\mathrm{d}t} \right)^2 \tag{103}$$

The potential energy V is given by

$$V = \frac{1}{2} \sum_{k=1}^{3N} \lambda_k Q_k^2 \tag{104}$$

with λ_k being functions of the force constants F_{ij}. This allows us now to write the classical Hamiltonian for every separate vibrational mode and the total vibrational Hamiltonian as a sum over all the modes:

$$H = \sum_{i=1}^{3N} H_i \left(Q_i, \frac{\mathrm{d}Q_i}{\mathrm{d}t} \right) \tag{105}$$

Translating this to quantum mechanics and solving the appropriate Schrödinger equation (*See* Merkt and Quack 2011: **Molecular Quantum Mechanics and Molecular Spectra, Molecular Symmetry, and Interaction of Matter with Radiation**, this handbook, Wilson *et al.* 1955) one obtains energy levels $E_{\mathrm{v}_1,\mathrm{v}_2,\mathrm{v}_3\ldots}$ and wave functions $\Psi_{\mathrm{v}_1,\mathrm{v}_2,\mathrm{v}_3\ldots}$:

$$E_{\mathrm{v}_1,\mathrm{v}_2,\mathrm{v}_3\ldots} = \sum_{i=1}^{3N} E_{\mathrm{v}_i} \tag{106}$$

$$\Psi_{\mathrm{v}_1,\mathrm{v}_2,\mathrm{v}_3\ldots}(Q_1, Q_2, Q_3, \ldots) = \prod_{i=1}^{3N} \Psi_{\mathrm{v}_i}(Q_i) \tag{107}$$

As in classical mechanics, one can describe the vibrational molecular motion as a superposition of $3N$ harmonic vibrations. For the quantum energy levels of the ith mode, one has

$$E_{\mathrm{v}_i} = \left(\mathrm{v}_i + \frac{1}{2} \right) h\nu_i \tag{108}$$

with

$$\nu_i = \frac{1}{2\pi}\sqrt{\lambda_i} = \frac{1}{2\pi}\sqrt{\frac{f_i}{\mu_i}} \tag{109}$$

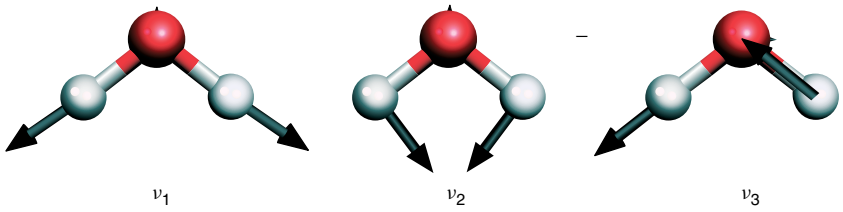

Figure 15 Graphical representation of the classical harmonic vibrations of water.

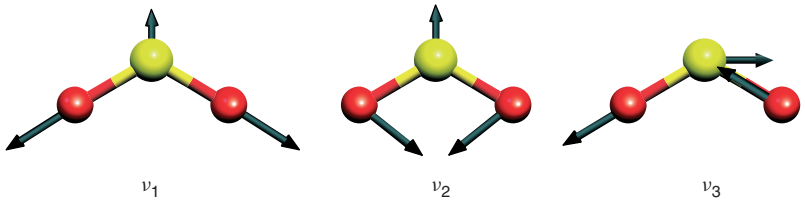

Figure 16 Graphical representation of the classical harmonic vibrations of SO_2.

where f_i are generalized force constants (depending on the F_{ij} and the masses) and μ_i are similarly generalized reduced masses. For the discussion of the modes of zero frequency (translation and rotation) as well as the mathematical treatment in terms of $\boldsymbol{F}$ and $\boldsymbol{G}$ matrix formalism, we refer to Wilson *et al.* (1955).

In general, the normal coordinates Q_i involve an in-phase motion of all the atoms in a molecule. This is usually graphically represented by arrows indicating the relative size of the displacement of the atoms in the classical vibrational motion associated with each mode.

As an example, we show in Figure 15 the graphical representation of the classical harmonic vibrations of the water molecule with nine degrees of freedom and three vibrational modes (six zero frequency modes corresponding to three translational and three rotational degrees of freedom). Because of the relatively light hydrogen atoms, all three vibrational modes involve mostly a motion of the two hydrogen atoms with the heavy oxygen atom moving only slightly. In contrast, the more even mass distribution in the SO_2 molecule leads to a substantial displacement of all three atoms in the three harmonic normal vibrations (Figure 16).

Figure 17 shows the normal vibrations of CO_2, and the fundamental transition wavenumbers are given in Table 4. This is an example of a linear molecule with two degenerate bending vibrations, leading to a vibrational angular momentum. We use here the notation ν_{2a} and ν_{2b} for the two degenerate bending vibrations. Another common notation uses the vibrational angular momentum quantum number l (v_1, v_2^l, v_3), see equation (112). A spectrum of CO_2 can be found in Albert *et al.* 2011: **High-resolution Fourier Transform Infrared Spectroscopy**, this handbook. Figure 18 shows the normal vibrations of $CHClF_2$, and the fundamental frequencies are

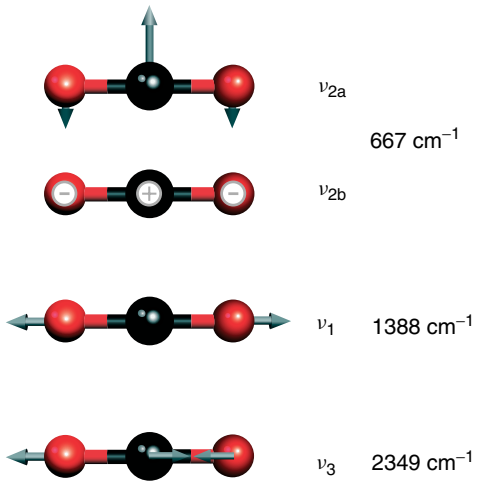

Figure 17 Graphical representation of the classical harmonic vibrations of CO_2.

Table 4 Fundamental wavenumbers of CO_2.

Mode	$\tilde{\nu}$/cm^{-1}	Description
ν_{2a}	667	Bending
ν_{2b}	667	Bending
ν_1	1388	Symmetric stretching
ν_3	2349	Asymmetric stretching

summarized in Table 5. Finally, Figure 19 shows the normal modes of CHD_2I, with three light and one very heavy substituent at the C atom. Table 6 summarizes harmonic normal vibrational frequencies as well as the fundamental transition frequencies. We discuss some additional aspects of the vibrational overtone spectra for these molecules in the following subsection. Many other examples of

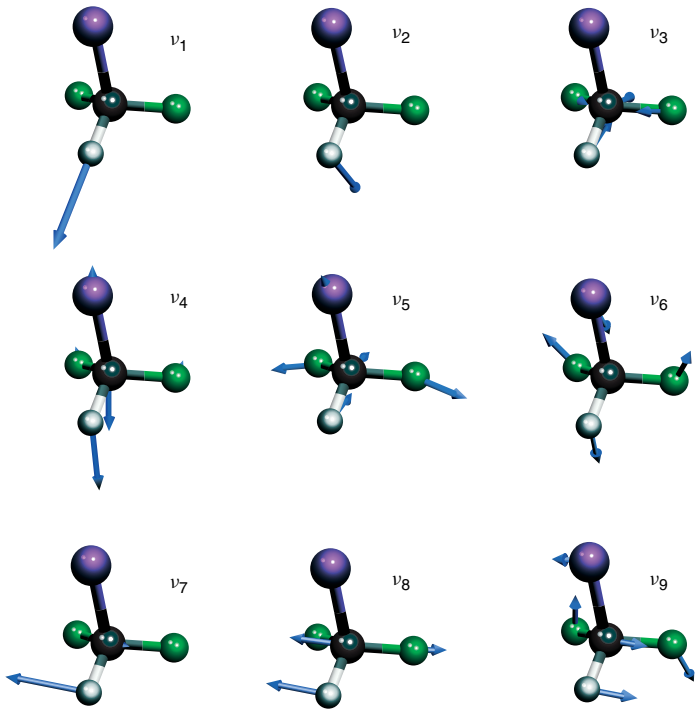

Figure 18 Graphical representation of the classical harmonic vibrations of $CHClF_2$.

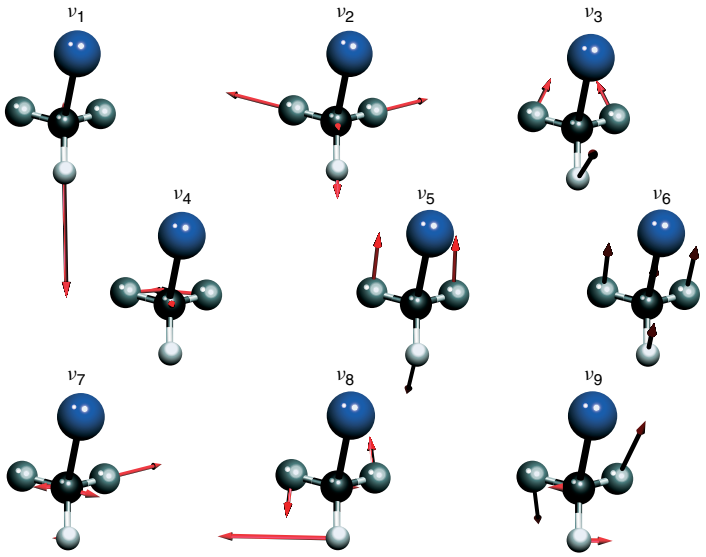

Figure 19 Graphical representation of the classical harmonic vibrations of CHD_2I.

normal vibrations and spectra can be found in various articles of this handbook (*see* Albert *et al*. 2011: **High-resolution Fourier Transform Infrared Spectroscopy**, Weber 2011: **High-resolution Raman Spectroscopy of Gases**, Herman 2011: **High-resolution Infrared Spectroscopy of Acetylene: Theoretical Background and Research Trends** and Hippler *et al*. 2011: **Mass and Isotope-selective Infrared Spectroscopy**, this handbook). Programs for normal-mode calculations are also readily available, including didactic examples (see, for instance McIntosh and Michaelian 1979a,b,c). In the separable normal-mode picture of molecular vibrations, the molecular vibrational motion is described by a collection of independent harmonic oscillators, not too different from the harmonic oscillator picture of a diatomic molecule. Each normal vibration has its own vibrational spectrum. It turns out, however, that anharmonicity is very important in reality.

Table 5 Fundamentals of $CH^{35}ClF_2$ (band centers in cm^{-1}).

Mode	$\Gamma^{(a)}$	$\tilde{\nu}_i/cm^{-1}$	References	Approximate Description
ν_1	A′	3021 63351(4)	(c)–(e)	s-(CH)
ν_2	A′	1313 09551(2)	(c),(f)	b-(CH)
ν_3	A′	1108 72738(2)	(g)–(i)	s-(CF)
		1108 72704(2)	(j)	
ν_4	A′	812 9300(45)[(b)]	(k),(l)	s-(CCl)
ν_5	A′	596 371399(5)	(m),(n)	b-(CF)
ν_6	A′	412 928543(5)	(o)–(q)	b-(CCl)
ν_7	A″	1351 70198(2)	(c),(f)	b-(CH)
ν_8	A″	1127 28175(2)	(g)–(i)	s-(CF)
		1127 28149(2)	(j)	
ν_9	A″	366 197216(5)	(o)–(q)	b-(CF)

In the given approximate assignments the following abbreviations are used: s refers to a stretching and b to a bending mode (after Albert *et al.* (2006)).
[(a)] Γ gives the vibrational symmetry species in the C_s point group.
[(b)] deperturbed value.
[(c)] Amrein *et al.* (1985).
[(d)] Amrein *et al.* (1988a).
[(e)] Fraser *et al.* (1992).
[(f)] Thompson *et al.* (2003).
[(g)] Albert *et al.* (2004b).
[(h)] Luckhaus and Quack (1989).
[(i)] Snels and D'Amico (2001).
[(j)] Thompson *et al.* (2004).
[(k)] Albert *et al.* (2006).
[(l)] Ross *et al.* (1989a).
[(m)] Klatt *et al.* (1996).
[(n)] Gambi *et al.* (1991).
[(o)] Kisiel *et al.* (1997).
[(p)] Kisiel *et al.* (1995).
[(q)] Merke *et al.* (1995).

Table 6 Harmonic ω_i and experimental $\tilde{\nu}_i$ band centers of the nine fundamental vibrational modes of CHD_2I. References of high-resolution analyses are also indicated when available.

Mode	Symmetry	Description	ω_i/cm^{-1}[(a)]	$\tilde{\nu}_i/cm^{-1}$
ν_1	A′	CH stretching	3199.4	3029.6790[(b)]
ν_2	A′	CD stretching	2280.1	2194[(c)–(e),(a)]
ν_3	A′	CH bending	1216.8	1170[(c)–(e),(a)]
ν_4	A′	CD bending	1047.7	1018[(c)–(e),(a)]
ν_5	A′	CD-bending	780.0	754.4738[(g)]
ν_6	A′	CI-stretching	543.9	508.7898[(f)]
ν_7	A″	CD-stretching	2401.7	2313[(d)–(e),(a)]
ν_8	A″	CH-bending	1332.3	1287[(d)–(e),(a)]
ν_9	A″	CI-bending	680.1	659.8692[(g)]

[(a)] Horká *et al.* (2008).
[(b)] Hodges and Butcher (1996).
[(c)] Riter and Eggers (1966).
[(d)] Duncan and Mallinson (1971).
[(e)] Santos and Orza (1986).
[(f)] Kyllönen *et al.* (2004).
[(g)] Kyllönen *et al.* (2006).

3.3 Anharmonic Resonances and Effective Hamiltonians

3.3.1 General Aspects

As discussed in Quack 2011: **Fundamental Symmetries and Symmetry Violations from High-resolution Spectroscopy**, this handbook, the normal mode approximation introduces a far too high symmetry and too many constants of the motion into the vibrational dynamics of polyatomic molecules. In reality, anharmonic terms in the potential break this high symmetry, resulting in much more complex spectra and dynamics. One can, in principle, retain a description in normal coordinates but introduce anharmonic terms in the potential (cubic, quartic, etc.) (Nielsen 1951, 1959, Wilson *et al.* 1955, Mills 1974, Califano 1976, Papoušek and Aliev 1982, Aliev and Watson 1985):

$$V(Q) = \frac{1}{2}\sum_k \lambda_k Q_k^2 + \frac{1}{6}\sum_{k,l,m} \Phi_{k,l,m} Q_k Q_l Q_m + \frac{1}{24}\sum_{k,l,m,n} \Phi_{k,l,m,n} Q_k Q_l Q_m Q_n + \cdots \quad (110)$$

This type of expansion is useful if there is a unique deep minimum on the potential hypersurface. The corresponding equilibrium geometry is taken as the reference configuration for the expansion. The normal coordinates Q_k are orthogonal, and with this choice of coordinates, the quadratic terms in the potential are diagonal, the first mixed terms being cubic as shown in equation (110). The minimum of the potential energy is taken as zero. Because the normal coordinates depend on masses, the potential constants Φ are different for different isotopomers even within the Born–Oppenheimer approximation. However, because one usually starts with a formulation of the potential in terms of a set of coordinates in which the potential is independent of the masses, such as internal coordinates, the anharmonic potential constants for each isotopomer can be derived to satisfy the conditions of the Born–Oppenheimer approximation or any other effective potential, which is independent of the atomic masses (*see* Marquardt and Quack 2011: **Global Analytical Potential Energy Surfaces for High-resolution Molecular Spectroscopy and Reaction Dynamics**, this handbook). For *ab initio* calculations of such "force fields" or potential functions, we refer to Yamaguchi and Schaefer 2011: **Analytic Derivative Methods in Molecular Electronic Structure Theory: A New Dimension to Quantum Chemistry and its Applications to Spectroscopy**, Tew *et al.* 2011: **Ab Initio Theory for Accurate Spectroscopic Constants and Molecular Properties** and Breidung and Thiel 2011: **Prediction of**

Vibrational Spectra from Ab Initio Theory, this handbook. In this article, we do not go into the details of the normal coordinate treatment including anharmonic potentials (see the extensive literature cited above) but rather restrict our discussion to the basic concepts. In a manner very similar to the case of diatomic molecules, one can now either handle the quantum mechanical problem of molecular vibrations with an exact variational (numerical) technique or can use perturbation theory, leading to simple term formulae and "effective Hamiltonians". The latter treatment is most commonly used in spectroscopy and first we discuss it briefly, with the emphasis on anharmonic resonance. We then summarize some recent developments on the relation of the relevant parameters in these two treatments. This relation has been shown to be more complex than previously anticipated with some unexpected consequences for spectra and dynamics (Lewerenz and Quack 1988, Quack 1990, Marquardt and Quack 1991, 2001, *see also* Marquardt and Quack 2011: **Global Analytical Potential Energy Surfaces for High-resolution Molecular Spectroscopy and Reaction Dynamics**, this handbook). We then briefly discuss local vibrations and group frequencies in IR spectra, as well as some aspects of tunneling problems arising in "nonrigid" molecules with multiple minima.

3.3.2 Term Formulae from Anharmonic Perturbation Theory for Polyatomic Molecules

If the Taylor expansion of equation (110) converges rapidly and if there are no "resonances" between close-lying states (see below), excluding degenerate vibrations, one can write the anharmonic term formula for a polyatomic molecule on the basis of perturbation theory in analogy to diatomic molecules as

$$\begin{aligned}\frac{E_{\mathrm{v}_1\mathrm{v}_2\ldots}}{hc} &= G(\mathrm{v}_1, \mathrm{v}_2, \ldots) \\ &= \sum_k \omega_k \left(\mathrm{v}_k + \frac{1}{2}\right) \\ &\quad + \sum_{k\geq l} x_{kl} \left(\mathrm{v}_k + \frac{1}{2}\right)\left(\mathrm{v}_l + \frac{1}{2}\right) + \cdots \end{aligned} \tag{111}$$

The harmonic frequencies and anharmonic constants can be related to the more fundamental force constants and other properties of the molecules (see for example Papoušek and Aliev 1982). For symmetric top molecules with twofold denegerate vibrations, one has similarly

$$\begin{aligned}\frac{E_{\mathrm{v}_1\mathrm{v}_2\ldots}}{hc} &= G(\mathrm{v}_1, \mathrm{v}_2, \ldots;\ l_i, l_{i+1}, \ldots) \\ &= \sum_s \omega_s \left(\mathrm{v}_s + \frac{1}{2}\right) + \sum_t \omega_t \left(\mathrm{v}_t + 1\right) \\ &\quad + \sum_{s'} \sum_{s\geq s'} x_{ss'} \left(\mathrm{v}_s + \frac{1}{2}\right)\left(\mathrm{v}_{s'} + \frac{1}{2}\right) \\ &\quad + \sum_s \sum_t x_{st} \left(\mathrm{v}_s + \frac{1}{2}\right)\left(\mathrm{v}_t + 1\right) \\ &\quad + \sum_{t'} \sum_{t\geq t'} x_{tt'} \left(\mathrm{v}_t + 1\right)\left(\mathrm{v}_{t'} + 1\right) \\ &\quad + \sum_{t'} \sum_{t\geq t'} g_{tt'} l_t l_{t'} + \cdots \end{aligned} \tag{112}$$

where s and s' denote non degenerate and t and t' twofold degenerate vibrational normal modes. Here, the l quantum number is related to the projection of the vibrational angular momentum of the twofold degenerate vibration on the symmetry axis. Analogous expressions hold if there are modes with higher degeneracy $d_t = 3, 4\ldots$, replacing the expressions in parentheses $(\mathrm{v}_t + 1)$ by appropriate terms with $(\mathrm{v}_t + d_t/2)$ in equation (112).

Alternatively, one can relate the level energies to the energy E_0 of the vibrational ground state as being set to zero. Then, one obtains

$$\begin{aligned}\frac{E_{\mathrm{v}_1\mathrm{v}_2\ldots} - E_0}{hc} &= G_0(\mathrm{v}_1, \mathrm{v}_2, \ldots) \\ &= \sum_j \tilde{\nu}'_j \mathrm{v}_j + \sum_i \sum_{j\geq i} x'_{ij} \mathrm{v}_i \mathrm{v}_j \\ &\quad + \sum_i \sum_{j\geq i} g'_{ij} l_i l_j + \ldots \end{aligned} \tag{113}$$

Again the corresponding "spectroscopic constants" $\tilde{\nu}'_j$, x'_{ij}, $g'_{ij}\ldots$ can be expressed in terms of the potential parameters and other molecular properties. These expressions are useful in describing vibrational spectra of polyatomic molecules. They frequently fail, however, if two or more vibrational states are close in energy, which may lead to an anharmonic resonance interaction.

3.3.3 Elementary Description of a Two-level Anharmonic Resonance (Fermi Resonances, Darling–Dennison Resonances, etc.)

We give here a brief summary of the two-level resonance, closely retaining the original notation from Herzberg (1945) for didactic reasons. Let us assume that the harmonic energies from equation (106) in the normal-mode picture are labeled as zero-order energies for one energy level

$E_i^0 = E_{v_1 v_2 v_3 \ldots}$ and also for a second energy level "accidentally" very close in energy in the normal-mode approximation $E_n^0 = E_{v_1' v_2' v_3' \ldots}$. The corresponding zero-order wavefunctions according to equation (107) are $\Psi_i^0 = \Psi_{v_1 v_2 v_3 \ldots}$ and $\Psi_n^0 = \Psi_{v_1' v_2' v_3' \ldots}$. The effect of including the higher order terms beyond the first sum in equation (110) can be taken into account locally for these two close-lying levels by computing the matrix element

$$W_{in} = \int \ldots \int \Psi_i^{0*} \hat{W} \Psi_n^0 \mathrm{d}Q_1 \mathrm{d}Q_2 \mathrm{d}Q_3 \ldots \tag{114}$$

where the integration is understood to cover the complete space of the coordinates. W_{in} is supposed to include all terms in the anharmonic Hamiltonian contributing to the integral. The effective Hamiltonian matrix for coupling just the two levels in "resonance", with "resonance" being defined as a similar magnitude of the coupling $|W_{in}|$ and the zero-order energy separation of the two levels

$$|W_{in}| \approx |E_i^0 - E_n^0| = |\delta| \tag{115}$$

takes the simple matrix form

$$\boldsymbol{H}_{\text{eff}} = \begin{pmatrix} E_i^0 & W_{in} \\ W_{ni} & E_n^0 \end{pmatrix} = \begin{pmatrix} H_{11} & H_{12} \\ H_{21} & H_{22} \end{pmatrix} \tag{116}$$

This matrix is Hermitian ($W_{ni}^* = W_{in}$) and in many cases real and symmetric ($W_{ni} = W_{in} = W$), which we assume here, without loss of generality, because we need only $|W_{ni}|^2 = |W_{in}|^2 = W^2$. The situation is schematically drawn in Figure 20. The eigenvalues of the two-level Hamiltonian are

$$E_{i,n} = \overline{E_{ni}} \pm \frac{1}{2}\sqrt{4W^2 + \delta^2} \tag{117}$$

$$\overline{E_{ni}} = \frac{(E_i^0 + E_n^0)}{2} = \frac{(E_i + E_n)}{2} \tag{118}$$

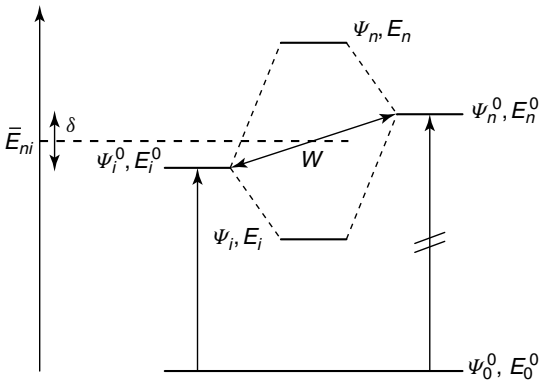

Figure 20 Energy diagram of a Fermi resonance between two energy levels.

with the eigenfunctions

$$\Psi_i = a\Psi_i^0 - b\Psi_n^0 \tag{119}$$

$$\Psi_n = b\Psi_i^0 + a\Psi_n^0 \tag{120}$$

If one has $\delta^2 \gg 4W^2$, one has approximately

$$E_{i,n} \simeq \overline{E_{ni}} \pm \left(\frac{\delta}{2} + \frac{W^2}{\delta}\right) \tag{121}$$

or $E_i \to E_i^0$ and $E_n \to E_n^0$ with $E_n^0 - E_i^0 = \delta$ and $\Psi_i \to \Psi_i^0$, $\Psi_n \to \Psi_n^0$ and thus a very small effect of the "non-resonant" perturbation, which provides a justification for neglecting non-resonant levels in isolating just the two-level resonance problem. For the coefficients in equations (119) and (120), one has

$$a = \left(\frac{\sqrt{4W^2 + \delta^2} + \delta}{2\sqrt{4W^2 + \delta^2}}\right)^{1/2} \tag{122}$$

$$b = \left(\frac{\sqrt{4W^2 + \delta^2} - \delta}{2\sqrt{4W^2 + \delta^2}}\right)^{1/2} \tag{123}$$

In the classic case of a Fermi resonance (Fermi 1931), Ψ_i corresponds to a fundamental level of one vibration ($v_1 = 1$, $v_2 = 0$, and all other $v_k = 0$) and Ψ_n to an overtone of a second vibration ($v_1 = 0$, $v_2 = 2$, and all other $v_k = 0$). If one assumes that the electric dipole transition strength for IR absorption is large for the fundamental ($|\langle \Psi_o^0 | \hat{\mu} | \Psi_i^0 \rangle|^2 = |M_{oi}^0|^2$) and essentially zero for the overtone ($|\langle \Psi_o^0 | \hat{\mu} | \Psi_n^0 \rangle|^2 = 0$), then one can readily see that the transition strengths for the observable transitions to the eigenstates Ψ_i and Ψ_n in the high-resolution spectrum are proportional to the squares of a and b, respectively. This is a common assumption in the analysis of spectra, allowing one to determine all parameters of the Fermi resonance equations from the observed line frequencies and intensities. The classic case of the Fermi resonance actually concerned the Raman spectrum of CO_2, in which one assumed that the Raman cross section for the symmetric stretching fundamental $\Psi_i^0 = \Psi_{100}$ is large, but small for the bending overtone $\Psi_n^0 = \Psi_{02^0 0}$. The zero-order energies are $E_i^0/(hc) \approx 1335\,\mathrm{cm}^{-1} \approx E_n^0/(hc)$, whereas the observed levels are at about 1388 and 1285 cm^{-1}, both giving a strong Raman signal. Furthermore, only the Σ_g^+ component $\Psi_{02^0 0}$ (with vibrational angular momentum quantum number $l = 0$, indicated by the superscript $(0,2^0,0)$) can give a nonzero matrix element W, whereas the Π component $\Psi_{02^2 0}$ has a vanishing W because of the symmetry selection rule on the integral in equation (114). Therefore, $E(0, 2^2, 0)$ is not shifted by the resonance and the level separation $|E(0, 2^0, 0) - E(0, 2^2, 0)|/(hc)$ is about 50 cm^{-1}, in the observed eigenstate spectrum, where the

harmonic level labels have obviously no exact meaning for the $E(0, 2^0, 0)$ level, which is heavily mixed. A more detailed discussion of the Fermi resonance in CO_2 can be found in Herzberg (1945) and Califano (1976). Numerous resonances of similar type have been observed in many other molecules since the first discussion of the CO_2 resonance by Fermi (1931). Another type of "named" resonance is the so-called Darling–Dennison resonance in which the two modes of different symmetry but similar harmonic frequency exchange two quanta (thus $\Psi_i^0 = \Psi_{20\ldots}$ and $\Psi_n^0 = \Psi_{02\ldots}$). This type of resonance was discussed by Darling and Dennison (1940) for H_2O and frequently occurs in not only dihydrides but also in many other molecules. More general types of resonances are simply called *anharmonic resonances*. If rotational levels are involved, one speaks of rovibrational resonances. We have given this introductory discussion to provide some basis for a commonly used analysis for two-level resonances. Several questions deserve attention in this context:

1. Is the assumption that only one state results in a zero-order line strength (either Raman or IR, and also others such as fluorescence) justified? Such a state is sometimes called the *bright state* or, perhaps to be preferred, the *chromophore state*.
2. Is the neglect of further interacting levels justified?
3. Is the common assumption that the first low-order term in the Taylor expansion of the potential equation (110) is sufficient to describe the resonance using the matrix element in equation (114) justified? For a Fermi resonance, this would be a $\Phi_{kl^2} Q_k Q_l^2$ term and for a Darling–Dennison resonance the $\Phi_{k^2l^2} Q_k^2 Q_l^2$ term, which might thus then be directly evaluated from the resonance analysis (Mills 1974). This is furthermore frequently complemented by the assumption that low-order terms are generally larger than higher order terms in the Taylor expansion.

It turns out that all of these assumptions must be questioned under many circumstances. They are also obviously not necessary in a more general treatment, of which we outline some aspects with some pertinent examples.

3.4 Many-level Anharmonic Resonances in Molecules Containing an Isolated CH Chromophore

3.4.1 Overtone Spectra of CHX_3 Molecules and Polyad Structure

Figure 21 shows a survey spectrum of the CH-stretching overtone absorption in CHF_3 (second overtone corresponding to three quanta of CH-stretching, Dübal and Quack 1984a). As the CH-stretching wavenumber is about twice the CH-bending wavenumber, one expects a strong Fermi resonance. There are, indeed, two bands of almost equal strength, each showing the characteristic P, Q, R structure of a parallel band, as for CH-stretching overtones in this symmetric top molecule.

Thus, one might be tempted to analyze this observed spectrum using a two-level Fermi resonance model, and this was, indeed, the basis of the first analysis by Bernstein and Herzberg (1948). Although the other bands are quite weak, nevertheless, they are important for the multistate Fermi resonance. The effective Hamiltonian is shown in Figure 22. The Fermi resonance system is, in fact, described by a polyad (here tetrad) of four strongly coupled zero-order levels. In the effective Hamiltonian, one takes the term formula in equation (113) as a diagonal structure, and one assumes a general form similar to the one from perturbation theory on a harmonic oscillator model as the off-diagonal structure. The effective Hamiltonian is assumed to be block-diagonal in the polyad quantum number N

$$N = \mathrm{v_s} + \frac{1}{2}\mathrm{v_b} \tag{124}$$

where $\mathrm{v_s}$ is the CH-stretching quantum number and $\mathrm{v_b}$ the quantum number for the degenerate CH-bending mode

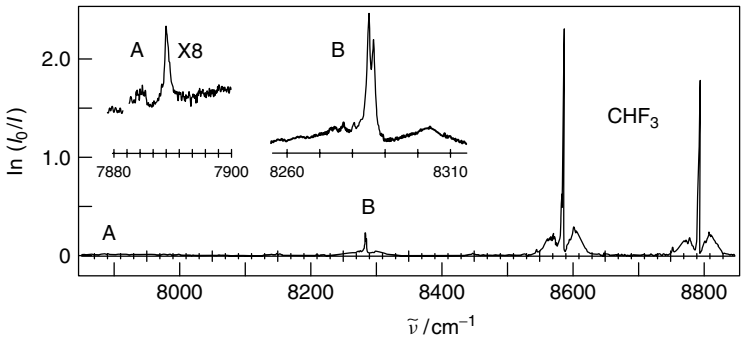

Figure 21 Survey spectrum of the $N = 3$ Fermi resonance polyad in CHF_3. The inserts are magnified portions from the same survey spectrum ($P = 0.5 \times 10^5$ Pa, resolution 1 cm^{-1}). [Reproduced with permission from Dübal and Quack (1984a).]

$$H^3 = \begin{array}{c} \begin{matrix} |3,0,0\rangle & |2,2,0\rangle & |1,4,0\rangle & |0,6,0\rangle \end{matrix} \\ \begin{pmatrix} H^3_{11} & -\sqrt{3/2}k_{\mathrm{sbb}} & 0 & 0 \\ -\sqrt{3/2}k_{\mathrm{sbb}} & H^3_{22} & -2k_{\mathrm{sbb}} & 0 \\ 0 & -2k_{\mathrm{sbb}} & H^3_{33} & -\frac{3}{\sqrt{2}}k_{\mathrm{sbb}} \\ 0 & 0 & -\frac{3}{\sqrt{2}}k_{\mathrm{sbb}} & H^3_{44} \end{pmatrix} \end{array} \begin{matrix} |3,0,0\rangle \\ |2,2,0\rangle \\ |1,4,0\rangle \\ |0,6,0\rangle \end{matrix}$$

$$\begin{pmatrix} 8684 & +130 & 0 & 0 \\ +130 & 8526 & +213 & 0 \\ 0 & +213 & 8310 & +226 \\ 0 & 0 & +226 & 8036 \end{pmatrix}$$

Figure 22 Structure of the Fermi resonance Hamiltonian for the $N = 3$ polyad in CHF_3. Top: General form. Bottom: Numerical values in cm^{-1} units from the best fit. [Reproduced with permission from Dübal and Quack (1984a).]

(l_b is the corresponding vibrational angular momentum quantum number). The structure of the Hamiltonian takes the following form for nonzero matrix elements:

$$\begin{aligned} H^N_{\mathrm{v_s},\mathrm{v_b},l_b;(\mathrm{v_s}-1),(\mathrm{v_b}+2),l_b} &= \left\langle \mathrm{v_s}, \mathrm{v_b}, l_b | k'_{\mathrm{sbb}} Q'_s {Q'_b}^2 | \mathrm{v_s}-1, \mathrm{v_b}+2, l_b \right\rangle \\ &= -\frac{1}{2}k'_{\mathrm{sbb}} \left(\frac{1}{2}\mathrm{v_s}(\mathrm{v_b} - l_b + 2)(\mathrm{v_b} + l_b + 2) \right)^{1/2} \end{aligned} \tag{125}$$

where we introduce primed quantities for Q'_s and Q'_b for effective dimensionless reduced normal coordinates and k'_{sbb} for the effective anharmonic coupling constant, which is related to the structure defined by the expansion in equation (110) but not identical to the corresponding force constant, as we shall see. Such effective Hamiltonians have been shown to describe the overtone spectra of many CHX_3 molecules reliably. Such success would be interpreted as a success of low-order perturbation theory to describe the many-level Fermi resonance. A more careful investigation shows, however, that some caution is necessary with such a conclusion.

3.4.2 *Variational Treatment and Effective Fermi Resonance Hamiltonian*

Lewerenz and Quack (1988), Dübal *et al.* (1989), and Marquardt and Quack (1991) have investigated the relation between a full vibrational variational treatment of the CH-stretching and bending Fermi resonance in the subspace of the relevant normal coordinates and the effective Hamiltonian. For the variational treatment, one uses reduced dimensionless normal coordinates and a Taylor expansion of the potential as follows:

$$\begin{aligned} V(Q'_s, Q'_b) = {} & \frac{1}{2}\omega_s y^2 + \frac{1}{2}\omega_b Q'^2_b + C_{\mathrm{sbb}} y Q'^2_b \\ & + C_{\mathrm{ssbb}} y^2 Q'^2_b + C_{\mathrm{bbbb}} Q'^4_b + C_{\mathrm{sbbbb}} y Q'^4_b \\ & + C_{\mathrm{sssbb}} y^3 Q'^2_b + \cdots \end{aligned} \tag{126}$$

Here, we use the "Morse coordinate"

$$y = \frac{[1 - \exp(-a Q'_s)]}{a} \tag{127}$$

with an effective Morse parameter a to describe the one-dimensional, very anharmonic C–H stretching potential ($D = \omega_s/(2a^2)$ is the corresponding dissociation wavenumber) and about 30 terms in the expression of equation (126) are generally needed for an accurate representation of either *ab initio* potentials or empirically derived potentials. The anharmonic vibrational problem is solved numerically either by basis set representation methods (Lewerenz and Quack 1988, Marquardt and Quack 1991) or by discrete variable techniques (Luckhaus and Quack 1992, Beil *et al.* 1994, 1997). As both the effective (experimental) and the vibrational variational spectra are well described by the simple effective Hamiltonian $\hat{H}_{\mathrm{eff}}$ of the previous subsections, one can derive the following transformations:

$$\boldsymbol{Z}^{\mathrm{T}} \boldsymbol{H}_{\mathrm{eff}} \boldsymbol{Z} = \mathbf{Diag}(E_1, E_2 \ldots E_n) \tag{128}$$

$$\boldsymbol{V}^{\mathrm{T}} \boldsymbol{H}_{\mathrm{var}} \boldsymbol{V} = \mathbf{Diag}(E_1, E_2 \ldots E_n) \tag{129}$$

where $\boldsymbol{Z}$ and $\boldsymbol{V}$ are the corresponding eigenvector matrices of the effective and variational Hamiltonians. Thus, one can derive the matrix representation of the effective Hamiltonian using the similarity transformation:

$$\boldsymbol{H}_{\mathrm{eff}} = (\boldsymbol{V}\boldsymbol{Z}^{\mathrm{T}})^{\mathrm{T}} \boldsymbol{H}_{\mathrm{var}} \boldsymbol{V}\boldsymbol{Z}^{\mathrm{T}} \tag{130}$$

If we arrange the eigenfunctions ψ_n of eigenvalues E_n as the column vector

$$\boldsymbol{\psi} = (\psi_1, \psi_2, \psi_3 \ldots \psi_n)^{\mathrm{T}} \tag{131}$$

and similarly the basis functions ϕ_n of the variational Hamiltonian $\hat{H}_{\mathrm{var}}$ as

$$\boldsymbol{\phi} = (\phi_1, \phi_2, \phi_3 \ldots \phi_n)^{\mathrm{T}} \tag{132}$$

and the *a priori* unknown basis functions χ_n of $\hat{H}_{\mathrm{eff}}$ as

$$\boldsymbol{\chi} = (\chi_1, \chi_2, \chi_3 \ldots \chi_n)^{\mathrm{T}} \tag{133}$$

we can write in matrix notation

$$\boldsymbol{\psi} = \boldsymbol{V}^{\mathrm{T}}\boldsymbol{\phi} = \boldsymbol{Z}^{\mathrm{T}}\boldsymbol{\chi} \tag{134}$$

and obtain an explicit expression for $\boldsymbol{\chi}$ in terms of the functions ϕ_n, which are known in real coordinate space

$$\boldsymbol{\chi} = \boldsymbol{Z}\boldsymbol{V}^{\mathrm{T}}\boldsymbol{\phi} \tag{135}$$

Because of the block diagonal structure of $\boldsymbol{Z}$, one can restrict the expansion of χ_i to the N_ith block with explicit notation as follows:

$$\chi_i = \sum_{k(N_i)} Z_{ik} \sum_j V_{jk}\phi_j \tag{136}$$

These relations are, in fact, generally useful, when relating a treatment using an effective "spectroscopic" Hamiltonian defined by a small number of spectroscopic parameters such as the Hamiltonian of Section 3.4.1 with a full variational Hamiltonian defined in real coordinate space. These investigations during the decade following 1980 have resulted in the following, perhaps surprising, conclusions:

1. Often anharmonic resonance spectra can be described using effective Hamiltonians similar in structure to normal coordinate expansions of very low order in equation (110) with very few parameters.
2. These parameters may not be interpreted, in general, as potential parameters in real coordinate space, even though equation (110) might suggest this. This would only be the case if the expansion of the actual potential were to stop after very few terms, which is not the case for the real molecular systems. Rather, the few effective Hamiltonian parameters are complicated combinations of very many potential parameters appearing in a long expansion of the type of equation (110) or (126).
3. The vibrational variational treatment combined with the effective Hamiltonian treatment allows a compact representation of spectroscopic data on the one hand. At the same time, it establishes the nontrivial relation between the effective Hamiltonian parameters and the true potential parameters and it allows for a representation of molecular eigenfunctions and of basis functions of the effective Hamiltonians in terms of wavefunctions in real coordinate space by means of transformations given by equations (128)–(136).
4. In particular, the long-believed dogma of the simple perturbation theoretical relation between the anharmonic potential constants and the effective Hamiltonian constants cannot be maintained.

We illustrate this last point with some results for prototypical molecules in Table 7. One can readily see the fairly similar magnitude of the various "spectroscopic" effective Hamiltonian parameters and their difference from the corresponding potential constants. Clearly, the traditional relation due to perturbation theory (Nielsen 1951, 1959, Mills 1974)

$$k'_{\mathrm{sbb}} = C_{\mathrm{sbb}} \tag{137}$$

Table 7 Spectroscopic constants and force constants for the Fermi resonance in CHX_3 molecules (after Quack 1990).

	CHD_3[a]		CHF_3[b]		$CHCl_3$[c]	$CHBr_3$[d]	$CH(CF_3)_3$[e]
Constant	Exp.	*Ab initio*	Exp.	*Ab initio*	Exp.	Exp.	Exp.
$\tilde{\nu}_s/(\mathrm{cm}^{-1})$	3048	3148	3086	3126	3096	3110	305
$\tilde{\nu}_b/(\mathrm{cm}^{-1})$	1292	1326	1370	1432	1221	1148	1353
$x'_{ss}/(\mathrm{cm}^{-1})$	−58	−67	−64	−67	−65	−66	−68
$x'_{bb}/(\mathrm{cm}^{-1})$	−4.5	−5.0	−5.6	−7.5	−6.5	−5.0	1.2
$x'_{ab}/(\mathrm{cm}^{-1})$	−22	−34	−29	−34	−26	−21	−22
$g'_{bb}/(\mathrm{cm}^{-1})$	2.6	3.8	9.7	11.5	7.8	3.2	1.9
$\lvert k'_{sbb}\rvert/(\mathrm{cm}^{-1})$	30 ± 15	31	100 ± 10	99	85 ± 15	75 ± 30	70 ± 15
$C_{sbb}/(\mathrm{cm}^{-1})$	97 ± 50	140 ± 15	187	187	265[f]	245	115
$C_{ssbb}/(\mathrm{cm}^{-1})$	−50	−78	−92	−85	−116	−94	−50

[a] Experiments: Campargue and Stoeckel (1986), Ben Kraiem *et al.* (1989), Campargue *et al.* (1989a,b), Lewerenz and Quack (1988), Lewerenz (1987), Ha *et al.* (1987), Peyerimhoff *et al.* (1984). Theory: Dübal *et al.* (1989), Lewerenz and Quack (1988), Lewerenz (1987), Ha *et al.* (1987), Peyerimhoff *et al.* (1984), Segall *et al.* (1987).

[b] Experiments: Dübal and Quack (1984a), von Puttkamer and Quack (1989), Quack (1982). Theory: Dübal *et al.* (1989), Lewerenz and Quack (1988), Lewerenz (1987), Ha *et al.* (1987). For $^{13}CHF_3$, see Hollenstein *et al.* (1990).

[c] Dübal *et al.* (1989), Lewerenz and Quack (1986), Baggott *et al.* (1986), Green *et al.* (1987), Wong *et al.* (1987). For $^{13}CHCl_3$, see Hollenstein *et al.* (1990).

[d] Ross *et al.* (1989a), Hollenstein *et al.* (1990), Davidsson *et al.* (1991), Manzanares *et al.* (1988).

[e] Dübal *et al.* (1989), von Puttkamer *et al.* (1983b), Baggott *et al.* (1985).

[f] An *ab initio* calculation (Amos *et al.* 1988) gives $C_{sbb} = 278\,\mathrm{cm}^{-1}$ in surprisingly good agreement with experiment (Dübal *et al.* 1989).

does not hold very well. Marquardt and Quack (1991) have derived improved approximations:

$$k'_{\mathrm{sbb}} = \frac{8\omega_{\mathrm{b}}^2}{\omega_{\mathrm{s}}(2\omega_{\mathrm{b}} + \omega_{\mathrm{s}})} C_{\mathrm{sbb}} \tag{138}$$

and

$$k'_{\mathrm{sbb}} = \left(1 - \frac{3}{4}a^2\overline{N}\right)\left(\left[\frac{8\omega_{\mathrm{b}}^2}{\omega_{\mathrm{s}}(2\omega_{\mathrm{b}} + \omega_{\mathrm{s}})} + \frac{4\omega_{\mathrm{b}} + \omega_{\mathrm{s}}}{2\omega_{\mathrm{b}} + \omega_{\mathrm{s}}}a^2\overline{N}\right] C_{\mathrm{sbb}} + a\overline{N}C_{\mathrm{ssbb}}\right) + \Delta k'_{\mathrm{sbb}} \tag{139}$$

where a is the Morse parameter as defined above, $\overline{N}$ an averaged polyad quantum number for the polyads retained in the description, and $\Delta k'_{\mathrm{sbb}}$ a correction term defined as:

$$\Delta k'_{\mathrm{sbb}} \approx -a\overline{N} \times 2.6\,\frac{C_{\mathrm{sbb}}^2}{\omega_{\mathrm{s}}} \tag{140}$$

We do not discuss in detail additional efforts extended to treatments in curvilinear coordinates (Carrington *et al*. 1987, Green *et al*. 1987, Wong *et al*. 1987, Voth *et al*. 1984) including contributions by Sibert and coworkers (Sibert 1990) and other kinds of perturbation theoretical approaches. Table 8 summarizes the results from the approximations discussed here. In general, full accuracy can be achieved only with a complete vibrational variational treatment. The general Fermi resonance treatment has been extended to the CH-chromophore in C_{s} and C_1 symmetrical environments; in addition to the Fermi resonances, Darling–Dennison resonances (of a "quartic" type) involving the two CH-bending modes and "cubic" anharmonic resonances coupling the two bending modes a and b with the stretching mode s by an effective coupling constant k_{sab} are included. We refer to Horká *et al*. (2008) as a paper which also includes a summary of results for many molecules. An extensive treatment of various aspects of effective Hamiltonians can be found in the article by Field *et al*. 2011: **Effective Hamiltonians for Electronic Fine Structure and Polyatomic Vibrations**, this handbook.

Table 8 Fermi resonance coupling constants; values in cm^{-1} (after Marquardt and Quack 1991).

	$k'^{(a)}_{\mathrm{sbb}}$	$C^{(a)}_{\mathrm{sbb}}$	$k'^{(b)}_{\mathrm{sbb}}$	$k'^{(c)}_{\mathrm{sbb}}$
CHF_3	100 ± 10	187	118	113
CHD_3	30 ± 15	97	75	54
$CHCl_3$	89	265	129	115
$CH(CF_3)_3$	65	115	82	74
$CHBr_3$	$55\pm^{55}_{15}$	181	114	81

[(a)] From direct fit to experimental data (Segall *et al*. 1987, Lewerenz and Quack 1988, Dübal *et al*. 1989, Ross *et al*. 1989b, Davidsson *et al*. 1991).
[(b)] Prediction from equation (138).
[(c)] Prediction from equation (139); constants from Dübal *et al*. (1989), Ross *et al*. (1989b), Davidsson *et al*. (1991); $\overline{N} = 3.5$ assumed.

3.4.3 Concluding Remarks on Multistate Anharmonic Resonances

Many spectra of polyatomic molecules are analyzed with the effective Hamiltonian as illustrated in Section 3.4.2, and, even more frequently, only local resonances are identified, if any, as discussed in Section 3.3. The connection to the full variational treatment as discussed in Section 3.4.2 is carried out only rarely, but it is very important for the understanding of the underlying dynamics, in particular, also time-dependent wavepacket dynamics as discussed in Section 4.

The very extensive work of Amat *et al*. (1971) in terms of various contact transformations should be seen in the tradition of effective Hamiltonian analyses. Beyond the discussion of Field *et al*. 2011: **Effective Hamiltonians for Electronic Fine Structure and Polyatomic Vibrations**, this handbook, already mentioned, the article by Herman 2011: **High-resolution Infrared Spectroscopy of Acetylene: Theoretical Background and Research Trends**, this handbook, discusses effective Hamiltonian analyses. Polyad dynamics of effective Hamiltonians has been discussed by a number of authors from various points of view (Jung *et al*. 2001, Kellman and Lynch 1986). Reviews covering effective Hamiltonian analyses include those by Quack (1990), Lehmann *et al*. (1994), Nesbitt and Field (1996), Gruebele and Bigwood (1998), Perry *et al*. (1996), and Herman *et al*. (1999). In addition, more extensive references can be found in the article by Hippler *et al*. 2011: **Mass and Isotope-selective Infrared Spectroscopy**, this handbook.

The question of treating the anharmonic vibrational problem in small polyatomic molecules variationally, including all degrees of freedom, is dealt with in the articles by Tennyson 2011: **High Accuracy Rotation–Vibration Calculations on Small Molecules**, this handbook and Carrington 2011: **Using Iterative Methods to Compute Vibrational Spectra**, this handbook. So far this is restricted to small molecules. Our discussion of treating only a subspace variationally (Lewerenz and Quack 1988) finds its justification in the substantial separation of timescales and coupling strengths, when one considers additional degrees of freedom. We discuss this question in Section 4.

The final topic concerns the polyad structure, when an increasing number of degrees of freedom are coupled. Figure 23 shows the zero-order polyad levels for CHF_3 for A_1 polyads from $N = 1$ to 7. The number of coupled levels in each polyad is $N + 1 \propto N$, because the vibrational angular momentum l for the bending vibration is approximately

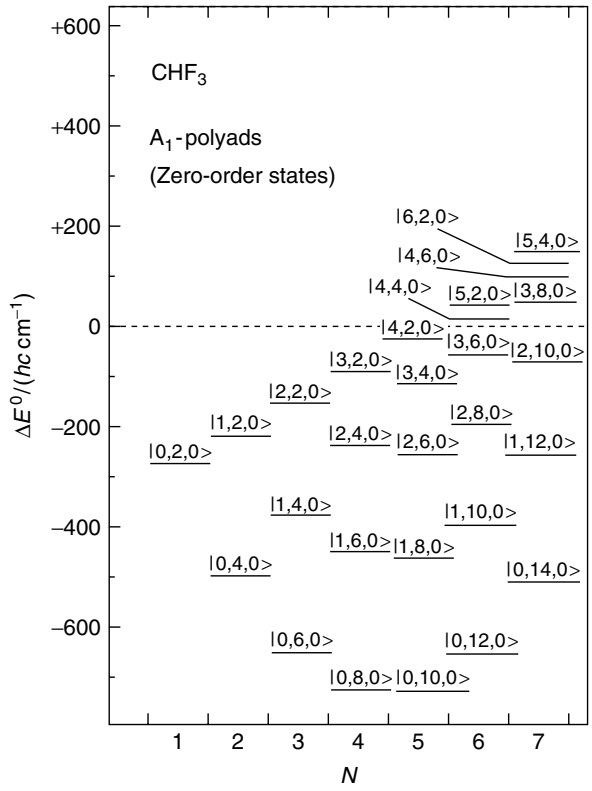

Figure 23 Reduced energy plot for the zero-order states $|v_s, v_b, l_b\rangle$ of CHF_3. The zero of energy is redefined at each N to be the energy of the $|v_s, 0, 0\rangle$ state, which is not shown explicitly. The coupled states for one polyad appear as one column with a given N. [Reproduced with permission from Dübal and Quack (1984a).]

conserved on short timescales in C_{3v} molecules (Luckhaus and Quack 1993). Figure 24 shows a coupling scheme just for one ($N = 4$) CH-stretching chromophore polyad in a C_1 or C_s symmetrical environment. Then, the number of coupled levels in each polyad increases approximately proportional to N^2. Finally, if all s vibrational degrees of freedom are included, the number of levels coupled in each polyad would increase approximately as $N^{(s-1)}$, proportional to the vibrational density of states. Ultimately, this leads to a sequential scheme for intramolecular vibrational and finally rotational–vibrational redistribution in polyatomic molecules and the concept of the global vibrational state, which would be delocalized over all degrees of freedom (Quack 1981, Quack and Kutzelnigg 1995).

Given the possibility of variational vibrational calculations and analysis, one might also wonder whether an effective Hamiltonian analysis has any justification at all. It turns out that, in practice, a fit to experimental spectra requires a compact description in terms of few parameters. For this purpose, fits of effective Hamiltonian parameters are an ideal intermediate step in spectroscopic analyses. A direct approach starting with a potential hypersurface and vibrational variational calculations would be much more difficult, although perhaps not impossible (*see* Marquardt and Quack 2011: **Global Analytical Potential Energy Surfaces for High-resolution Molecular Spectroscopy and Reaction Dynamics**, this handbook).

3.5 Local Modes, Group Frequencies, and IR Chromophores

When discussing the CH stretching overtone spectra, one implicitly uses the notion of a fairly localized normal vibration of the isolated CH chromophore. Indeed, it is the "infrared chromophore" nature of this localized vibration that results in a simple appearance of overtone spectra, where we have a very dense set of vibrational states that are "dark" and do not appear in spectra except by coupling to the chromophore levels. Indeed, the chromophore concept can be made the basis for a description of such spectra (Quack 1990). Another closely related concept is that of group frequencies, which are characteristic for certain types of functional groups. For high-frequency modes such as O–H stretching in alkanols and N–H stretching in amines, the relationship to fairly localized normal vibrations is clear and sometimes a quasi-diatomic treatment of the local vibrations is possible. However, there are also functional groups leading to more delocalized vibrations such as the C=O stretching in organic amides and others, on which there is extensive literature available. A more interesting variant of the local mode theory has been developed over many decades for hydrides with two or more high-frequency modes (XH_2, XH_3, etc.) and H_2O provides a simple example. Here, the normal modes are, by definition, delocalized over both X–H coordinates (symmetric and antisymmetric stretching). It has been argued, however, that at high excitations a zero-order Hamiltonian starting from localized X–H stretching modes provides a better approach than the normal-mode approach (Mecke 1936, 1950, Henry and Siebrand 1968, Child and Lawton 1981). We refer to Quack (1990) for a summary of the historical development of this approach. On the other hand, in large polyatomic molecules, the "high-resolution" eigenstates at high densities of states may be assumed to be very delocalized, lending themselves perhaps to a statistical treatment in terms of global vibrational states (Quack 1981, 1990, Lehmann *et al.* 1994). These concepts go beyond an introductory survey and we refer to some relevant articles in this handbook (*see* Herman 2011: **High-resolution Infrared Spectroscopy of Acetylene: Theoretical Background and Research Trends** and Quack 2011: **Fundamental Symmetries and Symmetry Violations from High-resolution Spectroscopy**, this handbook).

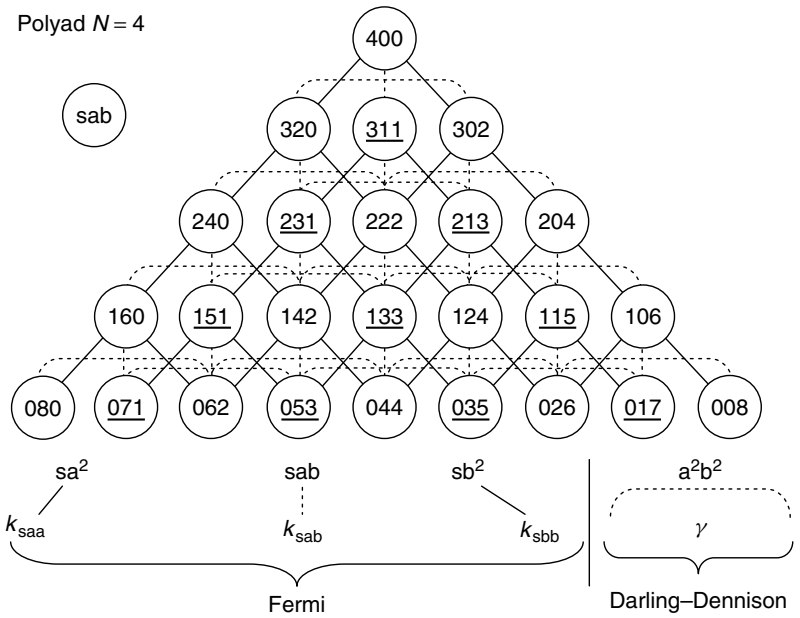

Figure 24 The coupling scheme for polyad $N = 4$ of CHD_2I, where the states are labeled in the circles by the quantum numbers $v_s v_a v_b$ in the zero-order picture, where v_s is the quantum number for stretching mode and v_a and v_b are quantum numbers for the bending modes. The underlined states have A″ symmetry in a C_s symmetric molecule. [Reproduced with permission from Horká *et al.* (2008).]

3.6 Large Amplitude Motion in Nonrigid Molecules Including Several Equivalent Minima

A straightforward treatment of large-amplitude motions of very nonrigid molecules with several equivalent or nonequivalent potential minima of very similar energy clearly is not possible. In such cases, one may sometimes define a reaction path connecting the minima and define normal modes along this path, for instance, inversion in ammonia and internal rotation in ethane or methanol. The dynamics and spectra of such nonrigid molecules have been discussed in the article by Bauder 2011: **Fundamentals of Rotational Spectroscopy**, this handbook. Coupling to vibrational degrees of freedom leads to mode selective tunneling, studied for instance in ammonia isotopomers (*see* Snels *et al.* 2011: **High-resolution FTIR and Diode Laser Spectroscopy of Supersonic Jets**, this handbook), aniline (Fehrensen *et al.* 1998, 1999), or H_2O_2 (Fehrensen *et al.* 2007, *see* Marquardt and Quack 2011: **Global Analytical Potential Energy Surfaces for High-resolution Molecular Spectroscopy and Reaction Dynamics**, this handbook). For more details on this topic, we refer to these articles and also to others present in this handbook (*see* Bauder 2011: **Fundamentals of Rotational Spectroscopy**, Caminati 2011: **Microwave Spectroscopy of Large Molecules and Molecular Complexes**, Hippler *et al.* 2011: **Mass and Isotope-selective Infrared Spectroscopy**, Amano 2011: **High-resolution Microwave and Infrared Spectroscopy of Molecular Cations** and Havenith and Birer 2011: **High-resolution IR-laser Jet Spectroscopy of Formic Acid Dimer**, this handbook). If one has very floppy systems such as clusters bound by van der Waals or hydrogen bonds, in general, the best approach is a variational treatment, for instance, using discrete variable representations (DVR) (*see* Bačić and Light 1989, Tennyson 2011: **High Accuracy Rotation–Vibration Calculations on Small Molecules** and Carrington 2011: **Using Iterative Methods to Compute Vibrational Spectra**, this handbook). In some cases, quantum Monte-Carlo techniques are useful (Quack and Suhm 1991).

4 MOLECULAR IR SPECTRA AND MOLECULAR MOTION

4.1 General Aspects

Deriving molecular motion from IR rotation–vibration spectra has a long history and can be discussed at several levels, leading to slightly differing pictures of molecular motion.

1. The historically oldest and still very widely used picture is derived from the classical normal-mode treatment. In this approach, spectroscopy is used to derive the normal vibrations and the motion of the

atoms is then described by the classical mechanical normal vibrations. If one considers the arrows in Figures 15–19 literally as describing atomic motions (not just relative displacements along a normal coordinate), then these figures give a schematic view of these classical vibrations. Didactic movies using classical dynamics showing these normal vibrations exist and are widely distributed. The overall motion when several normal vibrations are excited would correspond to a more complicated classical Lissajous motion. It turns out that the coherent-state description of the quantum harmonic oscillator also provides some justification for this picture for the true quantum motion. The coherent quantum state shown for a typical "molecular" harmonic oscillator in Figure 25 (with a fundamental wavenumber of 1000 cm^{-1}) is a Gaussian probability following the classical mechanical trajectory (Schrödinger 1926, Quack and Sutcliffe 1985, Marquardt and Quack 1989). This picture would then remain valid for all harmonic degrees of freedom and thus the classical picture of molecular vibrations would be qualitatively valid also for the true quantum motion, *if the harmonic normal-mode description were adequate to describe vibrational spectra and dynamics* (Quack 1995).

2. It turns out, as we have seen, that anharmonic contributions to the spectra are very important. One might then think of deriving anharmonic potentials from spectra and describing molecular motion quasi-classically by computing trajectories using the anharmonic potentials. Indeed, this approach is widely used. However, it turns out that anharmonicity (when large) leads to

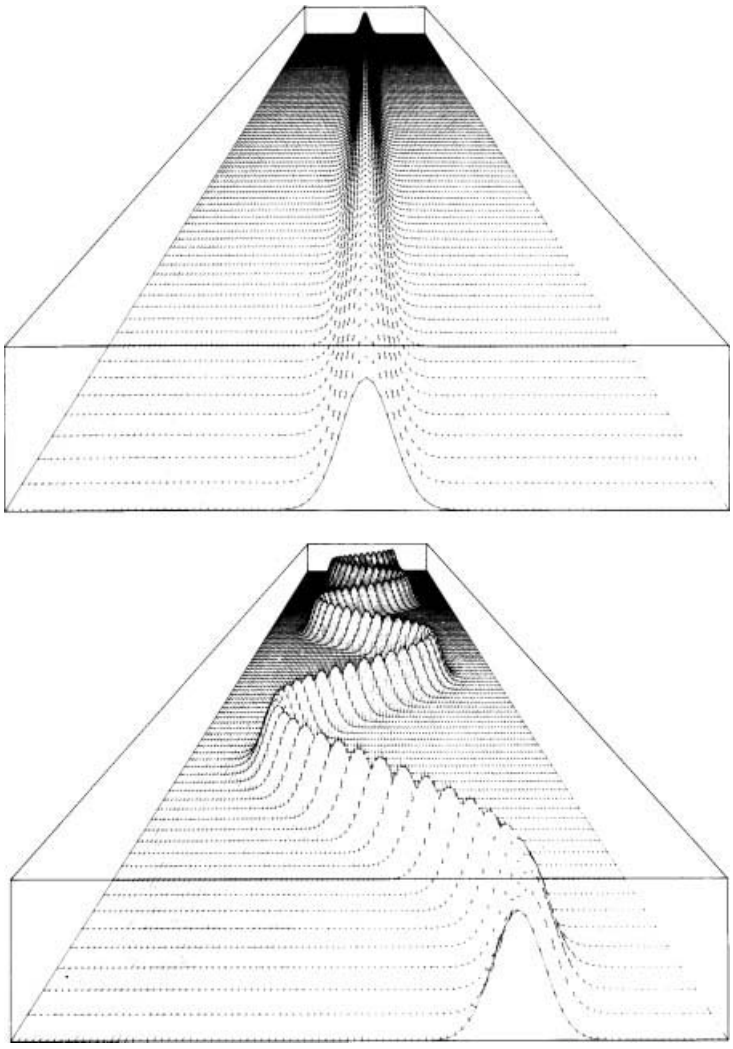

Figure 25 Quasi-classical oscillation of the harmonic oscillator with resonant, coherent excitation ($\tilde{\nu} = \tilde{\nu}_L = 1000\,cm^{-1}$) (after Quack and Sutcliffe 1985). The images show the axis t toward the back (the time step separating two lines is 1 fs). The abscissa from left to right shows the spatial coordinate q and the ordinate the probability density $|\Psi|^2$. Top: from $t = 0$ to 0.1 ps (practically unperturbed ground state). Bottom: from 16.5 to 16.6 ps (practically free oscillation after resonant excitation).

dynamical consequences, making a quantum description necessary.

3. A quantum description, which has come into wide use more recently, uses effective Hamiltonians, such as the Fermi resonance Hamiltonians as discussed in Section 3, and computes anharmonic intramolecular vibrational redistribution (IVR) in terms of time-dependent quantum basis state populations. This provides some insights into quantum redistribution processes. However, it does not provide a complete picture of the true quantum motion, because the wavefunctions corresponding to the basis states are either completely unknown or arbitrary, or they might be known as approximations, such as normal-mode wavefunctions. They still carry a large uncertainty, related to the uncertainties originating from the basis states.
4. If the transformation to a true variational Hamiltonian is known along the lines of Section 3.4.2, then a complete quantum description in terms of quantum mechanical wavepackets and time-dependent probability densities is possible, the accuracy of which is only limited by the uncertainties of the primary spectroscopic data and the accuracy of the corresponding spectroscopic analysis. We provide here some examples for analyses along the lines of the last two approaches.

4.2 Time-dependent Population Dynamics from Simple Coupling Models and Effective Hamiltonians

Simple coupling models relating spectra and time-dependent population dynamics can be traced to the early model of Bixon and Jortner (1968). This model for an exponential decay of an initial state into a dense set of background states was motivated by the need to understand the irreversible relaxation of excited electronic states by internal conversion and intersystem crossing processes (*see* Merkt and Quack 2011: **Molecular Quantum Mechanics and Molecular Spectra, Molecular Symmetry, and Interaction of Matter with Radiation**, this handbook). The essence of the result of Bixon and Jortner (1968) is the realization that exponential decay of an initial state can occur not only with truly continuous spectra, such as in predissociation (Herzberg 1966), but also with quasi-continua, such as in internal conversion processes. In addition, the Bixon–Jortner model provides an important result: the "Golden Rule"

$$k = \frac{2\pi\Gamma}{h} = \frac{4\pi^2 V^2}{h}\rho \tag{141}$$

This provides a relation between the exponential decay rate constant k and the full width at half maximum Γ (FWHM) of a Lorentzian line shape with the coupling strength V^2 to a quasi-continuum of state density ρ. It can be derived from an (almost) exactly solvable model and is not a consequence of first-order perturbation theory. The application of this idea to an exponential decay of a highly excited vibrational state into a quasi-continuum of vibrational states by IVR and an exponential line shape analysis was done by Bray and Berry (1979), deriving very short (100 fs) decay times for highly excited CH-stretching states in benzene. Numerous analyses of this kind have appeared since then. Of course, one can also find exponential decay through IVR by vibrational predissociation into true continua, for instance, for $(HF)_2$ (Hippler *et al.* 2007, Manca *et al.* 2008).

More generally, one can go beyond these simple coupling schemes (Quack 1981) and finally derive state populations p_k for some spectroscopic effective Hamiltonian. The basic equations, given some Hamiltonian matrix $\boldsymbol{H}$ ("effective" or "true"), are given by the propagator

$$\boldsymbol{U}(t, t_0) = \exp\left(-2\pi \mathrm{i}\boldsymbol{H}(t - t_0)/h\right) \tag{142}$$

$$\boldsymbol{b}(t) = \boldsymbol{U}(t, t_0)\boldsymbol{b}(t_0) \tag{143}$$

$$p_k = |b_k|^2 \tag{144}$$

For the two-level Fermi resonance problem, the full time evolution matrix can be easily written (*see* Merkt and Quack 2011: **Molecular Quantum Mechanics and Molecular Spectra, Molecular Symmetry, and Interaction of Matter with Radiation**, this handbook, for the mathematically identical Rabi problem, which is explicitly solved in terms of the $\boldsymbol{U}$ matrix therein). The numerical calculation for more complicated examples is straightforward. Figure 26 shows the result for basis state populations of the

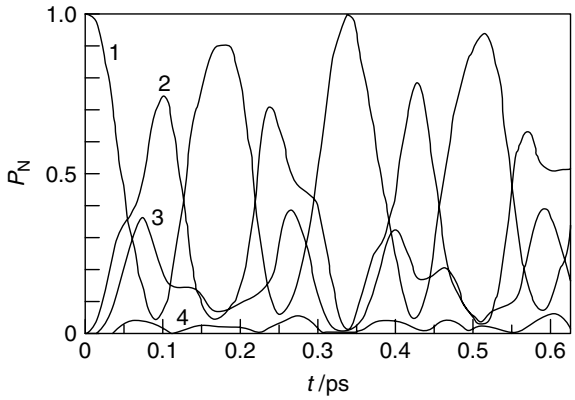

Figure 26 Time evolution for the populations of states interacting in the $N = 3$ polyad of CHF_3 calculated with the spectroscopic Fermi resonance Hamiltonian and the initial condition $p(|3, 0, 0\rangle) = 1$. [Reproduced with permission from Dübal and Quack (1984a).]

Table 9 Typical IVR lifetimes of initial CH-stretching excitation in alkyl and acetylene compounds estimated from spectroscopic data. See reviews (Quack 1990, 1991, Lehmann *et al*. 1994) for further tables (after Quack and Kutzelnigg 1995).

Example	τ_{IVR}/ps	Method and reference
Alkyl CH	<0.1[a]	Effective Hamiltonian H_{eff} dynamics
X_3CH		(Quack 1990, 1991, Baggott *et al*. 1985)
(X=D,F,Cl,Br,CF_3)		or real molecular Hamiltonian dynamics H_{mol} in subspace (Quack 1991, Marquardt *et al*. 1986, Marquardt and Quack 1991)
XF_2CH	<0.1[a]	H_{eff} (Dübal and Quack 1984a,b
X_2FCH	<0.1[a]	Amrein *et al*. 1985, Quack 1991) or H_{mol}
(X=D,Cl,(CF_3))		(Luckhaus and Quack, 1992, 1993, Quack 1991, Quack and Stohner 1993)
Acetylene CH		Temperature-dependent lineshape
$(CX_3)_3CC{\equiv}CH$(X=F)	$\geq$10–20	(von Puttkamer *et al*. 1983a)
(v=1)	$\geq$60	Molecular beam linewidth, bolometric
(X=F)		(Gambogi *et al*. 1993, Lehmann *et al*. 1994)
X=H	$>$200	Molecular beam, bolometric
		(Lehmann *et al*. 1994) linewidth
X=D	$\geq$40	Molecular beam, bolometric
		(Lehmann *et al*. 1994) linewidth
$(CH_3)_3Si{-}C{\equiv}C{-}H$	Inhomogeneous	FTIR, temperature dependent
(v=1)	$\geq$2000	(von Puttkamer, K. and Quack, M. (1983) unpublished work cited in Quack 1991) bolometric
		(Kerstel *et al*. 1991)
$CH_3CH_2C{\equiv}C{-}H$	$\geq$269	Statistical H_{eff} (band structure
		(McIllroy and Nesbitt 1990, Bethardy and Perry 1993)).

[a] Detailed dynamics (nonexponential) obtained from 10 to 1000 fs.

effective Hamiltonian represented for CHF_3 in Figure 22 (spectra in Figure 21). An interesting observation beyond the very short time for IVR ($<$100 fs for a complete initial decay of the $v_s = 3$ CH-stretching state) is the very substantial population of two other states (achieving maximum populations of about 80 and 40%), although the spectrum in Figure 21 shows only two prominent bands. Nevertheless, a two-level Fermi resonance analysis would be dynamically quite misleading as it would lead to a periodic beating of just two states instead of the correct involvement of three as shown in Figure 26.

Quite a few examples of this type have been analyzed in terms of IVR along those lines and Table 9 gives a summary of some results (Quack and Kutzelnigg 1995).

One of the more interesting results concerns the very different initial redistribution times for the isolated alkyl CH chromophore states ($\tau < 100$ fs) and the acetylenic CH chromophore ($\tau > 1$ ps) originally derived by von Puttkamer *et al*. (1983b) and since confirmed by many experiments, now also including time-resolved femtosecond-pump probe experiments (Kushnarenko *et al*. 2008a,b). Rather than discussing more such examples, we now consider evolution of the quantum mechanical wavepacket derived from high-resolution IR spectra, which provides an additional level of understanding.

4.3 Time-dependent Wavepacket Analysis

The state population analyses contain an element of arbitrariness, because the time evolution of populations depends upon the choice of basis states (Beil *et al*. 1997). For instance, if one chooses eigenstates as the basis there is no time evolution of populations, and if one chooses some very highly localized states, one might get evolution on a 1-fs or even shorter timescale. While often the physical situation may suggest some reasonable effective Hamiltonian, the ambiguities can be removed altogether if a transformation to a "true" variational Hamiltonian can be carried out along the lines of Section 3.4.2.

Figure 27 shows such a result for CHF_3, which was, in fact, the first example where such a wavepacket analysis was carried out (Marquardt *et al*. 1986, Marquardt and Quack 1991). The new aspect beyond the short timescale is now the evolution of probability density in space. As can be seen, this evolution is not simply a quasi-classical oscillation between two coupled pendula, but rather one finds a nonclassical delocalization. It has been found that with artificially very small anharmonicities one has a quasi-classical coherent state propagation, very similar to the behavior of two classical anharmonically coupled oscillators. On the other hand, with large anharmonicity (as

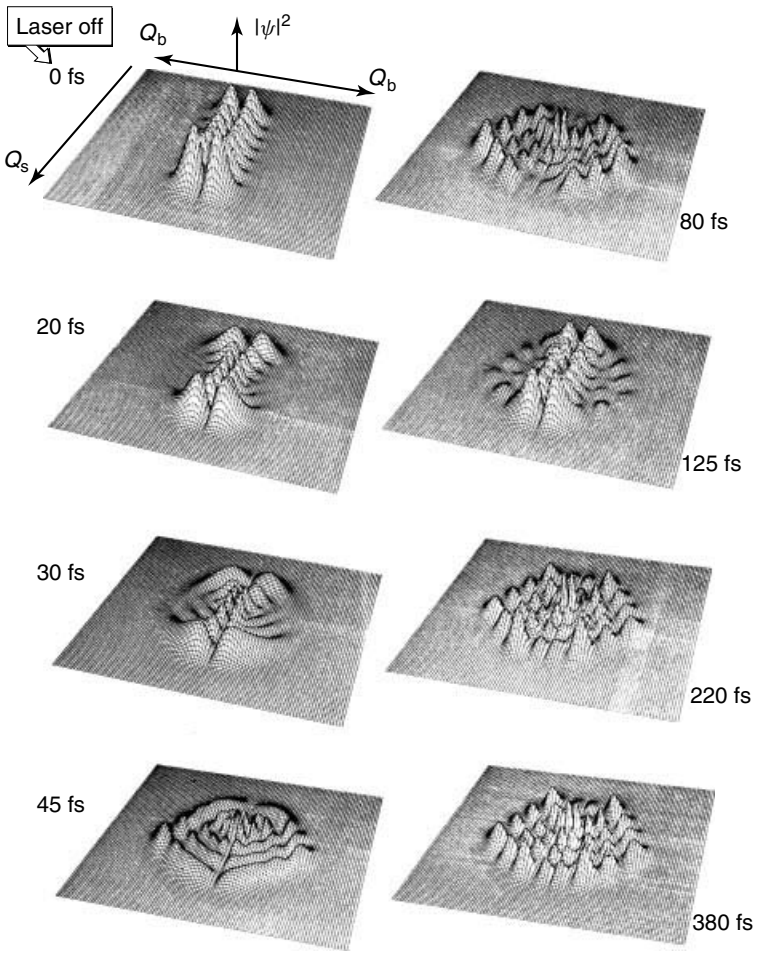

Figure 27 Wavepacket motion for the two strongly coupled CH-stretching (Q_s) and bending (Q_b) vibrations in the CHF_3 molecule. $|\Psi(Q_s, Q_b, t)|^2$ is the probability distribution on the femtosecond timescale after the initial CH-stretching excitation at $t = 0$. [Reproduced from Marquardt and Quack (2001).]

applicable to CHF_3), one finds nonclassical delocalization on the timescale of IVR. This introduces the new concept DIVR (delocalization IVR) as opposed to CIVR (classical IVR) and the tuning of this phenomenon by anharmonicity constitutes a fundamental finding for intramolecular dynamics (Marquardt and Quack 1991, 2001, Quack 1993, 1995).

These phenomena can be investigated both for isolated molecules as shown in Figure 27 and for molecules under coherent excitation (Quack and Stohner 1993). Figure 28 shows such an example for CH-stretching and bending wavepackets in CHD_2F (Luckhaus *et al.* 1993). One can recognize an initial almost coherent state oscillation for the first 100 fs, followed by IVR and delocalization on timescales <1 ps. In addition, with wavepacket analysis under coherent excitation, one finds the pronounced difference in timescales for the alkyl–CH chromophore and the acetylenic–CH chromophore as derived from the spectrum (Quack and Stohner 1993). Taking a slightly different line of thought, one can also analyze the dynamics in a very coarse-grained way by studying time-dependent entropy (Quack 1990, Luckhaus *et al.* 1993, Quack 2011: **Fundamental Symmetries and Symmetry Violations from High-resolution Spectroscopy**, this handbook).

5 ROTATION–VIBRATION SPECTRA OF POLYATOMIC MOLECULES

5.1 General Aspects

The basic concepts of the interaction of vibration and rotation in polyatomic molecules are similar to the ones discussed in Section 2 for diatomic molecules. However, the exact separation of rotational and vibrational motion possible for diatomic molecules cannot be directly translated to polyatomic molecules. Nevertheless, one can distinguish between the two approaches.

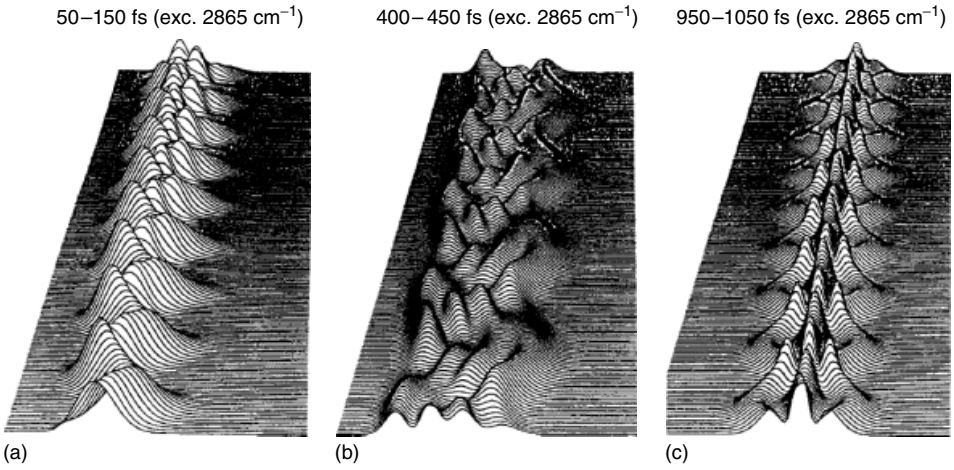

Figure 28 (a) Time-dependent probability density $P(q_v, t)$ of CHD_2F under IR-multiphoton excitation with $I = 20\,W\,cm^{-2}$, $\tilde{\nu}_{FL} = 2865\,cm^{-1}$. The abscissa shows a dimensionless CH-stretching normal coordinate range $-4.5 \leq q_s \leq +8.5$, the timestep separating two lines toward the back is 0.5 fs; total time range shown from 50 to 150 fs after the start of radiative excitation. (b) As (a) but from 400 to 450 fs with time step 0.25 fs. (c) As (a) but showing probability density $P(q_i, t)$, integrated over q_s, and the dimensionless CH-bending out-of-plane q_o, time range 950–1050 fs, time step 0.5 fs, range of the dimensionless CH-bending in-plane $-8 \leq q_i \leq +8$. [Reproduced with permission from Luckhaus *et al.* (1993).]

1. Exact (numerical) treatment of the rotation–vibration problem given an effective multidimensional potential hypersurface (the lowest dimension, for a triatomic molecule, would be a three-dimensional hypersurface in a four-dimensional space–with the fourth dimension being the potential energy coordinate). Such approaches are discussed in this handbook by Tennyson 2011: **High Accuracy Rotation–Vibration Calculations on Small Molecules**, and Carrington 2011: **Using Iterative Methods to Compute Vibrational Spectra**, this handbook. Until today, these approaches have been limited to triatomic, four atom, and at most five atom molecules and very few analyses of rotation–vibration spectra along these lines have been carried out, quite in contrast to diatomic molecules, where this type of "exact" approach is more common.
2. Effective Hamiltonian analyses leading to sets of spectroscopic parameters. Different from diatomic molecules, the effective rotation–vibration parameters, however, concern matrix representations of appropriate Hamiltonians prior to diagonalization; thus, rotation–vibration energies cannot, in general, be given as simple formulae for the Hamiltonian in diagonal structure. For the purely vibrational problem of anharmonic resonances, an example has already been given in Section 3, where we introduced diagonal term formulae for a zero-order Hamiltonian and other parameters defining the off-diagonal structures. The rotation–vibration problem has been addressed already in the preceding article by Bauder 2011: **Fundamentals of Rotational Spectroscopy**, this handbook, with emphasis on the rotational level structure. Here, we complement this with a brief summary of the basic theory and a short section on the practice of rotation–vibration analysis including a discussion of an efficient general program available for rotation–vibration analysis of asymmetric tops.

5.2 The Rotation–Vibration Hamiltonian

The rotation–vibration Hamiltonian of polyatomic molecules is discussed in the article by Bauder 2011: **Fundamentals of Rotational Spectroscopy**, this handbook, and has a long history. We may refer here to the classic papers by Nielsen (1951, 1959), the work by Wilson *et al.* (1955) (particularly Chapter 11 therein) and Watson (1968), with important subsequent work by Howard and Moss (1971), Louck (1976), Makushkin and Ulenikov (1977), Meyer (1979), and Islampour and Kasha (1983). We introduce here the basic concepts, with the aim of defining notations. The usual starting point is the classical Hamiltonian of equation (97) in Cartesian coordinates for all particles written in quantum mechanical operator form:

$$\hat{H} = -\frac{h^2}{4\pi^2}\sum_{i=1}^{3N}\frac{1}{2m_i}\frac{\partial^2}{\partial x_i^2} + \hat{V}(x_1, \ldots, x_{3N}) \quad (145)$$

$$= \sum_{i=1}^{3N}\frac{\hat{p}_i^2}{2m_i} + \hat{V}(x_1, \ldots, x_{3N})$$

Transformation to a system of arbitrary coordinates q_k following Podolsky (1928) gives

$$\hat{H} = \frac{1}{2}|\boldsymbol{g}|^{-1/4} \sum_{j,k} \hat{p}_j |\boldsymbol{g}|^{1/2} G_{jk} \hat{p}_k |\boldsymbol{g}|^{-1/4} + \hat{V}(q_1, \ldots, q_{3N}) \tag{146}$$

with the momentum operators $\hat{p}_k$ given by

$$\hat{p}_k = -\mathrm{i}\frac{h}{2\pi}\frac{\partial}{\partial q_k} \tag{147}$$

and

$$G_{jk} = \sum_i \frac{1}{m_i}\frac{\partial q_j}{\partial x_i}\frac{\partial q_k}{\partial x_i} \tag{148}$$

$$g_{jk} = \sum_i m_i \frac{\partial x_i}{\partial q_j}\frac{\partial x_i}{\partial q_k} \tag{149}$$

$$|\boldsymbol{g}| = \mathrm{Det}(\boldsymbol{g}) \tag{150}$$

This can be simplified to

$$\hat{H} = \frac{1}{2}\sum_{j,k} \hat{p}_j G_{jk} \hat{p}_k + \hat{u}(q_1, \ldots, q_{3N}) + \hat{V}(q_1, \ldots, q_{3N}) \tag{151}$$

$$\hat{u}(q_1, \ldots, q_{3N}) = \frac{h^2}{8\pi^2}\sum_{j,k}\left(\frac{1}{4}\frac{\partial}{\partial q_j}\left[G_{jk}\frac{\partial \ln(|\boldsymbol{g}|)}{\partial q_k}\right] + \frac{1}{16}\frac{\partial \ln(|\boldsymbol{g}|)}{\partial q_j} G_{jk} \frac{\partial \ln(|\boldsymbol{g}|)}{\partial q_k}\right) \tag{152}$$

Using center of mass separation, Euler angles for rotation, Eckart conditions, and transformation to normal coordinates, Watson (1968) has derived a simplified general effective rotation–vibration Hamiltonian, which we write here in the notation of Aliev and Watson (1985)

$$\hat{H} = \frac{1}{2M}\overline{p}_\mathrm{f}^2 + \frac{h^2}{8\pi^2}\sum_{\alpha,\beta}(\hat{J}_\alpha - \hat{\Pi}_\alpha)\mu_{\alpha\beta}(\hat{J}_\beta - \hat{\Pi}_\beta) + \frac{1}{2}\sum_k \hat{p}_k^2 + \hat{u} + \hat{V}(q_1, \ldots, q_{3N}) \tag{153}$$

where

$$\hat{u} = -\frac{h^2}{32\pi^2}\sum_\alpha \mu_{\alpha\alpha} \tag{154}$$

$\hat{J}_\alpha$ are the angular momentum operators in the molecule-fixed system, and $\overline{p}_f$ the total linear momentum in space-fixed direction f.

$$\mu_{\alpha\beta} = \left(I_{\alpha\beta} - \sum_{i,j,k}\zeta_{ik}^\alpha \zeta_{jk}^\beta q_i q_j\right)^{-1} \tag{155}$$

$I_{\alpha\beta}$ are the components of the moments of inertia tensor, with $\alpha, \beta = x, y, z$, and $i, j, k = 1, \ldots, 3N-6$, and ζ_{ik}^α the common Coriolis coupling parameters. $\hat{\Pi}_\alpha$ are the components of vibrational angular momentum:

$$\hat{\Pi}_\alpha = \sum_{i,j}\zeta_{ij}^\alpha q_i \hat{p}_j \tag{156}$$

$$\zeta_{ij}^\alpha = -\zeta_{ji}^\alpha = \sum_{n=1}^{N}(l_{n\beta,i} l_{n\gamma,j} - l_{n\gamma,i} l_{n\beta,j}) \tag{157}$$

where the matrix $\boldsymbol{l}$ defines the transformation from normal coordinates to mass-weighted Cartesian coordinates in the molecule-fixed system.

5.3 Effective Hamiltonian Analysis for Rotation–Vibration Spectra of Asymmetric Tops

The general Hamiltonian of the preceding section can be applied in several ways to rotation–vibration spectra. One can distinguish three cases depending on the moments of inertia I_a, I_b, I_c after transformation to the principal axis system (*see* Bauder 2011: **Fundamentals of Rotational Spectroscopy**, this handbook) or the corresponding rotational constants ordered by convention $A \geq B \geq C$ and with $X = A, B, C$:

$$X = \frac{h}{8\pi^2 {}_c I_X} \tag{158}$$

For rigid rotors, apparently simple forms can be derived for the rotational energy levels when some of the A, B, C are identical (*see* Bauder 2011: **Fundamentals of Rotational Spectroscopy**, this handbook). For $A = B = C$, one has a spherical rotor (or spherical top); for $A \neq B = C$, one has a prolate symmetric top and for $A = B \neq C$, one has an oblate symmetric top. We refer to Bauder 2011: **Fundamentals of Rotational Spectroscopy**, this handbook and Herzberg (1945, 1966) for rotational–vibrational energy level structures for these cases. It turns out, however, that the rotation–vibration problem for spherical and symmetric rotors is actually complicated by the occurrence of degeneracies, which are lifted at higher order. In general, spherical and symmetric rotors possess degenerate vibrations, if the identity of moments of inertia arises from the

symmetry of the molecule (Herzberg 1945). Here, we do not discuss these cases in more detail, referring to Bauder 2011: **Fundamentals of Rotational Spectroscopy**, this handbook, and in particular to Boudon *et al*. 2011: **Spherical Top Theory and Molecular Spectra**, this handbook, for spherical rotors.

Asymmetric rotors have no simple term value formulae; however, they have the advantage that degenerate vibrations do not occur, in general. This allows one to deal with the rotation–vibration problem in a fairly general way. We discuss here an implementation, which exists also in the form of a computer program (Luckhaus and Quack 1989), which was designed to allow for treating all kinds of interaction of rotation and vibration in a very general way. A similar approach was later also used by Pickett (1991). Following Watson, one can, on the basis of the general Hamiltonian discussed in Section 5.2, define effective Hamiltonians that form blocks of "polyads" similar to those discussed in Section 3. However, now both anharmonic and Coriolis-type rotation–vibration couplings are included (see the scheme in Figure 29). If the molecule has some symmetry, anharmonic interactions are allowed only between states of the same vibrational symmetry species (as indicated by vertical arrows in Figure 29), whereas rovibrational Coriolis interactions also couple states of different vibrational symmetry (but with the same total, rovibrational symmetry species, of course). Figure 29 shows a case of a C_s-symmetrical molecule (for example, $CHClF_2$ (Luckhaus and Quack 1989, Albert *et al*. 2006)). As an example with C_{2v} symmetry, we mention CH_2D_2 (Ulenikov *et al*. 2006). Watson (1968) has given several representations for such effective Hamiltonians and we give here the S-reduced effective Hamiltonian in the I^r representation as an example, with terms diagonal in the vibrational quantum number v

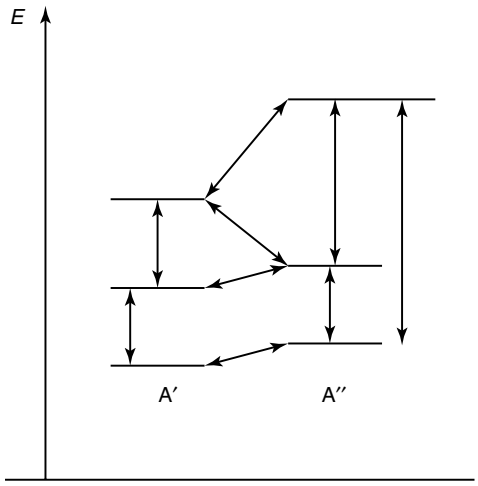

Figure 29 Illustration of a resonance polyad of an effective Hamiltonian including various types of interactions.

$$\begin{aligned}\hat{H}_{\mathrm{rot}}^{\mathrm{vv(S)}} = {} & A^{(\mathrm{S})}\hat{J}_z^2 + B^{(\mathrm{S})}\hat{J}_x^2 + C^{(\mathrm{S})}\hat{J}_y^2 - D_J\hat{J}^4 \\ & - D_{JK}\hat{J}^2\hat{J}_z^2 - D_K\hat{J}_z^4 \\ & + d_1\hat{J}^2(\hat{J}_+^2 + \hat{J}_-^2) + d_2(\hat{J}_+^4 + \hat{J}_-^4) + H_J\hat{J}^6 \\ & + H_{JK}\hat{J}^4\hat{J}_z^2 + H_{KJ}\hat{J}^2\hat{J}_z^4 + H_K\hat{J}_z^6 + h_1\hat{J}^4(\hat{J}_+^2 \\ & + \hat{J}_-^2) + h_2\hat{J}^2(\hat{J}_+^4 + \hat{J}_-^4) + h_3(\hat{J}_+^6 + \hat{J}_-^6) \end{aligned} \quad (159)$$

where

$$\hat{J}^2 = \hat{J}_x^2 + \hat{J}_y^2 + \hat{J}_z^2 \quad \text{and} \quad \hat{J}_\pm = \hat{J}_x \pm \mathrm{i}\hat{J}_y$$

Note that in Equation (159) as well as in the following equations in this section we do not explicitly write the v-dependence of the rotational constants to simplify the expressions.

We also give the A-reduced Hamiltonian in the I^r representation as another example with terms diagonal in the vibrational quantum number v:

$$\begin{aligned}\hat{H}_{\mathrm{rot}}^{\mathrm{vv(A)}} = {} & A^{(\mathrm{A})}\hat{J}_z^2 + B^{(\mathrm{A})}\hat{J}_x^2 + C^{(\mathrm{A})}\hat{J}_y^2 \\ & - \Delta_J\hat{J}^4 - \Delta_{JK}\hat{J}^2\hat{J}_z^2 - \Delta_K\hat{J}_z^4 \\ & - \frac{1}{2}[\delta_J\hat{J}^2 + \delta_K\hat{J}_z^2, \hat{J}_+^2 + \hat{J}_-^2]_+ \\ & + \phi_J\hat{J}^6 + \phi_{JK}\hat{J}^4\hat{J}_z^2 + \phi_{KJ}\hat{J}^2\hat{J}_z^4 + \phi_K\hat{J}_z^6 \\ & + \frac{1}{2}[\eta_J\hat{J}^4 + \eta_{JK}\hat{J}^2\hat{J}_z^2 + \eta_K\hat{J}_z^4, \hat{J}_+^2 + \hat{J}_-^2]_+ \end{aligned} \quad (160)$$

Note that in the following discussion the choice of the representation will not be explicitly mentioned in the notation of the rotational constants to simplify the expressions. For the off-diagonal terms representing a α-Coriolis coupling ($\alpha = x, y, z$), one has:

$$\hat{H}_{\mathrm{rot}}^{\mathrm{v'v}} = \mathrm{i}\xi_\alpha^{\mathrm{v'v}}\hat{J}_\alpha + \eta_{\beta\gamma}^{\mathrm{v'v}}[\hat{J}_\beta, \hat{J}_\gamma]_+ \quad (161)$$

where α, β, γ are all different. The ξ_α constants are related to the common Coriolis parameters ζ^α by

$$\xi_\alpha^{\mathrm{v'v}} = 2B_\alpha\zeta_{m,n}^\alpha\left(\sqrt{\frac{\omega_n}{\omega_m}} + \sqrt{\frac{\omega_m}{\omega_n}}\right)\left((\mathrm{v}_m + 1)\frac{\mathrm{v}_n}{4}\right)^{1/2} \quad (162)$$

in which ω_m and ω_n are the harmonic frequencies of the fundamentals, the coupling being between the $(\mathrm{v}_m, \mathrm{v}_n, \mathrm{v}_k)$ and the $(\mathrm{v}_{m+1}, \mathrm{v}_{n-1}, \mathrm{v}_k)$ states.

For anharmonic coupling, which can be of the Fermi resonance, Darling–Dennison type, or more complicated, one has

$$\hat{H}_{\mathrm{rot}}^{\mathrm{v'v}} = F + F_J\hat{J}^2 + F_{zz}\hat{J}_z^2 + F_{xy}(\hat{J}_x^2 - \hat{J}_y^2) \quad (163)$$

This introduces a rotational dependence of the anharmonic resonance. In the program WANG of Luckhaus and Quack (1989) all these couplings (and higher terms, if needed) are included. The symmetry of Hamiltonian and coupling schemes can be specified in a very simple and general way as described in the Appendix of Luckhaus and Quack (1989) which we almost literally recall here.

The number of diagonal blocks into which the Hamiltonian is split has to be specified. For each of these "symmetry blocks", a small matrix determines the mechanism that couples the different vibrational states and the Wang blocks that appear in the symmetry block. By the numbers contained in these matrices ("coupling schemes"), the program identifies the subroutines to be called for setting up the various diagonal (Wang) and off-diagonal (coupling) blocks. The diagonal numbers consist of two digits: the first one specifying the vibrational state and the second one the Wang block ($1, 2, 3, 4 = \mathrm{E}^+, \mathrm{E}^-, \mathrm{O}^+, \mathrm{O}^-$). The off-diagonal numbers stand for the type of coupling ($0, 1, 2, 3 =$ none, x-, y-, z-Coriolis coupling). The corresponding block structure of the program is very easily extended to include other types of coupling simply by assigning a new number to another subroutine containing the necessary formulae for the matrix elements.

As an example we give the coupling scheme used for the a-Coriolis interaction of the two CF-stretching fundamentals in $CH^{35}ClF_2$ (Luckhaus and Quack 1989): the lower state is identical with the vibrational ground state (state no. 1). There is no coupling and, therefore, each of the four Wang blocks forms a symmetry block by itself

11 12 13 14

The upper state consists of the two CF-stretching fundamentals ($a' : \nu_3 =$ state no. 2; $a'' : \nu_8 =$ state no. 3) coupled by a-Coriolis interaction (a-axis corresponding to z-axis in I^r representation). Neglecting the (symmetry allowed) c-Coriolis coupling (code:2) leads to four symmetry blocks containing two Wang blocks each

a':	21	3	24	3	a'':	22	3	23	3
	3	32	3	33		3	31	3	34

If c-Coriolis coupling were included, the Hamiltonian for the upper state would only split into two symmetry blocks:

a':	21	3	0	2	a'':	22	3	0	2
	3	32	2	0		3	31	2	0
	0	2	24	3		0	2	23	3
	2	0	3	33		2	0	3	34

The advantage of this method over simply setting the c-Coriolis coupling blocks equal to zero is obvious since the operations count for matrix diagonalization is roughly quadratic in the matrix dimension.

For the parameter refinement, the program uses the Marquardt (1961) algorithm (Press *et al*. 1986), a nonlinear least squares fit procedure. The required first derivatives of χ^2 (the sum of squared deviations) with respect to the spectroscopic parameters p_α are calculated analytically, using the Hellmann–Feynman theorem, i.e., the derivatives of the eigenvalues ε_i are obtained according to

$$\frac{\partial}{\partial p_\alpha}\varepsilon_i = \boldsymbol{c}_i^\dagger \left(\frac{\partial}{\partial p_\alpha}\boldsymbol{H}\right)\boldsymbol{c}_i \tag{164}$$

where ε_i is the ith eigenvalue, $\boldsymbol{c}_i$ is the ith eigenvector, $\boldsymbol{H}$ the Hamiltonian matrix, and p_α the αth spectroscopic parameter.

As long as there is no coupling between vibrational states, the usual set of rotational quantum numbers will generally provide an unambiguous assignment of a transition to a pair of eigenstates (the vibrational states involved have, of course, also to be specified). This is not true in the case of coupled vibrational states, as the energetical ordering of eigenstates belonging to different Wang blocks varies with the spectroscopic parameters. On the other hand, the ordering of rotational quantum numbers *within the same* Wang block is normally independent of the actual parameters. One, therefore, first assigns the eigenvectors of a given symmetry block (of a given J value) to the various Wang blocks, where care must be taken that the number of eigenvectors assigned to a Wang block is equal to its dimension. The sum over the squared coefficients of the corresponding basis functions serves as a criterion. Within these sets, the same correspondence between rotational quantum numbers and the eigenvalue-ordered eigenvectors as in the absence of coupling is assumed. This method guarantees a smooth transition from the cases of appreciable to those of vanishing coupling. The assignments have generally proved stable, i.e., there is no "switching" (or crossing) of assignments over a reasonable range of values of the coupling parameters.

Only assignments for which the deviations between observed and calculated wavenumbers are less than a given tolerance are considered for the calculation of χ^2 and its derivatives. The number of assignments considered changes, therefore, from one refinement cycle to the next (floating data base). Convergence is assumed for relative changes of the weighted mean square deviation (χ^2/Σ[statistical weights]) of less than 0.5×10^{-4}. This not only helps cope with typing errors in large sets of assignments but is also necessary when combining the program with a simple automatic assignment procedure.

In this case, a stick spectrum is calculated with the refined parameters and the experimental spectrum is searched for peaks coinciding within a given tolerance, with calculated transitions not yet assigned. An intensity limit helps avoid

Table 10 Spectroscopic parameters (in cm^{-1}) for the ν_3- and ν_8-fundamentals (C–F stretching) of $CH^{35}ClF_2$. Standard deviations are given in parentheses as uncertainties in the last digits (after Luckhaus and Quack 1989).

	ν_3	ν_8
$\tilde{\nu}_0$ /cm^{-1}	1108.7292(1)[a]	1127.2854(1)[a,b]
A /cm^{-1}	0.341271(39)	0.338478(38)
B /cm^{-1}	0.16226587(82)	0.16195055(61)
C /cm^{-1}	0.11616297(59)	0.11735914(52)
D_J /(10^{-6} cm^{-1})	0.02937(37)	0.05887(26)
D_{JK} /(10^{-6} cm^{-1})	0.0607(22)	0.2872(11)
D_K /(10^{-6} cm^{-1})	0.2237(71)	0.1318(83)
d_1 /(10^{-6} cm^{-1})	−0.02107(26)	−0.01081(21)
d_2 /(10^{-6} cm^{-1})	−0.01010(10)	−0.001183(92)
H_J /(10^{-12} cm^{-1})	0.227	0.227
H_K /(10^{-12} cm^{-1})	1.958	1.958
ξ_z /cm^{-1}	0.38370(94)	
rms error /cm^{-1}	0.0018	
Assignments	1424	2748
Max. J	40	51
Range/cm^{-1}	1095–1158	

[a] Corrected by a small average calibration shift of $+0.0018$ cm^{-1}.
[b] Here we correct a misprint of the original paper.

"assignment" of noise. A new fit is then performed and the whole procedure is repeated until no new assignments are found. As extrapolations beyond the range of quantum numbers for which a set of spectroscopic parameters has been optimized are rather unreliable, the simulation in each step is limited to quantum numbers only slightly higher than those already assigned. The range of assigned quantum numbers is thus extended stepwise. As the program can be run interactively, the necessary calculations can be carried out efficiently.

As an example, Table 10 gives the results for parameters obtained for the two Coriolis-coupled CF-stretching fundamentals in $CH^{35}ClF_2$ (a "dyad"). A more complicated example is provided by the tetrad of levels $2\nu_9(A')$, $2\nu_6(A')$, $\nu_6 + \nu_9(A'')$, and the fundamental $\nu_4(A')$ in that same molecule analyzed by Albert *et al.* (2006). Here, ν_4 and $2\nu_6$ are coupled by a Fermi resonance, whereas $2\nu_9$ and $2\nu_6$ are coupled to $\nu_6 + \nu_9$ by Coriolis interactions. The set of parameters obtained is given in Table 11. *See also* Snels *et al.* 2011: **High-resolution FTIR and Diode Laser Spectroscopy of Supersonic Jets**, this handbook, for an extended treatment of ν_3/ν_8 Coriolis resonance band of $CHClF_2$.

When considering the relatively large numbers of parameters in the effective Hamiltonians of this kind, one should also see the much larger number of line data analyzed in such spectra. Frequently, many thousands of lines are accurately measured and assigned and thus an enormous data set is described in a very compact form by such effective Hamiltonians. Line intensity information complements this, usually by comparing simulated and experimental data, although least squares analyses of intensities are also possible and sometimes carried out. These effective Hamiltonians can then be used for analyses of time-dependent state populations. One can also use the rotational constants in the various vibrational states to determine A_e, B_e, and C_e at the equilibrium geometry, very similar to diatomic molecules discussed in Section 2 but with added complexities. We refer here to the critical discussion of equilibrium structures of methane derived from spectra of CH_2D_2 (Ulenikov *et al.* 2006). Another approach to equilibrium structures of polyatomic molecules is to adjust parameters of a potential hypersurface in the calculation of vibrational ground-state properties and compare these with the experimental constants A_0, B_0, C_0 of the vibrational ground state (Hollenstein *et al.* 1994). Such calculations have been carried out even for high-dimensional (CH_4) and very floppy molecules (such as $(HF)_2$) (Quack and Suhm 1991). Along fairly similar lines, Gauss and Stanton (1999) have proposed computing the difference between A_e, B_e, C_e and A_0, B_0, C_0 from *ab initio* calculations combined with perturbation theory to derive semi-experimental equilibrium structures.

6 PATTERN RECOGNITION FOR SPECTROSCOPIC ASSIGNMENTS AND ANALYSIS OF ROVIBRATIONAL SPECTRA WITH LOOMIS–WOOD DIAGRAMS

6.1 General Aspects

The high-resolution rotation–vibration spectra of polyatomic molecules often show an enormous complexity, which makes assignment of the rotation–vibration states connected in a transition, the first step in any analysis, sometimes very difficult. There are several techniques that help to establish and confirm such quantum number assignments:

1. One can check the assignments by ground-state (or excited-state) combination differences, which must match to within the experimental accuracy (Section 2).
2. One can establish the symmetry assignment by means of nuclear spin statistical weights and the resulting line intensity alternations in high-resolution spectra.
3. One can simulate intensities in spectra obtained as a function of temperature and thereby gain effective information on the lower state of the observed line.

All these methods are quite widely used and the combination difference technique has even provided the basis for a

Table 11 Spectroscopic constants (in cm^{-1}) of the ν_4, $2\nu_6$, $\nu_6 + \nu_9$, and $2\nu_9$ tetrad of $CH^{35}ClF_2$ (after Albert *et al.* 2006).

	Ground state[a]	$\nu_4(A')$	$2\nu_6(A')$	$\nu_6 + \nu_9(A'')$[b]	$2\nu_9(A')$[b]
$\tilde{\nu}_0$	0.0	812.9300(45)	825.4091(45)	778.61	732.41
A	0.341392948	0.34103816(137)	0.34151924(138)	0.34218295	0.34302622
B	0.162153959	0.16119383(30)	0.16194755(30)	0.16195124	0.16197450
C	0.116995535	0.11651661(52)	0.11671129(40)	0.11658536	0.11648176
$\Delta_J/10^{-8}$	5.2247979	5.0155(35)	5.5275(30)	5.224797	5.2247979
$\Delta_{JK}/10^{-8}$	15.3149617	13.497(27)	10.741(22)	15.3149617	15.3149617
$\Delta_K/10^{-8}$	16.4159900	18.651(34)	20.507(37)	16.4159900	16.4159900
$\delta_J/10^{-8}$	1.4746802	1.4383(11)	1.4998(10)	1.4746802	1.4746802
$\delta_K/10^{-8}$	16.7271720	16.342(11)	13.4991(87)	16.7271720	16.7271720
$\Phi_J/10^{-12}$	0.02341953	0.02341953	0.02341953	0.02341953	0.02341953
$\Phi_{JK}/10^{-12}$	0.33456479	0.33456479	0.33456479	0.33456479	0.33456479
$\Phi_{KJ}/10^{-12}$	−0.03422368	−0.03422368	−0.03422368	−0.03422368	−0.03422368
$\Phi_K/10^{-12}$	0.09860155	0.09860155	0.09860155	0.09860155	0.09860155
$\phi_J/10^{-12}$	0.01093423	0.01093423	0.01093423	0.01093423	0.01093423
$\phi_{JK}/10^{-12}$	0.18072503	0.18072503	0.18072503	0.18072503	0.18072503
$\phi_K/10^{-12}$	3.05377929	3.05377929	3.05377929	3.05377929	3.05377929
F		−7.6839(36)			
$F_{zz}/10^{-3}$		1.4715(12)			
ξ_z				0.023	0.023
ξ_y				−0.218	−0.218
$\eta_{Kxz}/10^{-8}$			7.593(94)[c]		
n_{data}		2284	1590		
max J		78	78		
max K_a		30	30		
$d_{rms}/10^{-3}$		0.308	0.288		

[a] Blanco *et al.* (1996).
[b] Rotational constants and Coriolis interaction constants transferred from Kisiel *et al.* (1997).
[c] Interaction between ν_4 and $\nu_6 + \nu_9$.

computer program for automatic assignments in the Zürich group. Nevertheless, often the initial assignment is difficult and this cannot be readily carried out automatically. Here, interactive visual aids for pattern recognition can be helpful and we describe as an important example the method originally published by Loomis and Wood (1928) and now used in some laboratories.

The Loomis–Wood algorithm uses the periodicity of a recurring pattern of lines in the spectrum and organizes the lines in such a way that the periodicity is translated into emerging, recognizable, continuous patterns in the Loomis–Wood diagram. The concept of the Loomis–Wood diagram arose in 1928 (Loomis and Wood 1928): to assign the rotational structure of the blue-green bands of the diatomic molecule Na_2, Loomis and Wood plotted $\tilde{\nu}(J) - \tilde{\nu}[Q(J)]$, the difference between the observed transition and that corresponding to the Q-branch, as a function of the J quantum number for four measured bands. P- and R-branches always appear as smooth curves, nearly straight lines with different slopes.

These diagrams seem helpful but were not often used in the beginning since they are time consuming when built manually. The first significant improvement came with the development of personal computers. Scott and Rao (1966) studied the 13.7 μm region of the acetylene spectrum with the first program able to generate Loomis–Wood diagrams. Later, several interactive Loomis–Wood assignment programs were developed, including the pioneering work of Winnewisser *et al.* (1989). The so-called Giessen Loomis–Wood program was originally designed only for linear molecules (Haas *et al.* 1994, Schulze *et al.* 2000, Albert *et al.* 1996, 1997a,b, 1998, 2001) but is also useful in the analysis of spectra of asymmetric top molecules (Albert *et al.* 2003, 2004a,b, Albert and Quack 2007). The first generation of Loomis–Wood programs uses line positions and intensities to recognize spectral patterns (McNaughton *et al.* 1991, Winther *et al.* 1992, Stroh *et al.* 1992). Most of the programs were based on a DOS interface, which limits the resolution. Some programs already provided approaches to assign spectra of symmetric top molecules (Moruzzi *et al.* 1994, Brotherus 1999) and distinguish asymmetry splitting components (Moruzzi *et al.* 1998). Nowadays, the new programs take advantage of graphic tools and mouse-interactive approaches in order to make the assignment process easier. Here, we refer to the Giessen Loomis–Wood program adapted for Igor Pro (Neese 2001), the program

written by Gottselig (2004) for the Zürich group, the CAAARS package (Medvedev *et al*. 2005) and its alternative AABS (Kisiel *et al*. 2005) optimized for asymmetric top rotors, LWW (Lodyga *et al*. 2007) for symmetric rotors developed for Windows, PGOPHER (Western 2010), or ATIRS (Tasinato *et al*. 2007). Besides Loomis–Wood plots, some of these programs provide further help such as the calculation of combination differences or simulation of the experimental spectrum following a fit procedure.

In our group, we have recently developed a new package called LOOM4WANG (Albert *et al*. 2011) to plot Loomis–Wood diagrams, which has the advantage of working on Unix, Windows, and Mac platforms. The program was developed under Linux using the GTK+/Gnome Application Development suite (Version 2) package[a] for the graphical interface. For the optimization and fit procedures, the code uses the Fortran C-MINUIT package from the CERN program library (James 1998). All the C-MINUIT fitting facilities for the different expressions of the Hamiltonian operator can be used. The present version of the program can fit spectroscopic parameters of a linear molecule, taking the centrifugal distortion corrections up to the second-order into account, and the upcoming version will also be able to treat the case of symmetric top molecules. Furthermore, LOOM4WANG provides an interface for the external fit program WANG (Luckhaus and Quack 1989). All the Loomis–Wood diagrams shown in the following were generated with LOOM4WANG.

6.2 Linear Molecules

The concept of Loomis–Wood diagrams is based on the expression of the rovibrational transitions for linear molecules. Here, we detail the case of transitions for the P-branch with correction of the centrifugal distortion constants up to the first order as an example:

$$\begin{aligned}\tilde{\nu}[\mathrm{P}(J)] &= \tilde{\nu}_0 + F_{\mathrm{v}'}(J-1) - F_{\mathrm{v}''}(J) \\ &= \tilde{\nu}_0 + B_{\mathrm{v}'}J(J-1) - D_{\mathrm{v}'}(J-1)^2J^2 \\ &\quad - \left[B_{\mathrm{v}''}J(J+1) - D_{\mathrm{v}''}J^2(J+1)^2\right] \qquad (165)\end{aligned}$$

where $\tilde{\nu}_0 = G(\mathrm{v}') - G(\mathrm{v}'')$ is the band center of the vibrational transition, $B_{\mathrm{v}''}$ is the rotational constant for the lower vibrational state and $B_{\mathrm{v}'}$ for the upper vibrational state, $D_{\mathrm{v}''}$ is the correction of the centrifugal distortion to the first order for the lower vibrational state, and $D_{\mathrm{v}'}$ that for the upper vibrational state. We use the following relations

$$B_{\mathrm{v}'} = B_{\mathrm{v}''} + \Delta B \qquad (166)$$

$$D_{\mathrm{v}'} = D_{\mathrm{v}''} + \Delta D \qquad (167)$$

to rewrite equation (165) in powers of $(-J)$:

$$\begin{aligned}\tilde{\nu}[\mathrm{P}(J)] - \tilde{\nu}_0 &= (2B_{\mathrm{v}''} + \Delta B)(-J) + (\Delta B - \Delta D)(-J)^2 \\ &\quad -2(2D_{\mathrm{v}''} + \Delta D)(-J)^3 - \Delta D(-J)^4 \qquad (168)\end{aligned}$$

Equation (168) is a polynomial of fourth degree in $(-J)$. The same treatment can be done for transitions of the R-branch:

$$\tilde{\nu}[\mathrm{R}(J)] = \tilde{\nu}_0 + F_{\mathrm{v}'}(J+1) - F_{\mathrm{v}''}(J) \qquad (169)$$

Analogous to Equation (168), $\tilde{\nu}[\mathrm{R}(J)] - \tilde{\nu}_0$ can then be written as a polynomial, in $(J+1)$ this time, with the same coefficients:

$$\begin{aligned}\tilde{\nu}[\mathrm{R}(J)] - \tilde{\nu}_0 &= (2B_{\mathrm{v}''} + \Delta B)(J+1) + (\Delta B - \Delta D)(J+1)^2 \\ &\quad -2(2D_{\mathrm{v}''} + \Delta D)(J+1)^3 - \Delta D(J+1)^4 \qquad (170)\end{aligned}$$

In general, the transitions for P- and R-branches can be written as a polynomial of fourth degree in m with $m = -J$ for the P-branch and $m = J+1$ for the R-branch:

$$\tilde{\nu}_{\mathrm{LW}}(m) = \tilde{\nu}[\mathrm{P}(-m)] - \tilde{\nu}_0 \text{ for } m < 0 \qquad (171)$$

$$= \tilde{\nu}[\mathrm{R}(m-1)] - \tilde{\nu}_0 \text{ for } m \geq 1 \qquad (172)$$

with

$$\begin{aligned}\tilde{\nu}_{\mathrm{LW}}(m) &= (2B_{\mathrm{v}''} + \Delta B)m + (\Delta B - \Delta D)m^2 \\ &\quad -2(2D_{\mathrm{v}''} + \Delta D)m^3 - \Delta D m^4 \qquad (173)\end{aligned}$$

Usually, ΔB, $D_{\mathrm{v}''}$, and ΔD are several orders of magnitude smaller than $B_{\mathrm{v}''}$, which means that, in a first approximation, all the terms in m of degree higher than one are negligible compared to $2B_{\mathrm{v}''} + \Delta B$ in equation (173), at least for m values that are not very large. For example, in the case of carbonyl sulfide (OCS), the vibrational band at $\tilde{\nu}_0 = 3095.55442(9)\ \mathrm{cm}^{-1}$ has been assigned to the 12^00–00^00 transition of the main isotopomer $^{16}\mathrm{O}^{12}\mathrm{C}^{32}\mathrm{S}$ (Maki and Wells 1991); the analysis of the rotational transitions results in the following rotational constants: $B_{\mathrm{v}''} = 0.202849\,\mathrm{cm}^{-1}$, $\Delta B = 6.23025\,10^{-4}\,\mathrm{cm}^{-1}$, $D_{\mathrm{v}''} = 4.24954\,10^{-8}\,\mathrm{cm}^{-1}$, and $\Delta D = -7.14171\,10^{-9}\,\mathrm{cm}^{-1}$; in other words, terms with order higher than one are negligible up to $J = 64$.

The almost linear relationship between m and the transition (the higher order terms being negligible at first approximation) is exploited as follows: in the modern form of the Loomis–Wood diagram, the rovibrational spectrum is cut in segments of width $\sim 2B_{\mathrm{v}''}$ (actually $2B_{\mathrm{v}''} + \Delta B$) and stacked one beneath the other in order to

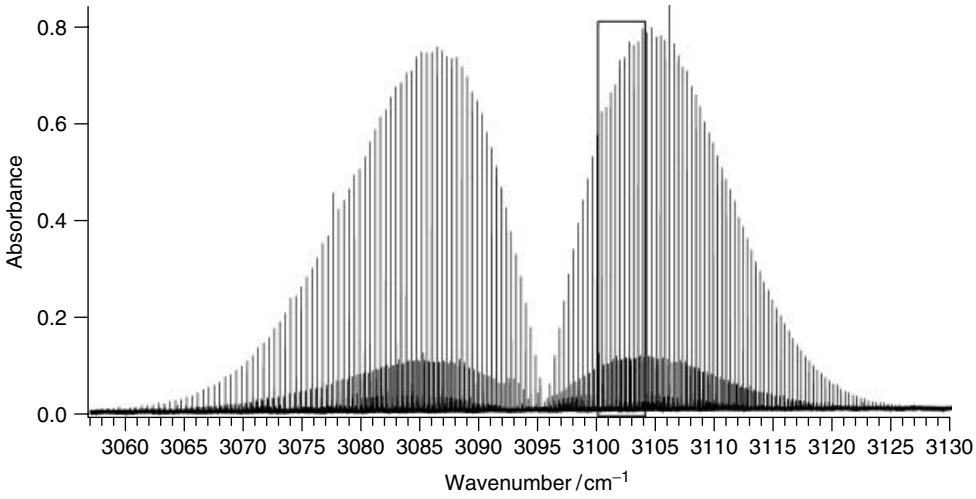

Figure 30 FTIR spectrum of OCS recorded with a White type cell of 19.2 m length with the Bruker IFS125 prototype ZP 2001 in the 3055–3130 cm^{-1} region. The box indicates the region illustrated in Figure 31 (pressure of OCS is ca 0.2 mbar, decadic absorbance $\lg(I_0/I)$ is shown).

highlight lines belonging to the same group of transitions. Figure 30 shows the FTIR spectrum of the OCS molecule in the 3055–3130 cm^{-1} region and Figure 31 shows how the $\sim 2B_{v''}$-wide slices of the 3100–3104 cm^{-1} region of the spectrum are arranged one beneath the other in order to reveal patterns in the spectrum.

The corresponding Loomis–Wood diagram constructed with the LOOM4WANG program is shown in Figure 32: the lines of the spectrum are represented by bars with lengths proportional to the intensity of the transitions in the spectrum. If a correct value of $B_{v''}$ is used, the bars corresponding to the same group of rovibrational transitions appear aligned in the Loomis–Wood diagram. The pattern at the center of Figure 32 is composed of the most intense lines of the spectrum and corresponds to the transitions of the $12^00–00^00$ band of the main isotopomer $^{16}O^{12}C^{32}S$.

The top of the diagram corresponds to the lower end of the spectral range shown in Figure 30, and as the wavenumber increases from left to right in Figure 30, it increases from top to bottom by row in Figure 32. Therefore, the top half of the diagram illustrates transitions lower than the band center $\tilde{\nu}_0$, i.e., the P-branch, and the bottom half of the diagram shows transitions higher than the band center, i.e., the R-branch. The closer the transition to the center of the diagram, the lower is the J value. Figures 33(a) and (b) illustrate the effect of neglecting the correction of the centrifugal distortion: the deviation from the vertical straight line for large J values (tails of the plot) in Figure 33(a) indicates the limitations of the linear approximation of the polynomial because $D_{v''}$ as well as ΔD were set to zero in Figure 33(a), whereas they were optimized in 33(b), all other parameters being kept the same.

For larger molecules, a more exact description of the transition, taking into account the correction of the centrifugal distortion constants up to the second or even higher order, may be required; it leads to a polynomial of at least the sixth degree in m:

$$\begin{aligned}\tilde{\nu}_{LW}(m) = {} & (2B_{v''} + \Delta B)m + (\Delta B - \Delta D)m^2 \\ & - 2(2D_{v''} + \Delta D - H_{v''} - \Delta H/2)m^3 \\ & + (3\Delta H - \Delta D)m^4 + 3(2H_{v''} + \Delta H)m^5 \\ & + \Delta H m^6 \\ & + \cdots \end{aligned} \tag{174}$$

$H_{v''}$ is the correction of the centrifugal distortion to the second order in the lower vibrational state, and $H_{v'}$ is that in the upper vibrational state with $\Delta H = H_{v'} - H_{v''}$. These terms are smaller than $D_{v''}$ and ΔD, which does not change the interpretation of the Loomis–Wood diagram.

Plotting the same Loomis–Wood diagram as in Figure 34, one beside the other three times, allows the user to recognize the continuity of the patterns. They are of weaker intensity and with different slopes: these patterns have been assigned to the splitting of the 131–010 transition (see Maki and Wells 1991 and references therein). Since $v_2'' > 0$, $l > 0$, the state is split into e and f components of l, corresponding to the B and C branches on the diagram (Figure 34).

Obviously, the interpretation of the spectrum of a linear molecule such as OCS is one of the simplest cases for a Loomis–Wood plot and may not require such graphical tools to get the proper assignment. This section has illustrated the key points of the Loomis–Wood diagram, which can be useful for more complex spectra.

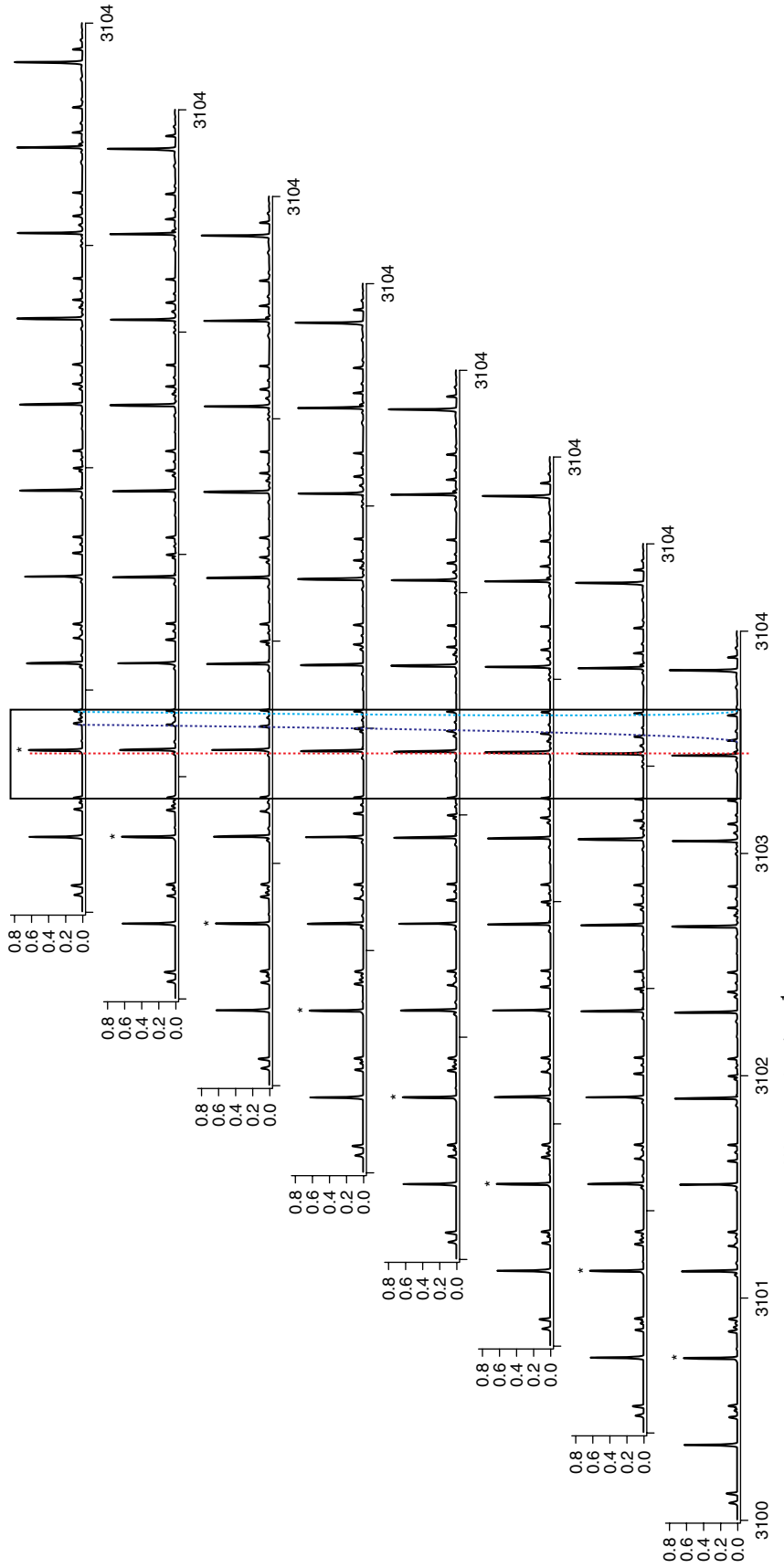

Figure 31 Superposition of slices of a section of the FTIR spectrum of OCS as indicated in Figure 30 in order to obtain the patterns aligned for a Loomis–Wood diagram. The star indicates the first line considered in this pattern here and is repeated on each slice to make the displacement of the spectrum clear. Only the indicated box is retained for the Loomis–Wood diagram shown in Figure 32.

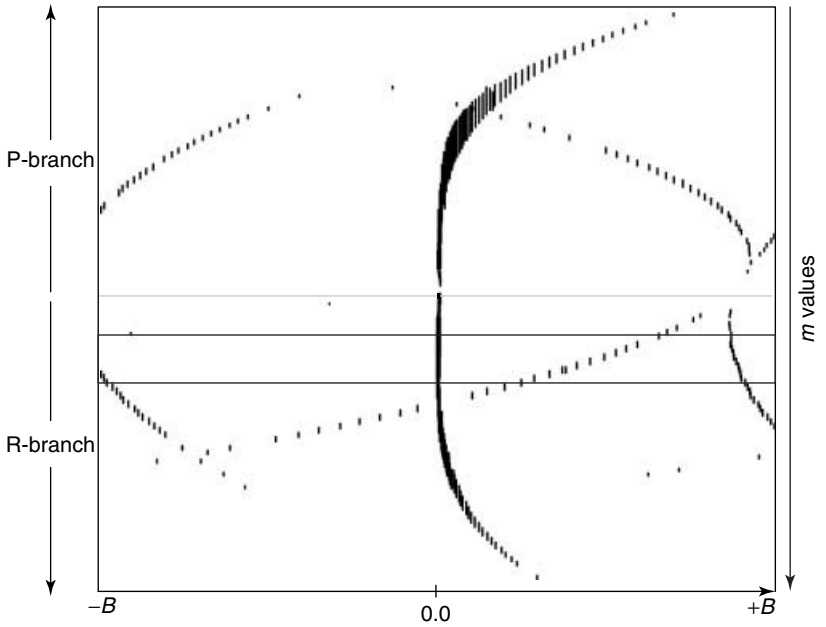

Figure 32 Loomis–Wood diagram of the FTIR spectrum of OCS shown in Figure 30. The box indicates the spectral region selected in Figure 30. The spectroscopic parameters are as follows: $\tilde{\nu}_0 = 3095.55442\ \text{cm}^{-1}$, $B = 0.2028567408\ \text{cm}^{-1}$, and $\Delta B = -0.0005455008\ \text{cm}^{-1}$.

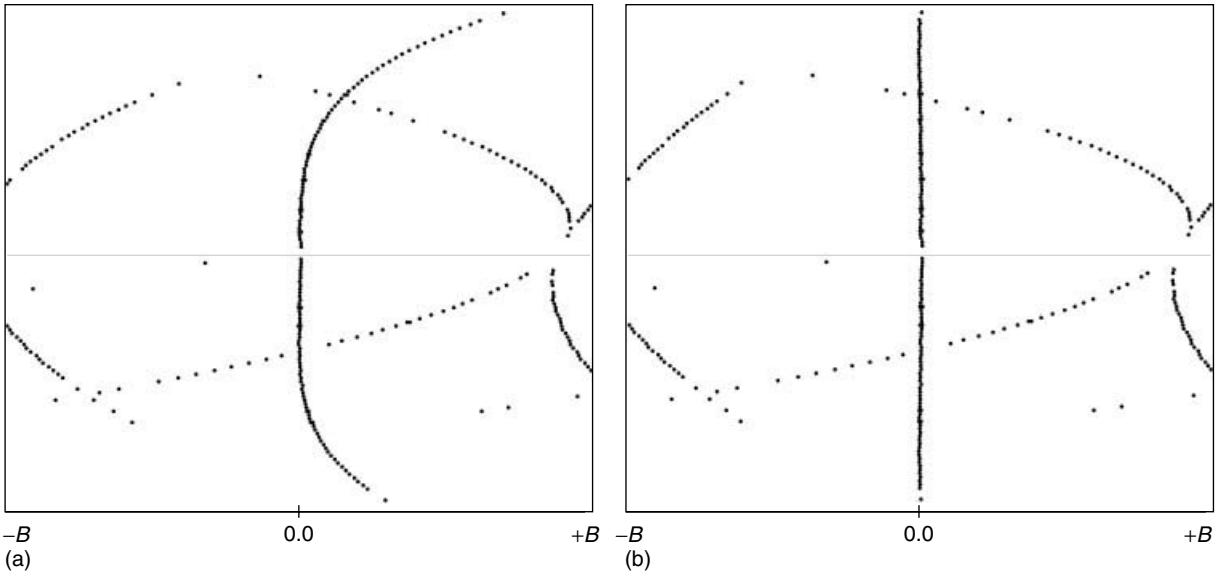

Figure 33 Loomis–Wood diagram of the FTIR spectrum of OCS shown in Figure 30. The spectroscopic parameters are as follows: $\tilde{\nu}_0 = 3095.55442\ \text{cm}^{-1}$, $B = 0.2028567408\ \text{cm}^{-1}$, and $\Delta B = -0.0005455008\ \text{cm}^{-1}$. (a) $D = 0\ \text{cm}^{-1}$ and $\Delta D = 0\ \text{cm}^{-1}$; (b) $D = 4.409752\,10^{-8}\ \text{cm}^{-1}$, and $\Delta D = -5.7191468\,10^{-9}\ \text{cm}^{-1}$.

6.3 Nonlinear Molecules

Each type of molecule has its own selection rules and, therefore, displays different patterns in Loomis–Wood diagrams. In this section, we describe how we can anticipate the Loomis–Wood plot patterns of nonlinear molecules, on the basis of that observed for linear molecules.

6.3.1 Symmetric Top Molecules

Here we discuss the case of the prolate symmetric top ($A > B = C$), and that for the oblate symmetric top ($A = B > C$) can be easily obtained by analogy (see below). Two kinds of bands are observable: parallel ($\Delta K = 0$ and

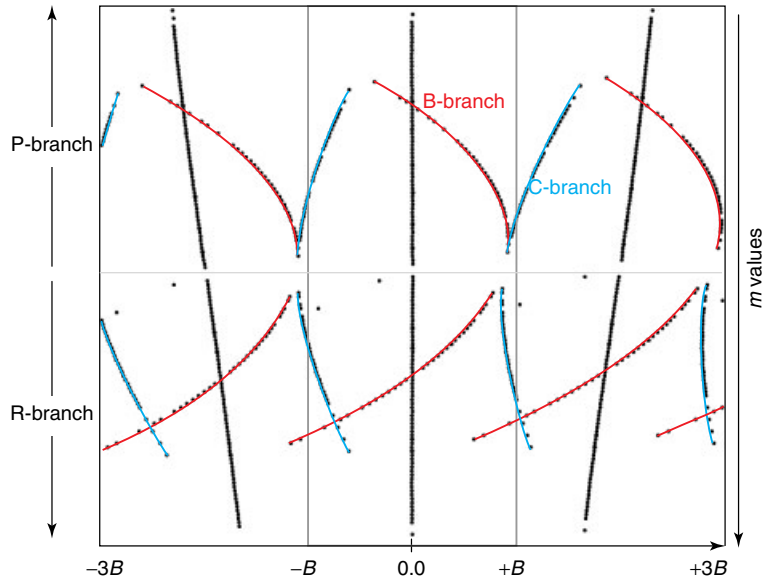

Figure 34 Loomis–Wood diagram of the FTIR spectrum of OCS shown in Figure 30 reproduced three times. The spectroscopic parameters are as follows: $\tilde{\nu}_0 = 3095.55442\ \text{cm}^{-1}$, $B = 0.2028567408\ \text{cm}^{-1}$, $\Delta B = -0.0005455008\ \text{cm}^{-1}$, $D = 4.409752\,10^{-8}\ \text{cm}^{-1}$, and $\Delta D = -5.7191468\,10^{-9}\ \text{cm}^{-1}$.

Table 12 Rotational constants (in cm^{-1}) of the ground state and the ν_1 state of CH_3I (after Paso and Antilla 1990).

Rotational constant X	Ground state	ν_1 state	$\Delta X = X_{\nu_1} - X''$
A	5.173931	5.121724	-52.207×10^{-3}
B	0.250215625	0.250167425	-0.0482×10^{-3}
D_J	0.2103983×10^{-6}	0.2118883×10^{-6}	1.49×10^{-9}
D_{JK}	3.294545×10^{-6}	3.254545×10^{-6}	-0.04×10^{-6}
D_K	87.34×10^{-6}	88.06×10^{-6}	0.72×10^{-6}

$\Delta J = \pm 1$ for $K = 0$, or $\Delta J = 0, \pm 1$ for $K \neq 0$), and perpendicular ($\Delta K = \pm 1$, $\Delta J = 0, \pm 1$).

The expression of the rotational term value is

$$F_v(J, K)_{\text{prolate}} = B_v J(J+1) + (A_v - B_v)K^2 - D_{J_v} J^2 \times (J+1)^2 - D_{JK_v} J(J+1)K^2 - D_{K_v} K^4 \quad (175)$$

where we have considered the centrifugal distortion correction up to the first order to simplify the mathematical treatment.

Parallel Band

In the case of parallel bands, the transition for the Loomis–Wood diagram can be written as follows for both P- and R-branches:

$$\tilde{\nu}_{LW}(m) = (2B_{v''} + \Delta B + \Delta D_{JK} K^2)m + (\Delta B - \Delta D_J - \Delta D_{JK} K^2)m^2 - 2(2D_{J''} + \Delta D_J)m^3 - \Delta D_J m^4 + (\Delta A - \Delta B)K^2 - \Delta D_K K^4 \quad (176)$$

For $K = 0$, the equation is analogous to equation (173) obtained in the case of the linear molecule as discussed in Section 6.2 with $D_{J''} = D_{v''}$, and therefore we expect a pattern similar to that shown in Figure 32 for the OCS molecule. Regarding $K \neq 0$, for each K value, we get a new pattern in the Loomis–Wood diagram, shifted from $(\Delta A - \Delta B)K^2 - \Delta D_K K^4$ compared to the $K = 0$ pattern. Since $(\Delta A - \Delta B)$ is generally much larger than ΔD_K, as soon as the $K = 0$ and $K = 1$ patterns are identified, the other are shifted by roughly K^2 times the difference between the $K = 0$ and $K = 1$ patterns. For instance, Table 12 lists the spectroscopic constants of the ν_1 band of the symmetric top molecule CH_3I. In this case, ΔD_{JK} is seven orders of magnitude smaller than $2B_{v''} + \Delta B$, and up to $K = 300$, $\Delta D_{JK} K^2$ is negligible compared to $2B_{v''} + \Delta B$: the patterns appear with almost the same slope as that for $K = 0$. The deviation from the "straight line", however, starts at lower J values with increasing K value since ΔD_J is only two orders of magnitude smaller than $2D_{J''}$ (third power of m in equation (176)).

Regarding the oblate symmetric top molecules, one has to replace $(A_v - B_v)$ in equation (175) by $(C_v - B_v)$, which leads to

$$F_v(J, K)_{\text{oblate}} = B_v J(J+1) + (C_v - B_v)K^2 - D_{J_v} J^2(J+1)^2 - D_{JK_v} J(J+1)K^2 - D_{K_v} K^4 \quad (177)$$

and the corresponding transition for the Loomis–Wood diagram:

$$\tilde{\nu}_{\text{LW}}(m) = (2B_{v''} + \Delta B + \Delta D_{JK} K^2)m + (\Delta B - \Delta D_J - \Delta D_{JK} K^2)m^2 - 2(2D_{J''} + \Delta D_J)m^3 - \Delta D_J m^4 + (\Delta C - \Delta B)K^2 - \Delta D_K K^4 \quad (178)$$

The treatment of the Loomis–Wood diagram is, therefore, exactly the same as for prolate symmetric top molecules.

Since the $\Delta J = 0$ transitions are allowed for $K \neq 0$, one could wonder how the Q-branches are handled in a Loomis–Wood diagram:

$$\begin{aligned}\tilde{\nu}[\text{Q}(J)] - \tilde{\nu}_0 &= F_{v'}(J, K) - F_{v''}(J, K) \\ &= B_{v'} J(J+1) + (A_{v'} - B_{v'})K^2 \\ &\quad - D_{J_{v'}} J^2(J+1)^2 - D_{JK_{v'}} J(J+1)K^2 \\ &\quad - D_{K_{v'}} K^4 - [B_{v''} J(J+1) + (A_{v''} - B_{v''})K^2 \\ &\quad - D_{J_{v''}} J^2(J+1)^2 - D_{JK_{v''}} J(J+1)K^2 \\ &\quad - D_{K_{v''}} K^4] \end{aligned} \quad (179)$$

$$\begin{aligned}\tilde{\nu}[\text{Q}(J)] - \tilde{\nu}_0 &= (\Delta B - \Delta D_{JK} K^2)J + (\Delta B - \Delta D_J - \Delta D_{JK} K^2)J^2 \\ &\quad - (2\Delta D_J)J^3 - (\Delta D_J)J^4 + [(\Delta A - \Delta B) \\ &\quad - \Delta D_K]K^4 \end{aligned} \quad (180)$$

Here again, the Loomis–Wood term can be considered to be a polynomial of fourth degree in m with $m = J$, but the coefficients of the first and third powers are different than those in equation (176). Since for the first power of the polynomial, ΔB is much smaller than the largest term $2B_{v''}$ found in the other expressions of $\tilde{\nu}[\text{P}(J)] - \tilde{\nu}_0$ and $\tilde{\nu}[\text{R}(J)] - \tilde{\nu}_0$, the pattern of the Q-branch appears as a horizontal line in the center of the diagram and cannot be as easily assigned with the help of the Loomis–Wood diagram as the P- and R-branches. Other programs have been developed to analyze this part of the spectrum, for example, QBRASS (Stroh 1991).

Perpendicular band

Here, we discuss the characteristics of the Loomis–Wood plot by comparing it to that corresponding to a parallel band. In the case of a perpendicular band, the transition can be written as follows:

$$\begin{aligned}\tilde{\nu}_{\text{LW}}(m) &= [2B_{v''} + \Delta B + \Delta D_{JK}(K \pm 1)^2 - D_{JK''} \times (2K \pm 1)]m + [\Delta B - \Delta D_J - (\Delta D_{JK} \times (K \pm 1)^2 - D_{JK''}(2K \pm 1))]m^2 - 2(2D_{J''} + \Delta D_J)m^3 - \Delta D_J m^4 + (\Delta A - \Delta B) \\ &\quad \times (K \pm 1)^2 - (A_{v''} - B_{v''})(2K \pm 1) - \Delta D_K(K \pm 1)^4 - D_{K''}(2K \pm 1)[K^2 + (K \pm 1)^2] \end{aligned} \quad (181)$$

with $\Delta K = \pm 1$, $m = -J$ for the P-branch and $m = (J + 1)$ for the R-branch.

Given the rotational constant X in equation (176) for a parallel band, $\Delta X K^2$ is replaced by $\Delta X(K \pm 1)^2 - X(2K \pm 1)$ in equation (181) for a perpendicular band. In this case, the added correction $-X(2K \pm 1)$ may be larger than the term $\Delta X(K \pm 1)^2$ itself. Moreover, this correction may be nonnegligible for the low powers of m in the polynomial. Therefore, no more straight line–like patterns can be expected, as seen in the Loomis–Wood plot for a parallel band, although patterns should still be recognizable. The main component of the distance to the band center $\tilde{\nu}_0$ is proportional to $D_{K''} K^3$: patterns with different values of K start at different slices of the spectrum in the diagram, and are apparently similar to those at different m values when the parameters of the diagram are optimized for a parallel band. For an oblate symmetric top molecule, the transition can be written as follows:

$$\begin{aligned}\tilde{\nu}_{\text{LW}}(m) &= [2B_{v''} + \Delta B + \Delta D_{JK}(K \pm 1)^2 - D_{JK''}(2K \pm 1)]m + [\Delta B - \Delta D_J - (\Delta D_{JK}(K \pm 1)^2 - D_{JK''}(2K \pm 1))]m^2 - 2(2D_{J''} + \Delta D_J)m^3 - \Delta D_J m^4 + (\Delta C - \Delta B)(K \pm 1)^2 - (C_{v''} - B_{v''})(2K \pm 1) - \Delta D_K(K \pm 1)^4 - D_{K''}(2K \pm 1) \times [K^2 + (K \pm 1)^2] \end{aligned} \quad (182)$$

6.3.2 *Spherical Top Molecules*

The similarity in the expressions for the rotational energy of a spherical top and that of a linear molecule makes the analysis of the spherical top's Loomis–Wood plot easier.

Indeed, a spherical top molecule can be considered to be the limiting case of a symmetric top molecule with $I_a = I_b = I_c$ (i.e., $A = B = C$) with all coefficients of K^2 in the expression of the term value equal to zero:

$$F_v(J, K)_{\text{sph. top}} = B_v J(J+1) - D_{J_v} J^2(J+1)^2 \quad (183)$$

In equation (183), we have once again considered the centrifugal distortion correction up to the first order to simplify the mathematical treatment. This equation is the same as that used in the case of linear molecules. The Loomis–Wood diagram of a spherical top molecule should, therefore, look similar to that of a linear molecule as described in Section 6.2.

6.3.3 Asymmetric Top Molecules

The case of asymmetric top molecules may seem to be the most complicated because the K degeneracy of the symmetric top is removed. The three kinds of allowed transitions are defined with J, K_a, and K_c:

$$\Delta J = \pm 1, \quad \Delta K_a = 0, \pm 2, \pm 4 \ldots, \quad \Delta K_c = \pm 1, \pm 3, \pm 5 \ldots, \text{ for } K_a = 0 \text{ and} \quad (184)$$

$$\Delta J = 0, \pm 1, \quad \Delta K_a = 0, \pm 2, \pm 4 \ldots, \quad \Delta K_c = \pm 1, \pm 3, \pm 5 \ldots, \text{ for } K_a \neq 0 \quad (185)$$

for a-type transitions,

$$\Delta J = \pm 1, \quad \Delta K_a = \pm 1, \pm 3, \pm 5 \ldots \quad \Delta K_c = \pm 1, \pm 3, \pm 5 \ldots \quad (186)$$

for b-type transitions, and

$$\Delta J = \pm 1, \quad \Delta K_a = \pm 1, \pm 3, \pm 5 \ldots, \quad \Delta K_c = 0, \pm 2, \pm 4 \ldots \text{ for } K_c = 0, \text{ and} \quad (187)$$

$$\Delta J = 0, \pm 1, \quad \Delta K_a = \pm 1, \pm 3, \pm 5 \ldots, \quad \Delta K_c = 0, \pm 2, \pm 4 \ldots \text{ for } K_c \neq 0 \quad (188)$$

for c-type transitions.

The second reason for the complexity of the treatment is the term W_τ in the expression of the rotational energy:

$$F(J_\tau) = \frac{(B+C)}{2} J(J+1) + \left[A - \frac{(B+C)}{2} \right] W_\tau \quad (189)$$

where τ is the subscript added to take the K-type doubling into account ($-J \leq \tau \leq J$) and W_τ is a function of the rotational constants A, B, and C and the quantum number J. For more details, see the algebraic expressions for $J = 0 - 6$ in Herzberg (1945) and citations therein. Nevertheless, it is sometimes possible, in the first approximation, for the analysis (and not for the determination of the rotational constants) to consider the molecule as a nearly symmetric top. In this case, the Loomis–Wood diagram is quite similar to that of a symmetric top molecule; $a-$ (respectively $b-$ and $c-$) type bands of an asymmetric top exhibit similar patterns to those of a parallel (respectively perpendicular) band of a symmetric top molecule. To illustrate this point, we discuss the case of CHD_2I, a molecule belonging to the C_s point group. Figure 35 shows the structure of the molecule with the principal axes a, b, and c.

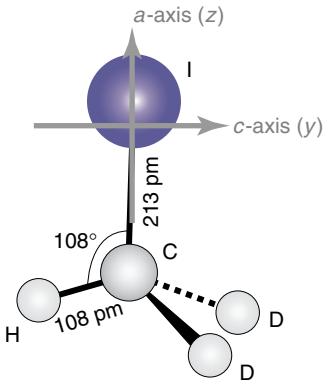

Figure 35 Illustration of the CHD_2I molecule and its principal axis system. The ac plane defines the C_s symmetry plane in the plane of the page, the b axis being perpendicular to the ac plane. The equilibrium geometry parameters are from *ab initio* calculations by Horká *et al*. (2008). [Reproduced with permission from Albert *et al*. 2010.]

The asymmetry parameter κ of CHD_2I defined by equation (190)

$$\kappa = \frac{2B - A - C}{A - C} \quad (190)$$

is close to -1 (-0.9978; Riter and Eggers 1966); therefore, the molecule can be considered to be a nearly prolate symmetric top. Figure 36 shows an overview of the ν_1 band of CHD_2I corresponding to the CH-stretching component (Albert *et al*. 2010). Typical features of an a/c-type hybrid band are visible: the more intense a-type transitions form the central Q-branch and the almost symmetric P- and R-branches are well resolved. The c-type transitions are detectable due to the strong $^{\Delta K_a = \pm 1}$Q-branches spaced by more than 5 cm^{-1}. The most intense region of the spectrum has already been assigned (Hodges and Butcher 1996) and data presented here include a larger spectral range.

The Loomis–Wood diagram of the a-type transitions of the ν_1 band is shown in Figure 37 in the approximation of a linear molecule Hamiltonian. In this case, each almost straight pattern corresponds to the P-(top half of the

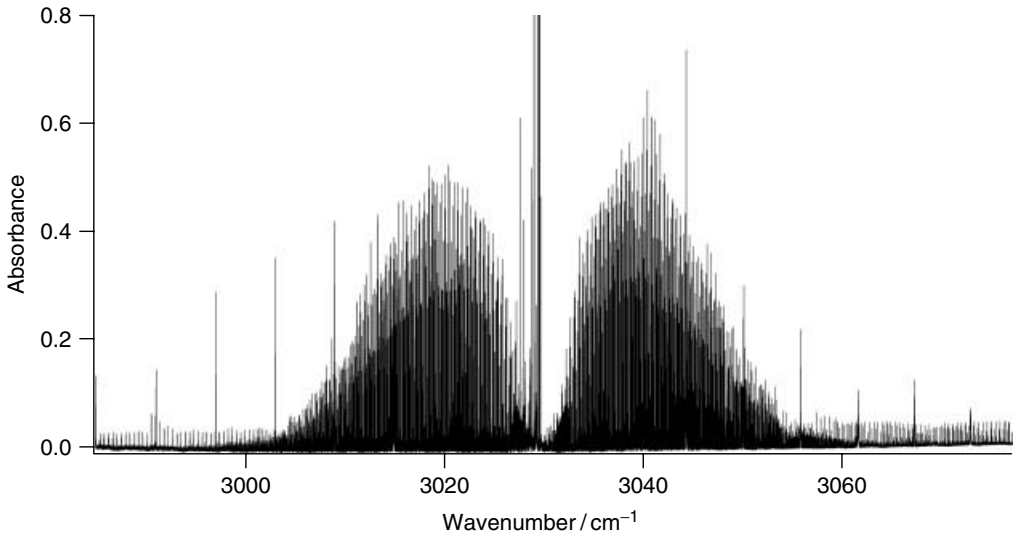

Figure 36 Overview of the FTIR spectrum of CHD_2I in the ν_1 region recorded in a White-type cell of 9.6 m length with the Bruker IFS125 prototype ZP 2001. [Reproduced with permission from Albert *et al*. (2010).]

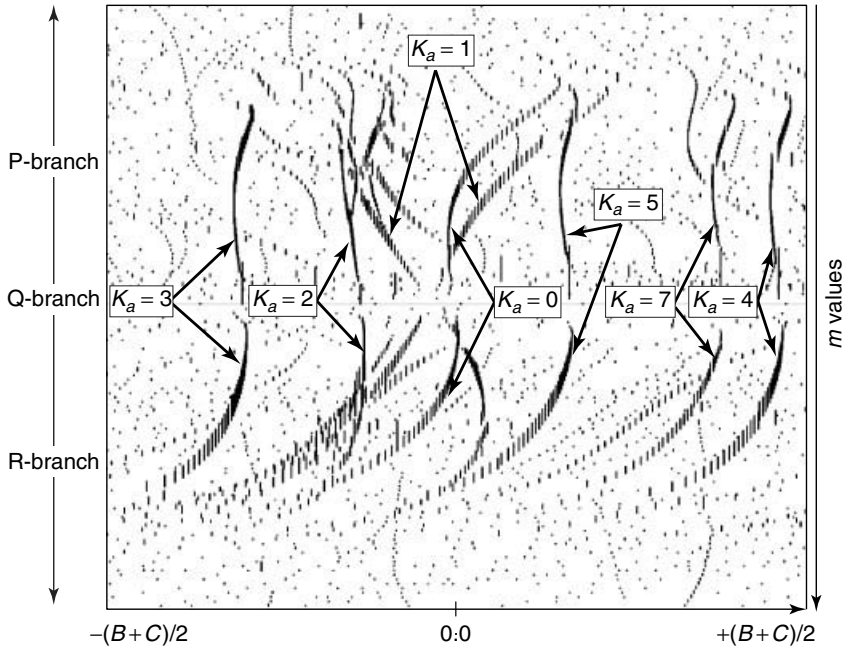

Figure 37 Loomis–Wood diagram of the a-type transitions of the ν_1 band of CHD_2I. The following parameters were used: $\tilde{\nu}_0 = 3029.68\ \text{cm}^{-1}$, $(B+C)/2 = 0.215\ \text{cm}^{-1}$, $\Delta[(B+C)/2] = 2.006\,10^{-6}\ \text{cm}^{-1}$, $D = 0\ \text{cm}^{-1}$, and $\Delta D = 0\ \text{cm}^{-1}$. [Reproduced with permission from Albert *et al*. 2010.]

diagram) and R-(bottom half of the diagram) branches of a-type transitions with the same K_a value; they are similar to those expected for a parallel band of a prolate symmetric top with the spacing between a given K_a pattern and the $K_a = 0$ pattern roughly proportional to K_a^2. The difference from a Loomis–Wood diagram of a prolate symmetric top is due to the asymmetry splittings ($K_a + K_c = J$ or $J+1$) observed for low K_a values ($K_a = 1, 2$): each P- and R-branch pattern is split into two components.

Figure 38 shows a larger view of the Loomis–Wood diagram of Figure 37, in which weaker patterns corresponding to the P-and R-branches of the c-type transitions are also visible. The middle part of the diagram corresponds to the a-type transitions discussed above. The curved patterns observed at the top of the diagram correspond to the

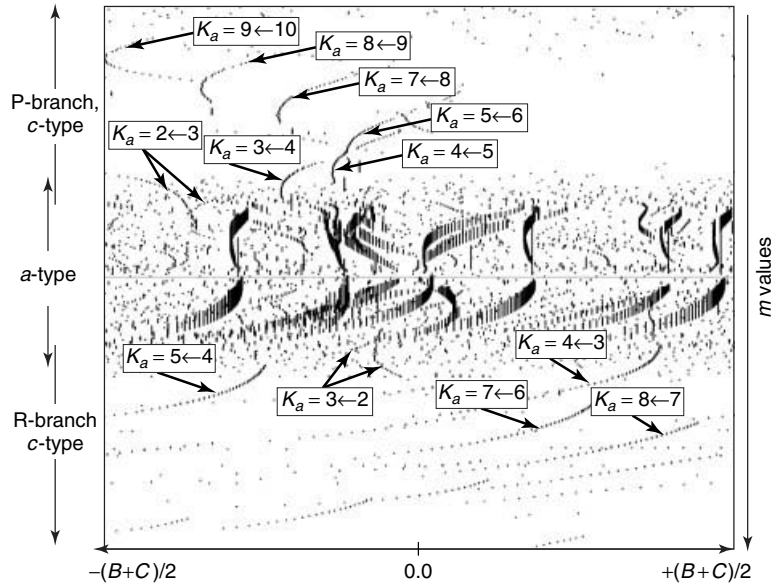

Figure 38 Loomis–Wood diagram of the *a*- (in the middle of the diagram) and *c*-type transitions (above the *a*-type transitions for the P-branch and below for the R-branch, respectively) of the ν_1 band of CHD_2I. The following parameters were used: $\tilde{\nu}_0 = 3029.68\ \text{cm}^{-1}$, $(B + C)/2 = 0.215\ \text{cm}^{-1}$, $\Delta[(B + C)/2] = 2.006\,10^{-6}\ \text{cm}^{-1}$, $D = 0\ \text{cm}^{-1}$, and $\Delta D = 0\ \text{cm}^{-1}$. [Reproduced with permission from Albert *et al*. 2010.]

P-branches of the *c*-type transitions, while those on the bottom of the diagram correspond to the R-branches. They are similar to those expected for a perpendicular band of a prolate symmetric top. The lines in a given pattern have the same $K'_a \leftarrow K''_a$ value but not the same K''_c (and therefore K'_c) value; the *c*-type patterns are no longer almost straight like the *a*-type patterns because of the correction in the expression of the transitions due to $\Delta K_a \neq 0$ compared to the linear molecule Hamiltonian approximation used to plot the Loomis–Wood diagram.

Figure 39 shows the same Loomis–Wood diagram as Figure 37, without taking the intensity of the spectral lines into account. This makes it possible to highlight small deviations observed from the smoothed patterns: these are

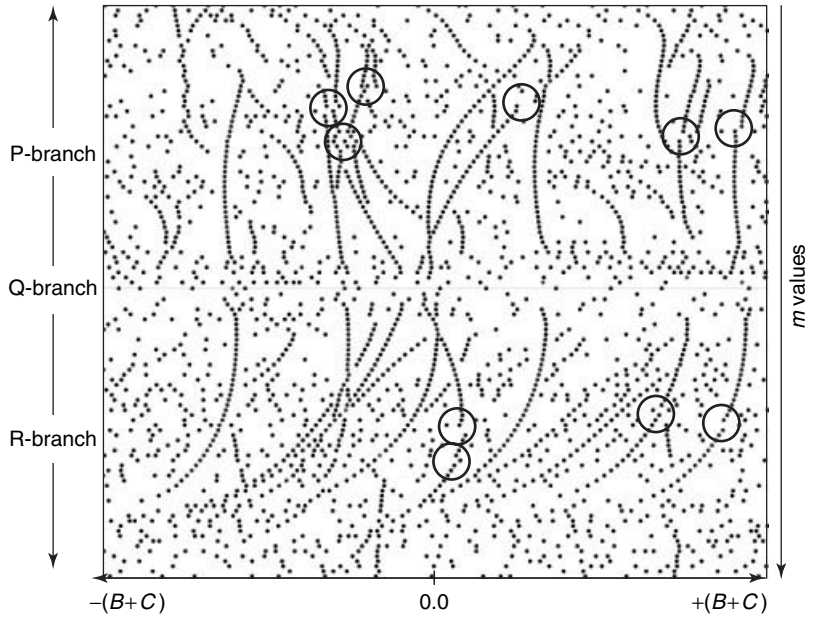

Figure 39 Loomis–Wood diagram of the *a*-type transitions of the ν_1 fundamental of CHD_2I. The diagram is obtained with the same parameters as in Figure 37. Circles highlight some of the weak resonances observed.

local resonances that can be revealed by Loomis–Wood diagrams. They prove the existence of at least one other vibrational state interacting with the ν_1 state, which must also be considered during the fitting procedure as discussed in Section 5.3.

7 CONCLUDING REMARKS

At high resolution, molecular rotation–vibration spectra contain an enormous amount of information on molecular structures and vibrational and rotational quantum motions. This information is encoded in spectral line intensities and positions, which can frequently be measured with stunning precision. In addition, the amount of information can be quantitatively enormous and involves the necessity of analyzing thousands and tens of thousands of rovibrational transitions. We have discussed here some of the fundamental aspects, ranging from the basic concepts for the relatively simple case of diatomic molecules to the tools available for analyzing the great complexity of the spectra of polyatomic molecules. Many of the other articles in this handbook provide further insight at the current level of research in this exciting area of spectroscopy.

ACKNOWLEDGMENTS

Our work is supported by ETH Zürich and the Schweizerischer Nationalfonds.

END NOTE

[a.] http://developer.gnome.org/.

ABBREVIATIONS AND ACRONYMS

BO	Born–Oppenheimer
DVR	discrete variable representations
FTIR	fourier transform infrared
GSCDs	ground-state combination differences
IR	infrared
MW	microwave

REFERENCES

Albert, S., Albert, K.K., and Quack, M. (2003) Very high resolution studies of chiral molecules with a Bruker IFS 120 HR: the rovibrational spectrum of CDBrClF in the range 600–2300 cm^{-1}. *Trends in Optics and Photonics*, **84**, 177–180.

Albert, S., Albert, K., and Quack, M. (2004a) Rovibrational analysis of the ν_4 and $\nu_5 + \nu_9$ bands of $CHCl_2F$. *Journal of Molecular Structure*, **695–696**, 385–394.

Albert, S., Albert, K.K., and Quack, M. (2011) High-resolution Fourier transform infrared spectroscopy, in *Handbook of High-resolution Spectroscopy*, Quack, M. and Merkt, F. (eds), John Wiley & Sons, Ltd., Chichester, UK.

Albert, S., Albert, K.K., Winnewisser, M., and Winnewisser, B.P. (1998) The rovibrational overtone spectrum of $H^{13}CNO$ up to 3600 cm^{-1}: a network of resonance systems. *Berichte der Bunsengesellschaft für Physikalische Chemie*, **102**(10), 1428–1448.

Albert, S., Albert, K.K., Winnewisser, M., and Winnewisser, B.P. (2001) The FT-IR spectrum of $H^{13}C^{15}NO$ in the ranges 1800–3600 and 6300–7000 cm^{-1}. *Journal of Molecular Structure*, **599**(1–3), 347–369.

Albert, S., Hollenstein, H., Quack, M., and Willeke, M. (2004b) Doppler-limited FTIR spectrum of the $\nu_3(a')/\nu_8(a'')$ Coriolis resonance dyad of $CHClF_2$: analysis and comparison with *ab initio* calculations. *Molecular Physics*, **102**(14–15), 1671–1686.

Albert, S., Hollenstein, H., Quack, M., and Willeke, M. (2006) Rovibrational analysis of the ν_4, $2\nu_6$ Fermi resonance band of $CH^{35}ClF_2$ by means of a polyad Hamiltonian involving the vibrational levels ν_4, $2\nu_6$, $\nu_6 + \nu_9$ and $2\nu_9$, and comparison with *ab initio* calculations. *Molecular Physics*, **104**(16–17), 2719–2735.

Albert, S., Keppler Albert, K.K., Manca Tanner, C., Mariotti, F., and Quack, M. (2011) in preparation.

Albert, S., Manca Tanner, C., and Quack, M. (2010) High resolution spectrum and rovibrational analysis of the ν_1CH-stretching fundamental in CHD_2I. *Molecular Physics*, **108**(18), 2403–2426.

Albert, S. and Quack, M. (2007) High resolution rovibrational spectroscopy of pyrimidine. Analysis of the B_1 modes ν_{10b} and ν_4 and the B_2 mode ν_{6b}. *Journal of Molecular Spectroscopy*, **243**(2), 280–291.

Albert, S., Winnewisser, M., and Winnewisser, B.P. (1996) Networks of anharmonic resonance systems in the rovibrational overtone spectra of the quasilinear molecule HCNO. *Berichte der Bunsengesellschaft für Physikalische Chemie*, **100**(11), 1876–1898.

Albert, S., Winnewisser, M., and Winnewisser, B.P. (1997a) The colorful world of quasilinearity as revealed by high resolution molecular spectroscopy. *Mikrochimica Acta*, **14**, 79–88.

Albert, S., Winnewisser, M., and Winnewisser, B.P. (1997b) The ν_1, ν_2, $2\nu_3$, $\nu_2 + \nu_3$ band systems and the overtone region of HCNO above 4000 cm^{-1}: a network of resonance systems. *Berichte der Bunsengesellschaft für physikalische Chemie*, **101**(8), 1165–1186.

Albritton, D.L., Schmeltekopf, A.L., and Zare, R.N. (1976) An Introduction to the Least Squares fitting of spectroscopic data, in *Molecular Spectroscopy: Modern Research*, Rao, K.N. (ed), Academic Press, New York, pp. 1–67, Vol. II.

Aliev, M.R. and Watson, J.K.G. (1985) Higher-order effects in the vibration-rotation spectra of semirigid molecules, in *Molecular Spectroscopy: Modern Research*, Rao, K.N. (ed), Academic Press, New York, pp. 2–67, Vol. III.

Amano, T. (2011) High-resolution microwave and infrared spectroscopy of molecular cations, in *Handbook of High-resolution Spectroscopy*, Quack, M. and Merkt, F. (eds), John Wiley & Sons, Ltd., Chichester, UK.

Amat, G., Nielsen, H.H., and Tarrago, G. (1971) *Rotation-vibration of Polyatomic Molecules: Higher Order Energies and Frequencies of Spectral Transitions*, Dekker, New York.

Amos, R.D., Gaw, J.F., Handy, N.C., and Carter, S. (1988) The accurate calculation of molecular-properties by *ab initio* methods. *Journal of the Chemical Society-Faraday Transactions II*, **84**(9), 1247–1261.

Amrein, A., Dübal, H.R., and Quack, M. (1985) Multiple anharmonic resonances in the vibrational overtone spectra of $CHClF_2$. *Molecular Physics*, **56**(3), 727–735.

Amrein, A., Luckhaus, D., Merkt, F., and Quack, M. (1988a) High-resolution FTIR spectroscopy of $CHClF_2$ in a supersonic free jet expansion. *Chemical Physics Letters*, **152**(4–5), 275–280.

Amrein, A., Quack, M., and Schmitt, U. (1988b) High-resolution interferometric Fourier transform infrared absorption spectroscopy in supersonic free jet expansions: carbon monoxide, nitric oxide, methane, ethyne, propyne, and trifluoromethane. *Journal of Physical Chemistry*, **92**(19), 5455–5466.

Bačić, Z. and Light, J.C. (1989) Theoretical methods for rovibrational states of floppy molecules. *Annual Review of Physical Chemistry*, **40**, 469–498.

Baggott, J., Chuang, M., Zare, R.N., Dübal, H.R., and Quack, M. (1985) Structure and dynamics of the excited CH—chromophore in $(CF_3)_3CH$. *Journal of Chemical Physics*, **82**(3), 1186–1194.

Baggott, J.E., Clase, H.J., and Mills, I.M. (1986) Overtone band shapes and IVR: C-H stretch overtones in $CHCl_3$. *Journal of Chemical Physics*, **84**(8), 4193–4195.

Bauder, A. (2011) Fundamentals of rotational spectroscopy, in *Handbook of High-resolution Spectroscopy*, Quack, M. and Merkt, F. (eds), John Wiley & Sons, Ltd., Chichester, UK.

Beil, A., Luckhaus, D., Marquardt, R., and Quack, M. (1994) Intramolcular energy transfer and vibrational redistribution in chiral molecules: experiment and theory. *Faraday Discuss*, **99**, 49–76.

Beil, A., Luckhaus, D., Quack, M., and Stohner, J. (1997) Intramolecular vibrational redistribution and unimolecular reaction: concepts and new results on the femtosecond dynamics and statistics in CHBrClF. *Berichte der Bunsengesellschaft für Physikalische Chemie*, **101**(3), 311–328.

Ben Kraiem, H., Campargue, A., Chenevier, M., and Stoeckel, F. (1989) Rotationally resolved overtone transitions of CHD_3 in the visible range. *Journal of Chemical Physics*, **91**, 2148–2152.

Bernstein, H.J. and Herzberg, G. (1948) Rotation-vibration spectra of diatomic and simple polyatomic molecules with long absorbing paths. 1. The spectrum of fluoroform (CHF_3) from 2.4μ to 0.7μ. *Journal of Chemical Physics*, **16**(1), 30–39.

Bethardy, G.A. and Perry, D.S. (1993) Rate and mechanism of intramolecular vibrational redistribution in the ν_{16} asymmetric methyl stretch band of 1-butyne. *Journal of Chemical Physics*, **98**(9), 6651–6664.

Bixon, M. and Jortner, J. (1968) Intramolecular radiationless transitions. *The Journal of Chemical Physics*, **48**(2), 715.

Blanco, S., Lesarri, A., López, J.C., Alonso, J.L., and Guarnieri, A. (1996) The rotational spectrum and nuclear quadrupole coupling of $(CHClF_2)-^{35}Cl$. *Zeitschrift für Naturforschung Section A-A Journal of Physical Sciences*, **51**(1–2), 129–132.

Boudon, V., Champion, J.-P., Gabard, T., Loëte, M., Rotger, M., and Wenger, C. (2011) Spherical top theory and molecular spectra, in *Handbook of High-resolution Spectroscopy*, Quack, M. and Merkt, F. (eds), John Wiley & Sons, Ltd., Chichester, UK.

Bray, R.G. and Berry, M.J. (1979) Intra-molecular rate-processes in highly vibrationally excited benzene. *Journal of Chemical Physics*, **71**(12), 4909–4922.

Breidung, J. and Thiel, W. (2011) Prediction of vibrational spectra from ab initio theory, in *Handbook of High-resolution Spectroscopy*, Quack, M. and Merkt, F. (eds), John Wiley & Sons, Ltd., Chichester, UK.

Brotherus, R. (1999) Infia—program for rotational analysis of linear molecular spectra. *Journal of Computational Chemistry*, **20**(6), 610–622.

Brown, J.M. and Carrington, A. (2003) *Rotational Spectroscopy of Diatomic Molecules*, Cambridge University Press, Cambridge.

Bunker, P.R. and Moss, R.E. (1977) Breakdown of Born-Oppenheimer approximation—effective vibration-rotation Hamiltonian for a diatomic molecule. *Molecular Physics*, **33**(2), 417–424.

Califano, S. (1976) *Vibrational States*, John Wiley & Sons, New York.

Callegari, C. and Ernst, W.E. (2011) Helium droplets as nanocryostats for molecular spectroscopy—from the vacuum ultraviolet to the microwave regime, in *Handbook of High-resolution Spectroscopy*, Quack, M. and Merkt, F. (eds), John Wiley & Sons, Ltd., Chichester, UK.

Caminati, W. (2011) Microwave spectroscopy of large molecules and molecular complexes, in *Handbook of High-resolution Spectroscopy*, Quack, M. and Merkt, F. (eds), John Wiley & Sons, Ltd., Chichester, UK.

Campargue, A., Chenevier, M., and Stoeckel, F. (1989a) High-resolution overtone spectroscopy of SiH_4 and $SiHD_3$ ($\Delta\nu_{SiH} = 6$) and CH_4 ($\Delta\nu_{CH} = 5$). *Chemical Physics*, **138**(2–3), 405–411.

Campargue, A., Chenevier, M., and Stoeckel, F. (1989b) Rotational structure of $\Delta\nu_{SiH} = 7$ and 8 overtone transitions of $SiHD_3$. *Chemical Physics*, **137**(1–3), 249–256.

Campargue, A. and Stoeckel, F. (1986) Highly excited vibrational states of CHF_3 and CHD_3 in the range of the $\nu_8 = 5$ CH chromophore. *Journal of Chemical Physics*, **85**(3), 1220–1227.

Carrington, T., Halonen, L., and Quark, M. (1987) *Chemical Physics Letters*, **140**, 512–519.

Carrington Jr., T. (2011) Using iterative methods to compute vibrational spectra, in *Handbook of High-resolution Spectroscopy*, Quack, M. and Merkt, F. (eds), John Wiley & Sons, Ltd., Chichester, UK.

Child, M.S. and Lawton, R.T. (1981) Local and normal vibrational-states—a harmonically coupled anharmonic-oscillator model. *Faraday Discussions*, **71**, 273–285.

Cohen, E.R., Cvitaš, T., Frey, J.G., Holmström, B., Kuchitsi, K., Marquardt, R., Mills, I., Pavese, F., Quack, M., Stohner, J., *et al*. (2007) *Quantities, Units and Symbols in Physical Chemistry*, 3rd edition, RSC Publishing, Cambridge.

Cohen-Tannoudji, C., Diu, B., and Laloë, F. (1977) *Mécanique Quantique, Deuxième Edition Revue, Corrigée, et Augmentée d'une Bibliographie Etendue*, Hermann, Paris.

Coxon, J.A. and Hajigeorgiou, P.G. (1999) Experimental Born-Oppenheimer potential for the $X^1\Sigma^{(+)}$ ground state of HeH^+: comparison with the *ab initio* potential. *Journal of Molecular Spectroscopy*, **193**(2), 306–318.

Darling, B.T. and Dennison, D.M. (1940) The water vapor molecule. *Physical Review*, **57**(2), 128–139.

Davidsson, J., Gutow, J.H., Zare, R.N., Hollenstein, H.A., Marquardt, R.R., and Quack, M. (1991) Fermi resonance in the overtone spectra of the CH chromophore in tribromomethane. 2. Visible spectra. *Journal of Physical Chemistry*, **95**(3), 1201–1209.

Demtröder, W. (2003) *Molekülphysik*, Oldenbourg Verlag, München.

Demtröder, W. (2011) Doppler-free laser spectroscopy, in *Handbook of High-resolution Spectroscopy*, Quack, M. and Merkt, F. (eds), John Wiley & Sons, Ltd., Chichester, UK.

Dübal, H.R., Ha, T., Lewerenz, M., and Quack, M. (1989) Vibrational spectrum, dipole moment function, and potential energy surface of the CH chromophore in CHX_3 molecules. *Journal of Chemical Physics*, **91**(11), 6698–6713.

Dübal, H.R. and Quack, M. (1984a) Tridiagonal Fermi resonance structure in the IR spectrum of the excited CH chromophore in CF_3H. *Journal of Chemical Physics*, **81**(9), 3779–3791.

Dübal, H.R. and Quack, M. (1984b) Vibrational overtone spectra and vibrational dynamics of $CFHCl_2$ and $(CH_3)_2CFH$. *Molecular Physics*, **53**(1), 257–264.

Duncan, J.L. and Mallinson, P.D. (1971) Infrared spectrum of CHD_2I and ground state geometry of methyl iodide. *Molecular Physics*, **39**(3), 471.

Dunham, J.L. (1932) The energy levels of a rotating vibrator. *Physical Review*, **41**(6), 721–731.

Ernst, R., Bodenhausen, G., and Wokaun, A. (1987) *Principles of Nuclear Magnetic Resonance in One and Two Dimensions*, Clarendon Press, Oxford. (and references cited therein).

Fehrensen, B., Hippler, M., and Quack, M. (1998) Isotopomer-selective overtone spectroscopy by ionization detected IR+UV double resonance of jet-cooled aniline. *Chemical Physics Letters*, **298**(4–6), 320–328.

Fehrensen, B., Luckhaus, D., and Quack, M. (1999) Inversion tunneling in aniline from high resolution infrared spectroscopy and an adiabatic reaction path Hamiltonian approach. *Zeitschrift für Physikalische Chemie*, **209**, 1–19.

Fehrensen, B., Luckhaus, D., and Quack, M. (2007) Stereomutation dynamics in hydrogen peroxide. *Chemical Physics*, **338**(2–3), 90–105.

Fermi, E. (1931) Über den Ramaneffekt des Kohlendioxids. *Zeitschrift für Physik*, **71**(3–4), 250–259.

Field, R.W., Baraban, J.H., Lipoff, S.H., and Beck, A.R. (2011) Effective hamiltonians for electronic fine structure and polyatomic vibrations, in *Handbook of High-resolution Spectroscopy*, Quack, M. and Merkt, F. (eds), John Wiley & Sons, Ltd., Chichester, UK.

Flaud, J.-M. and Orphal, J. (2011) Spectroscopy of the earth's atmosphere, in *Handbook of High-resolution Spectroscopy*, Quack, M. and Merkt, F. (eds), John Wiley & Sons, Ltd., Chichester, UK.

Fraser, G.T., Domenech, J., Junttila, M.-L., and Pine, A.S. (1992) Molecular-beam optothermal spectrum of the ν_1 C-H stretching fundamental band of CHF_2Cl, *Journal of Molecular Spectroscopy*, **152**, 307–316.

Frey, H.-M., Kummli, D., Lobsiger, S., and Leutwyler, S. (2011) High-resolution rotational Raman coherence spectroscopy with femtosecond pulses, in *Handbook of High-resolution Spectroscopy*, Quack, M. and Merkt, F. (eds), John Wiley & Sons, Ltd., Chichester, UK.

Gambi, A., Stoppa, P., Giorgianni, S., De Lorenzi, A., Visioni, R., and Ghersetti, S. (1991) Infrared study of the ν_5 fundamental of CF_2HCl by FTIR spectroscopy. *Journal of Molecular Spectroscopy*, **145**(1), 29–40.

Gambogi, J.E., Lehmann, K.K., Pate, B.H., and Scoles, G. (1993) The rate of intramolecular vibrational energy relaxation of the fundamental C–H stretch in $(CF_3)_3C-C\equiv C-H$. *Journal of Chemical Physics*, **98**(2), 1748–1749.

Gauss, J. and Stanton, J.F. (1999) The equilibrium structure of propadienylidene. *Journal of Molecular Structure*, **485–486**, 43–50.

Gottselig, M. (2004) *Spectroscopy, Quantum Dynamics and Parity Violation in Axially Chiral Molecules*, Dissertation, ETH Zürich, Laboratorium für Physikalische Chemie.

Green, W.H., Lawrence, W.D., and Moore, C.B. (1987) Kinetic anharmonic coupling in the trihalomethanes: a mechanism for rapid intramolecular redistribution of CH stretch vibrational energy. *Journal of Chemical Physics*, **86**(11), 6000–6011.

Gruebele, M. and Bigwood, R. (1998) Molecular vibrational energy flow: beyond the golden rule. *International Reviews in Physical Chemistry*, **17**(2), 91–145.

Ha, T.K., Lewerenz, M., and Quack, M. (1987) Anharmonic coupling in vibrationally highly excited CH-chromophores of CHX_3 symmetric tops: experiment and variational *ab initio* theory, in *Proceedings of* 10*th International Conference on Molecular Energy Transfer, Emmetten, Switzerland*, Dietrich, P. and Quack, M. (eds), ETH, Zürich, pp. 130–132.

Haas, S., Yamada, K.M.T., and Winnewisser, G. (1994) High-resolution Fourier transform spectrum of the ν_{13} fundamental band of triacetylene in the far-infrared region. *Journal of Molecular Spectroscopy*, **164**(2), 445–455.

Häber, T. and Kleinermanns, K. (2011) Multiphoton resonance spectroscopy of biological molecules, in *Handbook of High-resolution Spectroscopy*, Quack, M. and Merkt, F. (eds), John Wiley & Sons, Ltd., Chichester, UK.

Havenith, M. and Birer, Ö. (2011) High resolution IR-laser jet spectroscopy of formic acid dimer, in *Handbook of High-resolution Spectroscopy*, Quack, M. and Merkt, F. (eds), John Wiley & Sons, Ltd., Chichester, UK.

Heitler, W. and Herzberg, G. (1929) Do nitrogen nuclei follow the Bose statistics? *Naturwissenschaften*, **17**, 673–674.

Henry, B.R. and Siebrand, W. (1968) Anharmonicity in polyatomic molecules. CH-stretching overtone spectrum of benzene. *Journal of Chemical Physics*, **49**(12), 5369–5376.

Herman, M. (2011) High-resolution infrared spectroscopy of acetylene: theoretical background and research trends, in *Handbook of High-resolution Spectroscopy*, Quack, M. and Merkt, F. (eds), John Wiley & Sons, Ltd., Chichester, UK.

Herman, M., Lievin, J., and Vander Auwera, J. (1999) Advances in chemical physics—global and accurate vibration Hamiltonians from high-resolution molecular spectroscopy. *Advances in Chemical Physics*, **108**, 1–448.

Herzberg, G. (1939) *Molekülspektren und Molekülstruktur*, Theodor Steinkopff Verlag, Dresden/Leipzig.

Herzberg, G. (1945) *Molecular Spectra and Molecular Structure, Vol. II, Infrared and Raman Spectra of Polyatomic Molecules*, 1st edition, van Nostrand Reinhold, New York.

Herzberg, G. (1950) *Molecular Spectra and Molecular Structure, Vol. I, Spectra of Diatomic Molecules*, van Nostrand Reinhold, New York.

Herzberg, G. (1966) *Molecular Spectra and Molecular Structure Vol. III; Electronic Spectra and Electronic Structure of Polyatomic Molecules*, van Nostrand, New York.

Hippler, M., Miloglyadov, E., Quack, M., and Seyfang, G. (2011) Mass and isotope-selective infrared spectroscopy, in *Handbook of High-resolution Spectroscopy*, Quack, M. and Merkt, F. (eds), John Wiley & Sons, Ltd., Chichester, UK.

Hippler, M., Oeltjen, M., and Quack, M. (2007) High-resolution continuous-wave-diode laser cavity ring-down spectroscopy of the hydrogen fluoride dimer in a pulsed slit jet expansion: two components of the $N = 2$ triad near 1.3 μm. *The Journal of Physical Chemistry A*, **111**(49), 12659–12668.

Hodges, C.J. and Butcher, R.J. (1996) Difference frequency spectroscopy of methyl Iodide $^{12}CHD_2I$ in the ground and ν_1 vibrational states. *Journal of Molecular Spectroscopy*, **178**(1), 45–51.

Hollenstein, H., Lewerenz, M., and Quack, M. (1990) Isotope effects in the Fermi resonance of the CH chromophore in CHX_3 molecules. *Chemical Physics Letters*, **165**(2–3), 175–183.

Hollenstein, H., Marquardt, R., Quack, M., and Suhm, M. (1994) Dipole moment function and equilibrium structure of methane in an analytical, anharmonic nine-dimensional potential surface related to experimental rotational constants and transition moments by quantum Monte Carlo calculations. *Journal of Chemical Physics*, **101**(5), 3588–3602.

Horká, V., Quack, M., and Willeke, M. (2008) Analysis of the CH-chromophore spectra and dynamics in dideuteromethyliodide CHD_2I. *Molecular Physics*, **106**(9–10), 1303–1316.

Howard, B.J. and Moss, R.E. (1971) Molecular Hamiltonian. 2. Linear molecules. *Molecular Physics*, **20**(1), 147–159.

Huber, K.P. and Herzberg, G. (1979) *Molecular Spectra and Molecular Structure Vol. IV, Constants of Diatomic Molecules*, van Nostrand Reinhold, New York.

Hund, F. (1927) Zur Deutung der molekelspektren II. *Zeitschrift für Physik*, **42**, 93–120.

Islampour, R. and Kasha, M. (1983) Molecular translational rovibronic Hamiltonian. 1. Non-linear molecules. *Chemical Physics*, **74**(1), 67–76.

Jäger, W. and Xu, Y. (2011) Fourier transform microwave spectroscopy of doped helium clusters, in *Handbook of High-resolution Spectroscopy*, Quack, M. and Merkt, F. (eds), John Wiley & Sons, Ltd., Chichester, UK.

James, F. (1998) *Minuit—function minimization and error analysis, Reference manual*.

Jung, C., Ziemniak, E., and Taylor, H.S. (2001) Extracting the CH chromophore vibrational dynamics of CHBrClF directly from spectra: unexpected constants of the motion and symmetries. *Journal of Chemical Physics*, **115**(6), 2499–2509.

Kellman, M.E. and Lynch, E.D. (1986) Fermi resonance phase space structure from experimental spectra. *Journal of Chemical Physics*, **85**(12), 7216–7223.

Kerstel, T., Lehmann, K.K., Mentel, B.H., Pate, B.H., and Scoles, G. (1991) Dependence of intramolecular vibrational relaxation on central atom substitution: ν_1 and $2\nu_1$ molecular beam optothermal spectra of 3,3-dimethyl-1-butyne and trimethylsilylacetylene. *Journal of Physical Chemistry*, **95**(21), 8282–8293.

Kisiel, Z., Alonso, J.L., Blanco, S., Cazzoli, G., Colmont, J.M., Cotti, G., Graner, G., López, J.C., Merke, I., and Pszczółstrokowski, L. (1997) Spectroscopic constants for HCFC-22 from rotational and high-resolution vibration-rotation spectra: (CHF_2Cl)-^{37}Cl and (CHF_2Cl)-^{13}C-^{35}Cl isotopomers. *Journal of Molecular Spectroscopy*, **184**(1), 150–155.

Kisiel, Z., Pszczółstrokowski, L., Cazzoli, G., and Cotti, G. (1995) The millimeter-wave rotational spectrum and coriolis interaction in the 2 lowest excited vibrational-states of $CHClF_2$. *Journal of Molecular Spectroscopy*, **173**(2), 477–487.

Kisiel, Z., Pszczółstrokowski, L., Medvedev, I.R., Winnewisser, M., De Lucia, F.C., and Herbst, E. (2005) Rotational spectrum of trans-trans diethyl ether in the ground and three excited vibrational states. *Journal of Molecular Spectroscopy*, **233**(2), 231–243.

Klatt, G., Graner, G., Klee, S., Mellau, G., Kisiel, Z., Pszczółstrokowski, L., Alonso, J.L., and López, J.C. (1996) Analysis of the high-resolution FT-IR and millimeter-wave spectra of the $\nu_5 = 1$ state of CHF_2Cl. *Journal of Molecular Spectroscopy*, **178**(1), 108–112.

Klopper, W., Quack, M., and Suhm, M. (1998) HF dimer: empirically refined analytical potential energy and dipole hypersurfaces from *ab initio* calculations. *Journal of Chemical Physics*, **108**(24), 10096–10115.

Köppel, H., Cederbaum, L.S., and Mahapatra, S. (2011) Theory of the Jahn–Teller effect, in *Handbook of High-resolution Spectroscopy*, Quack, M. and Merkt, F. (eds), John Wiley & Sons, Ltd., Chichester, UK.

Kushnarenko, A., Krylov, V., Miloglyadov, E., Quack, M., and Seyfang, G. (2008a) Intramolecular vibrational energy redistribution measured by femtosecond pump-probe experiments in a hollow waveguide, in *Ultrafast Phenomena XVI, Proceedings of the 16th International Conference on Ultrafast Phenomena, Stresa, Italia, June 2008*, Corkum, P., Silvestri, S.D., Nelson, K., Riedle, E., and Schoenlein, R.W. (eds), *Springer Series in Chemical Physics*, Springer, Berlin, pp. 349–351. ISBN 978-3-540-95945-8.

Kushnarenko, A., Miloglyadov, E., Quack, M., and Seyfang, G. (2008b) Intramolecular vibrational energy redistribution in CH_2XCCH (X = Cl, Br, I) measured by femtosecond pump-probe experiments, in *Proceedings, 16th Symposium on Atomic and Surface Physics and Related Topics, Les Diablerets, Switzerland, 20. - 25.1.2008*, Beck, R.D., Drabbels, M., Rizzo, T.R. (eds), Innsbruck University Press, Innsbruck, pp. 149–152. ISBN 978-902571-31-1.

Kutzelnigg, W. (2007) Which masses are vibrating or rotating in a molecule? *Molecular Physics*, **105**(19–22), 2627–2647.

Kyllönen, K., Alanko, S., Baskakov, O.I., Ahonen, A.-M., and Horneman, V.M. (2006) High resolution FTIR spectroscopy on CH_2DI and CHD_2I: analyses of the fundamental bands ν_6' and ν_6''. *Molecular Physics*, **104**(16–17), 2663.

Kyllönen, K., Alanko, S., Lohilahti, J., and Horneman, V.M. (2004) High resolution Fourier transform infrared spectroscopy on CH_2DI and CHD_2I: evaluation of the ground state constants and analyses of the C-I stretching bands ν_3. *Molecular Physics*, **102**(14–15), 1597.

Le Roy, R.J. (2007) *Level 8.0, A Computer Program for Solving the Radial Schrödinger Equation for Bound and Quasibound Levels*.

Lehmann, K.K., Scoles, G., and Pate, B.H. (1994) Intramolecular dynamics from eigenstate-resolved infrared-spectra. *Annual Review of Physical Chemistry*, **45**, 241–274.

Lewerenz, M. (1987) *Spektroskopie und Dynamik hochangeregter Schwingungszustände des CH-Chromophore in vielatomigen Molekülen: Experiment und ab initio—Theorie*, Dissertation, ETH Zürich, Laboratorium für Physikalische Chemie.

Lewerenz, M. and Quack, M. (1986) Vibrational overtone intensities of the isolated CH and CD chromophores in fluoroform and chloroform. *Chemical Physics Letters*, **123**(3), 197–202.

Lewerenz, M. and Quack, M. (1988) Vibrational spectrum and potential energy surface of the CH chromophore in CHD_3. *Journal of Chemical Physics*, **88**(9), 5408–5432.

Łodyga, W., Kreglewski, M., Pracna, P., and Urban, Š. (2007) Advanced graphical software for assignments of transitions in rovibrational spectra. *Journal of Molecular Spectroscopy*, **243**(2), 182–188.

Loomis, F.W. and Wood, R.W. (1928) The rotational structure of the blue-green bands Na_2. *Physical Review*, **32**(2), 223–237.

Louck, J.D. (1976) Derivation of molecular vibration-rotation Hamiltonian from Schrödinger equation for molecular model. *Journal of Molecular Spectroscopy*, **61**(1), 107–137.

Luckhaus, D. and Quack, M. (1989) The far infrared pure rotational spectrum and the Coriolis coupling between ν_3 and ν_8 in $CH^{35}ClF_2$. *Molecular Physics*, **68**(3), 745–758.

Luckhaus, D. and Quack, M. (1992) Spectrum and dynamics of the CH chromophore in CD_2HF. I. Vibrational Hamiltonian and analysis of rovibrational spectra. *Chemical Physics Letters*, **190**(6), 581–589.

Luckhaus, D. and Quack, M. (1993) The role of potential anisotropy in the dynamics of the CH chromophore in CHX_3 (C_{3v}) symmetric tops. *Chemical Physics Letters*, **205**(2–3), 277–284.

Luckhaus, D., Quack, M., and Stohner, J. (1993) Femtosecond quantum structure, equilibration and time reversal for the CH-chromophore dynamics in CHD_2F. *Chemical Physics Letters*, **212**(5), 434–443.

Maki, A.G. and Wells, S. (1991) *Wavenumber Calibration Tables from Heterodyne Frequency Measurements*. NIST Special Publication 821, USA.

Makushkin, Y.S. and Ulenikov, O.N. (1977) Transformation of complete electron-nuclear Hamiltonian of a polyatomic molecule to intramolecular coordinates. *Journal of Molecular Spectroscopy*, **68**(1), 1–20.

Manca, C., Quack, M., and Willeke, M. (2008) Vibrational predissociation in hydrogen obnded dimers: the case of $(HF)_2$ and its isotopomers. *Chimia*, **62**(4), 235–239.

Manzanares, C., Yamasaki, N.L., and Weitz, E. (1988) Dye-laser photoacoustic overtone spectroscopy of $CHBr_3$. *Chemical Physics Letters*, **144**(1), 43–47.

Marquardt, D.W. (1961) An algorithm for least-squares estimation of nonlinear parameters. *Journal of the Society for Industrial and Applied Mathematics*, **11**(2), 431–441.

Marquardt, R. and Quack, M. (1989) Infrared-multiphoton excitation and wave packet motion of the harmonic and anharmonic oscillators: exact solutions and quasiresonant approximation. *Journal of Chemical Physics*, **90**(11), 6320–6327.

Marquardt, R. and Quack, M. (1991) The wave packet motion and intramolecular vibrational redistribution in CHX_3 molecules under infrared multiphoton excitation. *Journal of Chemical Physics*, **95**(7), 4854–4876.

Marquardt, R. and Quack, M. (2001) Energy redistribution in reacting systems, in *Encyclopedia of Chemical Physics and Physical Chemistry, Vol. 1 (Fundamentals), Chapter A.3.13*, Moore, J., and Spencer, N. (eds), IOP Publishing, Bristol, pp. 897–936.

Marquardt, R. and Quack, M. (2011) Global analytical potential energy surfaces for high-resolution molecular spectroscopy and reaction dynamics, in *Handbook of High-resolution Spectroscopy*, Quack, M. and Merkt, F. (eds), John Wiley & Sons, Ltd., Chichester, UK.

Marquardt, R., Quack, M., Stohner, J., and Sutcliffe, E. (1986) Quantum-mechanical wavepacket dynamics of the CH group in symmetric top X_3CH compounds using effective Hamiltonians from high-resolution spectroscopy. *Journal of the Chemical Society-Faraday Transactions II*, **82**, 1173–1187.

Mastalerz, R. and Reiher, M. (2011) Relativistic electronic structure theory for molecular spectroscopy, in *Handbook of High-resolution Spectroscopy*, Quack, M. and Merkt, F. (eds), John Wiley & Sons, Ltd., Chichester, UK.

McIllroy, A. and Nesbitt, D.A. (1990) Vibrational mode mixing in terminal acetylenes: high-resolution infrared laser study of isolated J states. *Journal of Chemical Physics*, **92**(4), 2229–2233.

McIntosh, D.F. and Michaelian, K.H. (1979a) Wilson-GF matrix-method of vibrational analysis. 1. General-theory. *Canadian Journal of Spectroscopy*, **24**(1), 1–10.

McIntosh, D.F. and Michaelian, K.H. (1979b) Wilson-GF-matrix-method of vibrational analysis. 2. Theory and worked examples of the construction of the B-matrix. *Canadian Journal of Spectroscopy*, **24**(2), 35–40.

McIntosh, D.F. and Michaelian, K.H. (1979c) Wilson-GF-matrix-method of vibrational analysis. 3. Worked examples of the vibrational analysis of CO_2 and H_2O. *Canadian Journal of Spectroscopy*, **24**(3), 65–74.

McNaughton, D., McGilvery, D., and Shanks, F. (1991) High resolution FTIR analysis of the ν_1 band of tricarbon monoxide: production of tricarbon monoxide and chloroacetylenes by pyrolysis of fumaroyl dichloride. *Journal of Molecular Spectroscopy*, **149**(2), 458–473.

Mecke, R. (1925) Zur Struktur einer Klasse von Bandenspektra. *Zeitschrift für Physik*, **31**(1), 709–712.

Mecke, R. (1936) Absorptionsuntersuchungen an Kohlenwasserstoffen im nahen Ultraroten. IV. Berechnung von anharmonischen Valenzschwingungen mehratomiger Moleküle. *Zeitschrift für Physik*, **99**, 217–235.

Mecke, R. (1950) Dipolmoment und chemische Bindung. *Zeitschrift für Elektrochemie*, **54**(1), 38–42.

Medvedev, I.R., Winnewisser, M., Winnewisser, B.P., De Lucia, F.C., and Herbst, E. (2005) The use of CAAARS (Computer Aided Assignment of Asymmetric Rotor Spectra) in the analysis of rotational spectra. *Journal of Molecular Structure*, **742**(1–3), 229–236.

Merke, I., Graner, G., Klee, S., Mellau, G., and Polanz, O. (1995) High-resolution FT-IR spectra of CHF_2Cl in the region between $335\,cm^{-1}$ and $450\,cm^{-1}$. *Journal of Molecular Spectroscopy*, **173**(2), 463–476.

Merkt, F. and Quack, M. (2011) Molecular quantum mechanics and molecular spectra, molecular symmetry, and interaction of matter with radiation, in *Handbook of High-resolution Spectroscopy*, Quack, M. and Merkt, F. (eds), John Wiley & Sons, Ltd., Chichester, UK.

Meyer, R. (1979) Flexible models for intra-molecular motion, a versatile treatment and its application to glyoxal. *Journal of Molecular Spectroscopy*, **76**(1–3), 266–300.

Mills, I.M. (1974) Harmonic and anharmonic force field calculations. *A Specialist Periodical Report / Royal Society of Chemistry. Theoretical Chemistry*, **1**, 110–159.

Moruzzi, G., Jabs, W., Winnewisser, B.P., and Winnewisser, M. (1998) Assignment and power series analysis of the FIR Fourier transform spectrum of cyanamide using a multimolecule RITZ program. *Journal of Molecular Spectroscopy*, **190**(2), 353–364.

Moruzzi, G., Xu, L.H., Lees, R.M., Winnewisser, B.P., and Winnewisser, M. (1994) Investigation of the ground vibrational state of CD_3OH by a new RITZ program for direct energy level fitting. *Journal of Molecular Spectroscopy*, **167**(1), 156–175.

Neese, C.F. (2001) An interactive Loomis–Wood Package for spectral assignment in Igor Pro, Version 2.0. *Abstracts of OSU International Symposium on Molecular Spectroscopy*, Columbus, pp. MG–03.

Nesbitt, D.J. and Field, R.W. (1996) Vibrational energy flow in highly excited molecules: role of intramolecular vibrational redistribution. *Journal of Physical Chemistry*, **100**(31), 12735–12756.

Nielsen, H.H. (1951) The vibration-rotation energies of molecules. *Reviews of Modern Physics*, **23**(2), 90–136.

Nielsen, H.H. (1959) The vibration-rotation energies of molecules and their spectra in the infra-red, in *Handbuch der Physik—Encyclopedia of physics*, Flugge, S. (ed), Springer, Berlin, pp. 173–313. Vol. 37 (1).

Nielsen, A.H. (1962) Infrared spectroscopy, in *Methods of Experimental Physics, Vol. 3 Molecular Physics*, Williams, D. (ed), Academic Press, New York, pp. 38–110.

Oka, T. (2011) Orders of magnitude and symmetry in molecular spectroscopy, in *Handbook of High-resolution Spectroscopy*, Quack, M. and Merkt, F. (eds), John Wiley & Sons, Ltd., Chichester, UK.

Papoušek, D. and Aliev, M.R. (1982) *Molecular Vibrational Rotational Spectra*, Elsevier, Amsterdam.

Paso, R. and Antilla, R. (1990) Perturbations in the ν_1 band of CH_3I. *Journal of Molecular Spectroscopy*, **140**(1), 46–53.

Pekeris, C.L. (1934) The rotation-vibration coupling in diatomic molecules. *Physical Review*, **45**(2), 98–103.

Perry, D., Bethardy, G.A., Davis, M.J., and Go, J. (1996) Energy randomisation: how much of rotational phase space is explored and how long does it take? *Faraday Discuss*, **102**, 215–226.

Peyerimhoff, S., Lewerenz, M., and Quack, M. (1984) Spectroscopy and dynamics of the isolated CH chromophore in CD_3H: experiment and theory. *Chemical Physics Letters*, **109**(6), 563–569.

Pickett, H.M. (1991) The fitting and prediction of vibration-rotation spectra with spin interactions. *Journal of Molecular Spectroscopy*, **148**(2), 371–377.

Podolsky, B. (1928) Quantum mechanically correct form of Hamiltonian function for conservative systems. *Physical Review*, **32**(5), 812–816.

Press, W.H., Flannery, B.P., Teukolsky, S.A., and Vetterling, W.T. (1986) *Numerical Recipes*, Cambridge University Press, Cambridge.

von Puttkamer, K., Dübal, H.R., and Quack, M. (1983a) Temperature-dependent infrared band structure and dynamics of the CH choromophore in $C_4F_9—C{\equiv}C—H$. *Chemical Physics Letters*, **95**(4–5), 358–362.

von Puttkamer, K., Dübal, H.R., and Quack, M. (1983b) Time-dependent processes in polyatomic molecules during and after intense infrared irradiation. *Faraday Discussions of the Chemical Society*, **75**, 197–210.

von Puttkamer, K. and Quack, M. (1989) Vibrational spectra of $(HF)_2$, $(HF)_n$ and their D-isotopomers: mode selective rearrangements and nonstatistical unimolecular decay. *Chemical Physics*, **139**(1), 31–53.

Quack, M. (1981) Discussion contributions on high resolution spectroscopy. (On normal, local, and global vibrational states). *Faraday discussions of the Chemical Society*, **71**, 359–364.

Quack, M. (1982) Reaction dynamics and statistical mechanics of the preparation of highly excited states by intense infrared radiation. *Advances in Chemical Physics*, **50**, 395–473.

Quack, M. (1990) Spectra and dynamics of coupled vibrations in polyatomic molecules. *Annual Review of Physical Chemistry*, **41**, 839–874.

Quack, M. (1991) Mode selective vibrational redistribution and unimolecular reactions during and after IR-laser excitation, in *Mode Selective Chemistry, Jerusalem Symposium*, Jortner, J., Levine, R.D. and Pullmann, B. (eds.) vol. 24, 47–65, Kluwer Academic Publishers, Dordrecht.

Quack, M. (1993) Molecular quantum dynamics from high resolution spectroscopy and laser chemistry. *Journal of Molecular Structure*, **292**, 171–195.

Quack, M. (1995) Molecular infrared spectra and molecular motion. *Journal of Molecular Structure*, **347**, 245–266.

Quack, M. (2011) Fundamental symmetries and symmetry violations from high-resolution spectroscopy, in *Handbook of High-resolution Spectroscopy*, Quack, M. and Merkt, F. (eds), John Wiley & Sons, Ltd., Chichester, UK.

Quack, M. and Kutzelnigg, W. (1995) Molecular spectroscopy and molecular dynamics: theory and experiment. *Berichte der Bunsengesellschaft für Physikalische Chemie*, **99**(3), 231–245.

Quack, M. and Stohner, J. (1993) Femtosecond quantum dynamics of functional groups under coherent infrared multiphoton excitation as derived from the analysis of high-resolution spectra. *Journal of Physical Chemistry*, **97**(48), 12574–12590.

Quack, M. and Suhm, M. (1991) Potential energy surfaces, quasiadiabatic channels, rovibrational spectra, and intramolecular dynamics of $(HF)_2$ and its isotopomers from quantum Monte Carlo calculations. *Journal of Chemical Physics*, **95**(1), 28–59.

Quack, M. and Sutcliffe, E. (1985) On the validity of the quasiresonant approximation for molecular infrared-multiphoton excitation. *Journal of Chemical Physics*, **83**(8), 3805–3812.

Rasetti, F. (1930) Über die Rotations-Ramanspektren von Stickstoff und Sauerstoff. *Zeitschrift für Physik*, **61**(06), 598–601.

Riter, J.R. and Eggers, D.F. (1966) Fundamental vibrations and force constants in the partially deuterated methyl halides. *Journal of Chemical Physics*, **44**(6), 745.

Ross, A., Amrein, A., Luckhaus, D., and Quack, M. (1989a) The rotational structure of the ν_4-band of $CH^{35}ClF_2$. *Molecular Physics*, **66**(6), 1273–1277.

Ross, A.J., Hollenstein, H.A., Marquardt, R.R., and Quack, M. (1989b) Fermi resonance in the overtone spectra of the CH chromophore in bromoform. *Chemical Physics Letters*, **156**(5), 455–462.

Santos, J. and Orza, J.M. (1986) Absolute Raman intensities of CH_3I, CH_2DI, CHD_2I and CD_3I—experimental results. *Journal of Molecular Structure*, **142**, 205–208.

Schrödinger, E. (1926) Der stetige Übergang von der Mikro-zur Makromechanik. *Naturwissenschaften*, **14**, 664–666.

Schulze, G., Koja, O., Winnewisser, B., and Winnewisser, M. (2000) High resolution FIR spectra of HCNO and DCNO. *Journal of Molecular Spectroscopy*, **518**, 307–325.

Schwartz, C. and Leroy, R.J. (1987) Nonadiabatic eigenvalues and adiabatic matrix-elements for all isotopes of diatomic hydrogen. *Journal of Molecular Spectroscopy*, **121**(2), 420–439.

Scott, J.F. and Rao, K.N. (1966) "Loomis-Wood" diagrams for polyatomic infrared spectra. *Journal of Molecular Spectroscopy*, **20**(4), 461–463.

Segall, J., Zare, R.N., Dübal, H.R., Lewerenz, M., and Quack, M. (1987) Tridiagonal Fermi resonance structure in the vibrational spectrum of the CH chromophore in CHF_3. II. visible spectra. *Journal of Chemical Physics*, **86**(2), 634–646.

Shipman, S.T. and Pate, B.H. (2011) New techniques in microwave spectroscopy, in *Handbook of High-resolution Spectroscopy*, Quack, M. and Merkt, F. (eds), John Wiley & Sons, Ltd., Chichester, UK.

Sibert, E.L. (1990) Variational and perturbative descriptions of highly vibrationally excited molecules. *International Reviews in Physical Chemistry*, **9**, 1–27.

Sigrist, M.W. (2011) High-resolution infrared laser spectroscopy and gas sensing applications, in *Handbook of High-resolution Spectroscopy*, Quack, M. and Merkt, F. (eds), John Wiley & Sons, Ltd., Chichester, UK.

Snels, M. and D'Amico, G. (2001) Diode laser jet spectra and analysis of the ν_3 and ν_8 fundamentals of CHF_2Cl. *Journal of Molecular Spectroscopy*, **209**(1), 1–10.

Snels, M., Horká-Zelenková, V., Hollenstein, H., and Quack, M. (2011) High-resolution FTIR and diode laser spectroscopy of supersonic jets, in *Handbook of High-resolution Spectroscopy*, Quack, M. and Merkt, F. (eds), John Wiley & Sons, Ltd., Chichester, UK.

Stanca-Kaposta, E.C. and Simons, J.P. (2011) High-resolution infrared–ultraviolet (IR–UV) double-resonance spectroscopy of biological molecules, in *Handbook of High-resolution Spectroscopy*, Quack, M. and Merkt, F. (eds), John Wiley & Sons, Ltd., Chichester, UK.

Stohner, J. and Quack, M. (2011) Conventions, symbols, quantities, units and constants for high-resolution molecular spectroscopy, in *Handbook of High-resolution Spectroscopy*, Quack, M. and Merkt, F. (eds), John Wiley & Sons, Ltd., Chichester, UK.

Stoicheff, B.P. (1962) Raman spectroscopy, in *Methods of Experimental Physics, Vol. 3 Molecular Physics*, Williams, D. (ed), Academic Press, New York, pp. 111–154.

Stroh, F. (1991) *Cyanoisocyan, CNCN: Identifikation und Charakterisierung einer neuen Spezies mittels hochauflösender Mikrowellen- und Fourier-Transform-Infrarot-Spektroskopie*, Dissertation Justus-Liebig-Universität, Giessen.

Stroh, F., Reinstädtler, J., Grecu, J.C., and Albert, S. (1992) *The Giessen Loomis–Wood program LW5.1* .

Tasinato, N., Pietropolli Charmet, A., and Stoppa, P. (2007) Atirs package: a program suite for the rovibrational analysis of infrared spectra of asymmetric top molecules. *Journal of Molecular Spectroscopy*, **243**(2), 148–154.

Tennyson, J. (2011) High accuracy rotation–vibration calculations on small molecules, in *Handbook of High-resolution Spectroscopy*, Quack, M. and Merkt, F. (eds), John Wiley & Sons, Ltd., Chichester, UK.

Tew, D.P., Klopper, W., Bachorz, R.A., and Hättig, C. (2011) Ab initio theory for accurate spectroscopic constants and molecular properties, in *Handbook of High-resolution Spectroscopy*, Quack, M. and Merkt, F. (eds), John Wiley & Sons, Ltd., Chichester, UK.

Thompson, C.D., Robertson, E.G., and McNaughton, D. (2003) Reading between the lines: exposing underlying features of high resolution infrared spectra ($CHClF_2$). *Physical Chemistry Chemical Physics*, **5**(10), 1996–2000.

Thompson, C.D., Robertson, E.G., and McNaughton, D. (2004) Completing the picture in the rovibrational analysis of chlorodifluoromethane ($CHClF_2$) : ν_3 and ν_8. *Molecular Physics*, **102**(14-15), 1687–1695.

Ulenikov, O.N., Bekhtereva, E.S., Grebneva, S.V., Hollenstein, H., and Quack, M. (2006) High-resolution rovibrational analysis of vibrational states of A_2 symmetry of the dideuterated methane CH_2D_2: the levels ν_5 and $\nu_7 + \nu_9$. *Molecular Physics*, **104**(20–21), 3371–3386.

Voth, G.A., Marcus, R.A., and Zewail, A.H. (1984) The highly excited C–H stretching states of CHD_3, CHT_3, and CH_3D. *The Journal of Chemical Physics*, **81**(12), 5494–5507.

Watson, J.K.G. (1968) Simplification of the molecular vibration-rotation hamiltonian. *Molecular Physics*, **15**(5), 479–490.

Watson, J.K.G. (2011) Indeterminacies of fitting parameters in molecular spectroscopy, in *Handbook of High-resolution Spectroscopy*, Quack, M. and Merkt, F. (eds), John Wiley & Sons, Ltd., Chichester, UK.

Weber, A. (2011) High-resolution Raman spectroscopy of gases, in *Handbook of High-resolution Spectroscopy*, Quack, M. and Merkt, F. (eds), John Wiley & Sons, Ltd., Chichester, UK.

Wester, R. (2011) Spectroscopy and reaction dynamics of anions, in *Handbook of High-resolution Spectroscopy*, Quack, M. and Merkt, F. (eds), John Wiley & Sons, Ltd., Chichester, UK.

Western, C.M. (2010) Pgopher, a Program for Simulating Rotational Structure, Technical Report, University of Bristol, http://pgopher.chm.bris.ac.uk.

Western, C.M. (2011) Introduction to modeling high-resolution spectra, in *Handbook of High-resolution Spectroscopy*, Quack, M. and Merkt, F. (eds), John Wiley & Sons, Ltd., Chichester, UK.

Wilson, E.B., Decius, J.C., and Cross, P.C. (1955) *Molecular Vibrations. The Theory of Infrared and Raman Vibrational Spectra*, McGraw-Hill, New York.

Winnewisser, B., Reinstädtler, J., Yamada, K., and Behrend, J. (1989) Interactive Loomis–Wood assignment programs. *Journal of Molecular Spectroscopy*, **136**(1), 12–16.

Winther, F., Schönhoff, M., LePrince, R., Guarnieri, A., Bruget, D.N., and McNaughton, D. (1992) The infrared rotation-vibration spectrum of dicyanoacetylene: the ground and $v_9 = 1$ state rotational constants. *Journal of Molecular Spectroscopy*, **152**(1), 205–212.

Wong, J.S., Green, W.H., Lawrence, W.D., and Moore, C.B. (1987) Coupling of CH stretching and bending vibrations in trihalomethanes. *Journal of Chemical Physics*, **86**(11), 5994–5999.

Wörner, H.J. and Merkt, F. (2011) Fundamentals of electronic spectroscopy, in *Handbook of High-resolution Spectroscopy*, Quack, M. and Merkt, F. (eds), John Wiley & Sons, Ltd., Chichester, UK.

Yamaguchi, Y. and Schaefer III, H.F. (2011) Analytical derivative methods in molecular electronic structure theory: a new dimension to quantum chemistry and its applications to spectroscopy, in *Handbook of High-resolution Spectroscopy*, Quack, M. and Merkt, F. (eds), John Wiley & Sons, Ltd., Chichester, UK.

Zare, R.N. (1988) *Angular Momentum: Understanding Spatial Aspects in Chemistry and Physics*, John Wiley & Sons, New York.

RELATED ARTICLES

Albert *et al*. 2011: **High-resolution Fourier Transform Infrared Spectroscopy**
Amano 2011: **High-resolution Microwave and Infrared Spectroscopy of Molecular Cations**
Bauder 2011: **Fundamentals of Rotational Spectroscopy**
Breidung and Thiel 2011: **Prediction of Vibrational Spectra from Ab Initio Theory**
Boudon *et al*. 2011: **Spherical Top Theory and Molecular Spectra**
Callegari and Ernst 2011: **Helium Droplets as Nanocryostats for Molecular Spectroscopy—from the Vacuum Ultraviolet to the Microwave Regime**
Carrington 2011: **Using Iterative Methods to Compute Vibrational Spectra**
Demtröder 2011: **Doppler-free Laser Spectroscopy**
Field *et al*. 2011: **Effective Hamiltonians for Electronic Fine Structure and Polyatomic Vibrations**
Flaud and Orphal 2011: **Spectroscopy of the Earth's Atmosphere**
Frey *et al*. 2011: **High-resolution Rotational Raman Coherence Spectroscopy with Femtosecond Pulses**
Häber and Kleinermanns 2011: **Multiphoton Resonance Spectroscopy of Biological Molecules**
Havenith and Birer 2011: **High-resolution IR-laser Jet Spectroscopy of Formic Acid Dimer**
Herman 2011: **High-resolution Infrared Spectroscopy of Acetylene: Theoretical Background and Research Trends**
Hippler *et al*. 2011: **Mass and Isotope-selective Infrared Spectroscopy**
Jäger and Xu 2011: **Fourier Transform Microwave Spectroscopy of Doped Helium Clusters**
Köppel *et al*. 2011: **Theory of the Jahn–Teller Effect**
Marquardt and Quack 2011: **Global Analytical Potential Energy Surfaces for High-resolution Molecular Spectroscopy and Reaction Dynamics**
Mastalerz and Reiher 2011: **Relativistic Electronic Structure Theory for Molecular Spectroscopy**
Merkt and Quack 2011: **Molecular Quantum Mechanics and Molecular Spectra, Molecular Symmetry, and Interaction of Matter with Radiation**
Oka 2011: **Orders of Magnitude and Symmetry in Molecular Spectroscopy**
Quack 2011: **Fundamental Symmetries and Symmetry Violations from High-resolution Spectroscopy**
Shipman and Pate 2011: **New Techniques in Microwave Spectroscopy**
Sigrist 2011: **High-resolution Infrared Laser Spectroscopy and Gas Sensing Applications**
Snels *et al*. 2011: **High-resolution FTIR and Diode Laser Spectroscopy of Supersonic Jets**

Stanca-Kaposta and Simons 2011: **High-resolution Infrared–Ultraviolet (IR–UV) Double-resonance Spectroscopy of Biological Molecules**
Stohner and Quack 2011: **Conventions, Symbols, Quantities, Units and Constants for High-resolution Molecular Spectroscopy**
Tennyson 2011: **High Accuracy Rotation–Vibration Calculations on Small Molecules**
Tew *et al*. 2011: **Ab Initio Theory for Accurate Spectroscopic Constants and Molecular Properties**
Watson 2011: **Indeterminacies of Fitting Parameters in Molecular Spectroscopy**
Weber 2011: **High-resolution Raman Spectroscopy of Gases**
Wester 2011: **Spectroscopy and Reaction Dynamics of Anions**
Wörner and Merkt 2011: **Fundamentals of Electronic Spectroscopy**
Yamaguchi and Schaefer 2011: **Analytic Derivative Methods in Molecular Electronic Structure Theory: A New Dimension to Quantum Chemistry and its Applications to Spectroscopy**